UNIVERSITÀ DEGLI STUDI DI PADOVA

DIPARTIMENTO DI INGEGNERIA DELL'INFORMAZIONE

University of Padua

Department of Information Engineering

BIOENGINEERING

Master's degree

# Detection of *L. Lactis* bacteriophages in milk samples by an electrochemical biosensor

21/02/2022

Candidate: Federico Magalini

Supervisor: Prof. Alessandro Paccagnella

Co-supervisor: Dr. Stefano Bonaldo

**Academic Year: 2021/22**

*To Greta and Alice,*
*don't be afraid to follow your dreams.*

**Abstract**

*Lactococcus Lactis* are among the most widely used lactic acid bacteria in the dairy industry. These micro-organisms catalyse the process of lactic fermentation, which is necessary to obtain products with desired characteristics. The presence of phages is one of the main causes of the failure of lactic fermentation and must be constantly monitored throughout the production process in order to avoid product wastage, delays in production with consequent environmental damage and economic repercussions. State-of-the-art techniques for detection of bacteriophages in milk have common disadvantages such as high cost, long detection time, need for trained personnel and specific equipments.

The aim of this thesis work is to develop an electrochemical biosensor capable of detecting the presence of *Lactococcus Lactis* bacteriophages, which is at the same time reliable, low cost, easy to use and portable. The device was characterised using electrochemical impedance spectroscopy (EIS), a technique that allows the monitoring and modelling of the electrode-solution interface. In parallel to the electrochemical measurements, the bacterial growth was tracked through optical absorbance measurements. The device was preliminarily tested with a milk-free solution with the goal of evaluating its stability, interchangeability and detection capability in ideal conditions. I developed an appropriate protocol called 'Spill-Out', which allowed me to detect the growth of *Lactococcus Lactis*. I detected the inhibition of bacterial growth due to the presence of phages in solution by evaluating the variation of the appropriate electrical parameters. After this preliminary characterisation, the device was tested in the presence of treated milk samples. I was able to measure electrically the inhibition of the growth of *L.Lactis*, induced by phages, in a solution that almost completely emulates a real milk sample.

# Contents

# Chapter 1

# Introduction

The goal of this thesis work is to develop an electrochemical biosensor capable to detect the presence of *Lactococcus Lactis* bacteriophages in milk samples. Biosensors represent one of the most innovative and successful areas of bioengineering. Technological advances in the field of biosensors have allowed the development of reliable, low-cost and portable devices with fast response times. Electrochemical biosensors based on screen-printed electrodes are one of the most promising technologies in the field of biosensor technology. They have all the above listed features and they can also be easily functionalized or modified according to analytical needs. The fields of application of this technology are very extensive, including healthcare, environmental applications and the food industry. Particularly in the dairy industry, it is crucial to monitor the product constantly, as any errors in the fermentation process could lead to low quality products, resulting in serious economic damage to the company. The presence of phages during production is one of the major problems for the dairy sector and prevents proper lactic fermentation, leading to product failure. Electrochemical biosensors represent a valid and economical alternative to the traditional techniques, in addition to the fact that their end use is designed for a non-specialist user.

In the first chapter, after a brief introduction of the basic biological aspects of *Lactococcus Lactis* and its bacteriophages, I describe the detection techniques currently in use, specifying the various advantages and disadvantages of each methodology.

Finally, I discuss how the use of electrochemical biosensors could be a possible solution to the problem.

The second chapter introduces the physico-chemical principles on which electrochemical biosensors are based, such as conduction in the material, the definition of the interface and the concept of the electrochemical cell. Then, I illustrate various measurement techniques used to characterize electrochemical cells.

The third chapter focuses on the first experimental tests carried out for an initial characterisation of the device. First, I present the experimental set-up, including the solutions, the software and the instrumentation used. Then, I explain the reasons why I chose a specific sensor produced by Metrohm DropSense called DRP-C223AT. I report the results of my test on stability over time, interchangeability and the ability to detect Lactis in solution, all of which are fundamental features for my purpose. Finally, I present the experimental results obtained by adding phages, verifying that my device is able to detect bacterial growth inhibition caused by phages.

In the fourth chapter, I report the results of experimental tests carried out with milk samples added in solution. First of all, I show the response of the sensor with the addition of milk in solution. Then, I present the experimental results of tests carried out with the addition of biological material (*Lactococcus Lactis* and phages) in a solution with milk that emulates a real sample.

In the final chapter, I discuss the obtained results and propose possible future experimental steps of validation and optimisation, necessary to lead to the commercial development of the biosensor.

This work has been carried out with the collaboration of ARC-Applied Research Centre s.r.l., Padova.

# Chapter 2

# Bacteriophages and dairy products

## 2.1 Lactic acid bacteria (LAB)

Food fermentation was the first biotechnological technique used by man. This process may have been a consequence of accidental contamination by environmental microorganisms, which would have caused an alteration of the raw material. In the case of milk, this contamination by lactic acid bacteria (LAB) resulted in products with an acceptable final taste, consistency and, above all, that could be stored for longer periods of time. In fact, LAB can convert lactose into lactic acid and consequently cause a decrease in pH that inhibits the growth of pathogens. Generally, LAB is Gram-positive, they growth in anaerobic conditions and do not form spores. Since the early 21st century, genomic data from more than 200 LAB strains has been collected in different public databases [1]. Comparative genomic analysis has revealed a large diversity among the LAB, which is attributed to their varying interactions with the environmental [2], [3]. Based on their metabolic activity, LAB can be divided into three groups:

1. Obligate homofermentative: they degrade glucose by the process of glycolysis. Pyruvate is then reduced to lactic acid, yielding two moluceles of ATP from a single molecule of glucose. Typical LAB of this group are *Lactobacillus*, *Enterococcus*, *Streptococcus* and *Pediococcus*.

2. Obligate heterofermentative: they cannot degrade glucose by glycolysis because they lack the enzyme 1,6-diphosphate aldolysis. They therefore degrade glucose via the pentose phosphate pathway, resulting in three equimolar products: lactic acid, ethanol and carbon dioxide.

3. Facultative heterofermentative: in presence of pentose, they use via the pentose phosphate pathway like an obbligate heterofementative. Alternatively, they can perform glycolysis, behaving as homofermentates.

### 2.1.1 *Lactococcus Lactis*

*Lactococcus Lactis* are used extensively in the production of buttermilk and cheese. They can't move autonomously, have spherical shape about 0.5/1.5um in size. They can grow at 10°C but not at 45°C (mesophilic) and usually tens to cluster in short chains. As reported in a review published by M.Wels et al.: "The industrial importance of *L. lactis* is demonstrated by a global cheese production of close to $2x10^7$ tons in 2015 (Bulletin of the International Dairy Federation 2016), and based on that we estimate that over $10^{20}$ lactococci are being consumed by humans annually" [4]. Their metabolism is homofermented with the production of L(+) lactic acid, but the production of D(-) lactic acid has sometimes been observed in an acidic environment.

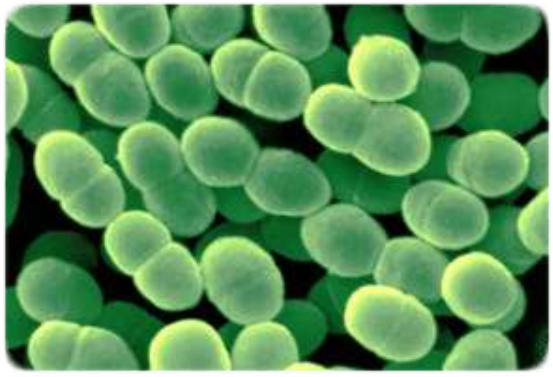

Figure 2.1: *Lactococcus Lactis* cells.

## 2.2 Bacteriophages

The success or failure of the fermentation process is closely dependent on the growth of LAB. This growth can be delayed or inhibited by many external factors, causing problems with the quality of production and consequent economic repercussions. The main cause of lactic fermentation failure is the presence of bacteriophages. Bacteriophages are viruses that infect bacterial cells, using their biosynthetic apparatus to carry out replication, causing lysis of the bacterium-infected [5].

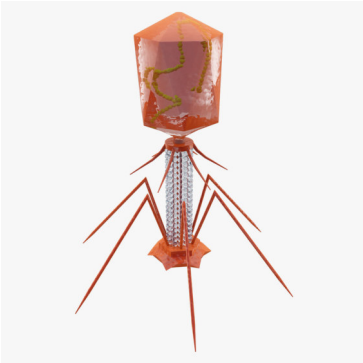

Figure 2.2: Typical structure of a bacteriophage.

Phage attack has always been the main problem for industrial milk fermentations and it has remained the major cause of fermentation failure. From first time that milk phages was isolated in 1935 onwards, the researchers isolated specific phages of all lactic bacteria species used by the industry: *Lactococcus*, which is widely used in the world; *Streptococcus termophilus*, *Leuconostoc*, the main bacteria for the production of blue cheese, butter and cream; and *Lactobacillus*, groups with highest number and diversity of species.

The bacteriophage infection of starter bacteria results in the slow production of lactic acid with the result of unacceptably long times of fermentation and, in extreme cases, may lead to loss of the product. The conditions prevailing in these industrial environments represent unique ecological niches that support phage proliferation. As previusly mentionated, phages is the main cause of economical loss in dairy industry; it is estimated that around 10% of production failures are due

to the presence of phages [6].

*Lactococcus Lactis* is the most used starter culture in the diary fermentation sector, and phages infecting this industrially significant species are probably the most studied group of Gram-positive infecting phages. These phages can be divided into ten groups, but three are the most encountered in diary industry: 936, C2 and P335 group. However, while lactococcal strain diversity may be limited, their infecting phages have proven to co-evolve with their hosts and resident prophages by genomic rearrangements. This coevolution is the driving force supporting the ever-increasing genetic diversity of lactococcal phages within 936 and P335 groups. As pointed out in the article "*Bacteriophages of lactic acid bacteria and their impact on milk fermentations*" written by J.Garneau and S.Moineau, *Lactococcal* and *Streptococcal* phages have been detected in 37% of the milk samples used for yogurt production in Spain [7].

There may be several sources of contamination, but the most important is certainly the milk itself. Phages can easily enter production processes and rapidly accumulate during formation. Phages can reach the raw material through external routes such as brine, ambient air, equipment or starter cultures. Other important sources of contamination are production residues. In a situation of poor hygiene, they can move into the environment through small droplets in the air (areosols). Whey is the largest source of phages in the dairy industry, as bacteria continue to grow in the whey even after it has been separated from the curds, and as a result of bacterial growth, phage growth occurs. Whey protein is often reused in the dairy industry, but if not well controlled it can be a major source of phage contamination.

Ideally, no phages should be present in a diary plant, but this condition is unrealistic in a milk sample. It is generally accepted as safe environment if phages are present at levels lower than $10^5 PFU mL^{-1}$. If they are present in milk at this level or greater, an inhibition, or even total failure, of the fermentation process is expected[8].

## 2.3 Phages detection methods

To ensure successful production, it is necessary to monitor the quantity of phages present in the milk sample and ensure that the critical threshold is never exceeded. An ideal detection system must have: high sensitivity, rapid response, high reliability and be as automated as possible [8]. But the techniques currently used to detect phage presence in milk do not have all the features outlined above. Detection techniques can be divided into two main strategies: microbiological analysis, based on direct visualisation of the virus; and molecular techniques, which demonstrate the presence or absence of specific viral components, such as genomic DNA or the protein envelope.

### 2.3.1 Molecular techniques

The main advantage of molecular technologies is quick detection and high specificity. However, they have the major limitation of not discriminating between infectious and inactivated phages, leading to an overestimation of the number of phages counted. The most commonly used detection techniques will be briefly described below:

#### Test ELISA

The ELISA test is based on the use of antibodies labelled with an enzyme, so that the resulting conjugates have both immunological and enzymatic activity. The antigen-antibody reaction is immobilised on the plate and can therefore easily be detected by the addition of the substrate, which reacts with the enzyme to produce a visually observable and quantifiable colour. There are three different applications methodologies [9]:

- Direct test: the antigen is adhered to the base of the solid support and its presence can be detected through the use of an antibody labelled with an enzyme which, when reacted with a specific substrate, allows the observation of a complex that will generate a coloration.
- Sandwich methods: In this case there is a specific antibody fixed on the substrate, the sample is added to test or not the presence of the antigen.

Then a secondary antigen-specific antibody is added, conjugated to a specific enzyme. If the antigen is present, the antibody will selectively bind to the antibody-antigen complex, forming a triple sandwich-like layer.

- Indirect test: The procedure involves the use of a labelled secondary antibody that is able to recognise the constant region of the primary antibody, previously incubated in the solid phase.

This technique has a good response time (4-5 h) but has a detection limit two orders of magnitude higher than the standard $10^5 \frac{pfu}{mL}$, not guaranteeing sufficient sensitivity.

### PCR

PCR is a technique that allows a specific DNA sequence to be amplified exponentially. [5]. Conceived in the 1980s by K. Mullis, this technique revolutionised many fields of research in the years that followed, finding numerous fields of application, including the dairy sector. The technique is based on a series of cyclic steps:

1. DNA strands are separated into individual strands by heating (denaturation process at 90°C).

2. A specific artificially synthesised primer (15-20 bases) complementary to a specific base sequence of the target strand is added in solution.

3. The addition of the DNA polymerase, starting with the primer, catalyses the production of the complementary strand. Taq-Polymerases are used, special polymerases obtained from thermophilic bacteria, which are therefore able to resist the high temperatures of the denaturation process.

This technique can be applied at different stages of dairy production to identify viruses and bacteria. A major limitation of this technique is that it does not allow discrimination between infectious and non-infectious phages, thus giving rise to a large number of false positives. A large number of samples can be identified in a short time with a sensitivity of $10^3/10^4 \frac{pfu}{mL}$.

#### RT-qPCR

With conventional PCR, it is not possible to specifically quantify the number of target sequences. RT-qPCR couples PCR with the use of fluorescent molecules. These molecules create a light that is detected by a sensing system, and based on the intensity of the light signal it is possible to estimate the number of phages present in the sample. This technology has shown remarkable sensitivity and specificity combined with a significant reduction in application time. With this technique it is possible to detect, quantify and classify phages in less than 30 minutes, without the need for prior sample preparation, making it suitable for routine use. In addition, the availability of various fluorescent dyes and the possibility of combining them allows the system to be extended for the simultaneous detection of multiple phage species [10]. Nevertheless, this is an expensive technique, requires specific instrumentation and trained personnel.

### 2.3.2 Microbiological analysis

#### Spot Test

These tests are based on inhibition of bacterial growth. The milk sample is collected and dissolved in a medium, then centrifuged and filtered to remove residual bacterial cells. A drop of solution is then taken and incubated under optimal growth conditions. If plaques are seen after the incubation time, this indicates the presence of phages in the sample. To ensure that no other inhibiting agents are present, serial dilutions are performed. This test is accurate, sensitive and allows us to have a quantitative analysis. Nevertheless, it takes a long time to perform, from a few hours to several days, depending on the interaction between bacteria and phages. In addition, it requires trained personnel and specific laboratory equipment, conditions that are rarely present on site.

### Electron Microscopy

In certain cases, many different bacterial strains are involved in fermentation processes, making phage identification difficult. In these cases, direct observation of a sample with electron microscopy is necessary. This technique is difficult to implement in routine analysis, because requires specific sample preparation, technical skills and experienced personnel. Electron Microscopy is only used in research and not in the dairy industry.

### Flow Cytomtric Detection

Flow Cytometry is a tecnique that for mesasuring and characterising cells suspended in a fluid medium. The cells in solution are injected into a microfluidic system which enables the cells to be organised in an ordely, constant and continuos flow. This process is called hydrodynamic focusing. Every single cell is crossed by a beam of ligth which excites the fluorochromes and results in the emmission of a fluorecent signal. The signals are colleted and sent to specific sensors who meausure the ligth intensity. The electrical signals coming from each sensor are amplified, digitized and then sent to a data analyser. It is possible to detect the presence of bacteriophages as this has a direct effect on the properties of the cell membrane. In fact, the infection causes a marked decrease of cellular membrane density, as observed in *L.Lactis* by Michelsen et.al also of 50% [11]. The method allows fast and early detection of phage-infected bacteria, independently of which phage has infected the culture. In addition, it can be performed in real time and therefore increases the chance of successful intervention in the fermentation process. The main disadvantages of this methodology are the high cost and the need of trained personnel.

### Optical Absorbance Spectroscopy

These techniques are based on the detection of bacterial lysis, an effect closely linked to the presence or absence of phages in the sample of interest. The variation of absorbance over time is monitored and compared to a control sample in which no phages are present. The control group, as time progresses, get higher absorbance values than in the sample containing the phages. These measurements are carried out using an instrument called spectrophotometer. The principle on which it is based is that each molecule absorbs, transmits or reflects light at a certain wavelength $\lambda$. By using different wavelengths, it is possible to detect the presence of a certain substance in the sample. This instrument allows the concentration of a substance to be determined by analysing the difference in light intensity between the light before and after passing through the sample. The physical law behind this detection system is the Lambert-Beer law [12], which allows us to calculate the ratio between the intensity of light before and after passing through a sample, $I_0$ and $I_d$ respectivily:

$$\frac{I_d}{I_0} = e^{\epsilon(\lambda)cd} \tag{2.1}$$

where $\epsilon$ is molar attenuation coefficient $\lambda$-dependent, $c$ is substance concentration and $d$ optical path. Absorbance $A$ is definited as natural logarithm of the ratio between $I_0$ and $I_d$:

$$A = \ln \frac{I_0}{I_d} \tag{2.2}$$

Taking 2.1 and combining $\epsilon$ and $d$ in a single parameter $K$, we obtain:

$$A = Kc \tag{2.3}$$

There is a direct proportionality between the absorbance, at a specificity wavelength, and the concentration of the substance. Usually, spectrophotometer contains a light source, the light is selected at a specific wavelength by a monochromator. The light, after passing through the cuvette, is detected by a photodetector. The signal obtained is processed through appropriate software.
These tests are very sensitive but have two major disadvantages: the presence of other inhibitory substances that could give false positives; they give long response

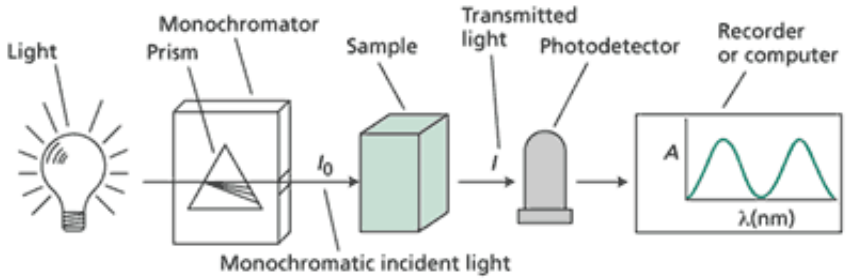


Figure 2.3: Example of spectrophotometer operation.

times ranging from 8 to 24 hours. In addition, culture maintenance and sample preparation require an operator with technical skills and laboratory equipment, resources that are often not available in a dairy industry.

## 2.4 New approach: electrochemical biosensing

In summary, the main problems with the systems currently used for phages detection in the dairy industry are:

1. Time issues: the tests presented give answers in too long a time, the possibly contaminated product may have already failed fermentation;
2. A microbiology laboratory is required, control can not be carried out on site;
3. Trained personnel are needed.

A possible solution could be electrochemical analysis techniques. These techniques can be considered as a kind of advanced version of optical absorbance spetroscopy. In fact, the presence or absence of phages is measured in relation to the change of appropriate electrical parameters, with respect to a sample tester.

New technologies in the field of electrochemical biosensors, in particular the development of thick film sensors, are ideal for the construction of a reliable, at the same time portable and user-friendly sensing system. These devices are manufactured using a simple process called screen printing technology. Using cut-out frames, it is possible to print on electrodes of any shape and size. Depending on the analytical

requirements, these devices can easily be customised with nanoparticles but also with real biological material such as enzymes, antibodies or nucleic acids, thus making them usable in many fields of application [13].

In literature, there are many examples of electrochemical biosensors, developed by different material and technologies, used in diary sector. Different type of this sensors are developed for monitoring the presence of lactate in milk, that is a specific indicator of the presence of bacterial fermentation, thus as an indicator for the freshness and quality of the product [14]. Other work is carried out for example to determinating the quantity of antibiotic in milk [15] or for revelation of *Salmonella* Typhimurium infection [16]. Thanks is hightly selectivity, bacteriophages was largely used for develope biosensors. Several examples are reported in the article *"Bacteriophage Based Biosensors: Trends, Outcomes and Challenges"* [17] written by Zahra Aliakbar Ahovan and his gruoup.

While if there is an extensive range of biosensor using phages as sensing element, there is not a large development of electrochemical biosensors for bacteriophage detection, especially for milk analysis and more in general for direct dairy application. A first example of this type of application is presented in the article *"On-chip impedimetric detection of bacteriophages in dairy samples"* [18] pubblished by C.Garcìa-Aljaro, X.Munoz-Berbel and F.J. Munoz. They developed an electrochemical device based on the formation of bacterial biofilm on a screen-printed electrode surface. The presence of the phages in solution causes lysis of the bacteria deposited on the surface, which leads to a change in the electrical properties of the system. They obtained a device capable of detecting the presence of bacteriophages in aqueous solution (milk and PBS).

Another example of this type of biosensor is presented in the article *"Inkjet Printed Interdigitated Biosensor for Easy and Rapid Detection of Bacteriophage Contamination: A Preliminary Study for Milk Processing Control Applications"* pubblished by the group of G.Rosati [15]. They were able to develop a specific device, capable of detecting *L.Lactis* phages, based on interdigitated electrode manufactured by inkjet tecnology. The working principle is different from that presented in the

previous article. In this case, there is not the formation of biofilm, but bacteria in the solution settle on the electrode by sedimentation, causing a change in the electrical properties of the system. Phage presence in solution lead to lysis of the bacteria, changing the electrical properties of the system comparated to a sample solution without phages. The system was tested in parallel with the traditionaly tecniques (plaque assay and turbinimetry) and proved to be sensitive and with good response time (3 hours from phage inoculation).

Based on the same working principle as the latter article, this thesis attempts to develop an electrochemical biosensor for the detection of *L.Lactis* phage that can overcome the limitations of traditional techniques. Before illustrating the materials, the strumentation and obtained data, it is neccesary to define some fundamental points such as the definition of a biosensor, the concept of electrochemical cell and the describing electrochemical measurements tecniques used for phage detection.

# Chapter 3

# Electrochemical Biosensors

A sensor is a device that measures physical input from its environment and converts it into data that can be interpreted by either a human or a machine. Most sensors are electronic (the data is converted into electronic data), but some are more simple, such as a glass thermometer, which presents visual data. People use sensors to measure temperature, gauge distance, detect smoke, regulate pressure and a myriad of other uses. With the development of microelectronics, sensors have invaded every field of technology and are now an integral part of everyday life, e.g. the most common smartphones are also equipped with more and more sensors. In addition to the already mentioned applications, sensors are widely used in the mechanical and robotic industry, in medicine, in the agri-food sector and in general wherever automation systems are needed. Conventionally, sensors can be divided into three macro-categories:

- Physical sensors: they measure distance, mass, temperature, pressure, current, voltage, impedance, light, etc.
- Chemical sensors: they measure chemical substances by chemical or physical responses
- Biosensor: they measure chemical substances by using a biological sensing element.

Today, biosensors represent one of the most interesting areas of bioengineering. Research on the development and application of biosensors is carried out by many international groups following different paths and approaches. The main feature of a biosensor is the presence of a sensitive biological element such as an enzyme, various enzymes, antibodies, components of natural or artificial biological membranes, bacteria, cells, living animal or plant tissue. These systems interact with the substrate to be measured and are responsible for the specificity of the sensor. The biosensor requires a transducer, i.e. an element capable of converting the quantity detected by the sensing element into a measurable quantity, such as an electrical signal.

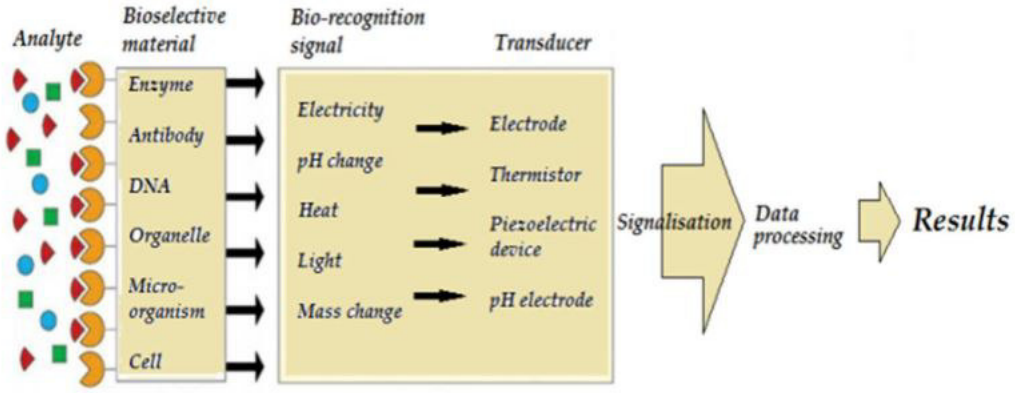


Figure 3.1: Illustration of typical biosensor components.

The birth of biosensors dates back to the early 1960s when Clark and Lyons (1962) developed a device by coupling an enzyme to an electrode. A few years later, Updike and Hicks (1967) developed the first enzyme using glucose oxidase immobilised on a gel and placed on an electrochemical sensor [19]. This sensor was used to measure the concentration of glucose in biological solutions. Rapid technological progress, together with the growing popularity of point of care diagnostics and the expansion of the application areas in the field of biomedical sciences, are among the major factors driving the growth of the global biosensors market. Taking advantage of interdisciplinary approaches from chemistry, electronics, medical science and nanotechnology, biosensors have rapidly paved their way into the biomedical field.

The performance of a bionsensor must be evaluated in terms of [9]:

1. Selectivity: is the ability to discriminate between different analytes.
2. Sensitivity: is the minimal detectable analyte concentration change
3. Precision: Is the degree to which repeated measurementes uder unchanged conditions show the same to the quantity's true value.
4. Accuracy: is the degreee of closensess of measurementes of a quantity to the quantity's true value.
5. Time influence: (i) Response time, time needed by the sensor to produce a stable response; (ii) Recovery time, time that elapses after a measurement before the sensor is ready to analyze the next sample ; (iii) Working lifetime, Time during which the sensor can be used maintaining its characteristics.
6. Operatibility: ability to work under different measurement conditions

Depending on the type of transducer, biosensors can be divided into several categories such as: electrochemical transducers; optical transducers; piezo-electric transducers and thermal transducers. Electrochemical biosensors represented more than 65% of the global market in 2016 [9].These provide better guarantees for analytical applications in terms of sensitivity, reproducibility and selectivity. An electrochemical biosensor generally consists of an electrical signal transducer called electrode.

The operating principle of such a sensor is as follows: a chemical species reacts with the biological element bonded to the surface of the electrode. The product of this reaction is an electroactive element which diffuses on the surface of the electrode and generates an electrical signal which is detected by an instrument and related to the concentration of the metabolite under examination. Electrochemical sensors are based on contact phenomena between a conducting electrode and a conducting liquid solution. The region of discontinuity between the two phases is called the interface, and it constitutes a region of discontinuity in the physical and chemical properties of the system.

Following this briefy introduction, the physical models used to describe conduction in metals and solutions will be explained. Subsequently, the various models that have been used over the years to describe the solid-liquid interface will be briefly presented, arriving at the model currently used, the BDM model. In the last part of the chapter, various measurement techniques used in electrochemical biosensors will be explained.

## 3.1 Electrochemical Interface

Interphase is the contact region between two regions with two different phases. Molecules in the region adjacent to the interface are contained in a region called interphase, they undergo physico-chemical interactions that are no longer balanced in all directions. Although it is small in size compared to the volumes of the two adjacent phases, the interface plays a decisive role in stabilising, creating and controlling the physico-chemical properties of many systems. The constituent particles of the two phases very often have electrical properties. The condition of heterogeneity and anisotropy in the interphase causes electrification, a phenomenon due to an excess of electric charges of opposite values from different sides of the interface. Electrical conductors are divided into two species, depending on the type of mobile charge carried:

- Electronic conductors, where the mobile charges are electrons. This species includes metals, semiconductors and some carbon compounds.
- Ionic conductors, where the mobile electrical charges are ions. To this species belong electrolic solutions, ionic cirstalls and fused electrolytes.

### 3.1.1 Electronic conductors

Conduction in electronic conductors is theorised quantum-mechanically using the so-called band theory. This theory allows us to understand the electrical properties of matter, explaining the properties of conductors, semiconductors and insulators. In conductors, the valence electrons are shared throughout the entire lattice, so

the orbitals occupied are diffused around the entire solid and not just around the individual atom. The outer orbital, which contains the valence electrons, gives rise to two energy bands: the low-energy valence band and the higher-energy conduction band, so there is no charge transport. In conductors, the valence band is partially overlapped by the conduction band, so that a valence electron can easily jump from one band to the other. However, in order for this jump to be possible, an external electric field must be applied to provide the necessary energy for the electron to make the energy jump. As regards insulating materials, the energy distance between the two bands is too great to allow the promotion of an electron from the valence band to the conduction band. Semiconductors have a completely full valence band and an empty conduction band, as in the case of insulating materials. However, the energy gap between the two bands is not so great: it is possible to provide the energy for an electron to be promoted from the valence band to the conduction band. When an electron is promoted in the conduction band, it leaves an empty electronic state in the valence band. This empty state is called hole and has its own electrical properties. In the presence of an electric field, hole exhibits a behaviour similar to that of a positive charge. Electrons in the conduction band and the holes in the valence band both contribute to electrical conduction, acting as charge carriers: the electrons carrying negative charge towards the end at positive electrical potential, the holes in the opposite direction.

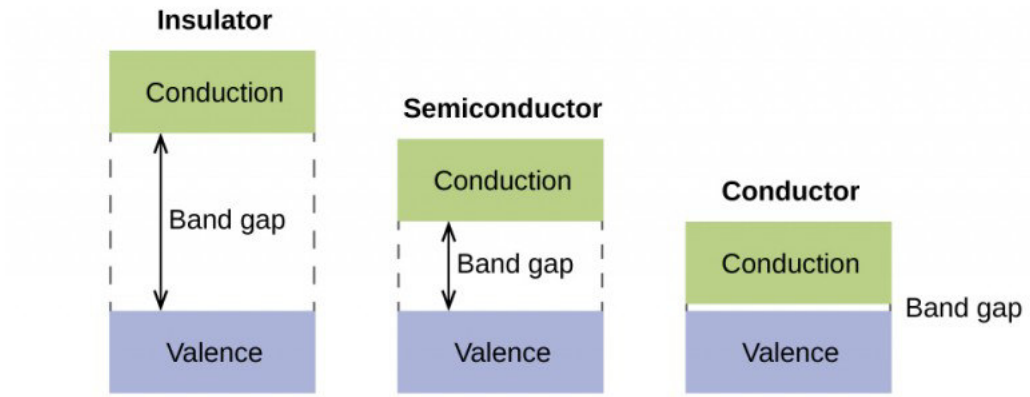


Figure 3.2: Representation of valence and conduction bands in different types of materials.

### 3.1.2 Ionic Conductors

Ionic conductors are materials in where charge transport is associated with ion transport. As previously explained, there are various type of this material, but for biosensor applications electrolytic solutions are of most interest. The main component of an electrolytic solution is the solvent. Solvents can be classified as: ionic solvent, consisting of species completely dissociated into ions; molecular solvent consisting of molecules and behaving as an insulator. In general, an electrolytic solution consists of a molecular solvent and the ions dissolved in it, with a conductivity that depends on the concentration of the electrolyte(s) dissolved in the solvent. The solvent-solute interaction is generally called solvation. This process induces the formation of solvation spheres around the ions of the electrolyte. The condution process in a solution depends on the:

- Electric field (which causes drift);
- Concentration gradient (which causes diffusion);
- Temperature gradient (which causes convection).

Through the Nernst-Planck equation it is possible to describe the solute flow $J$ (along the x-axis) as a function of the contributions just described:

$$J = -D\frac{dc}{dx} - \frac{zF}{RT}Dc\frac{d\Phi}{dx} + cv \tag{3.1}$$

where: D solute diffusion coefficient; c solute concentration, z charge stae, $\Phi$ eletric potential; v= speed of the solution (along x-axis); Faraday constant $F = 96485.3365\frac{C}{mol}$; Gas costant $R = 8.314472\frac{J}{mol}K$.

The conductivity of an electrolyte solution is a measure of its ability to conduct electricity. This parameter depends on the concentration of the electrolyte at a given temperature. It is convenient introduce a new term called molar conductivity:

$$\Lambda_m = \frac{k}{C} \tag{3.2}$$

where $k$ and $c$ are respectively the conductivity and the concentration. A clear difference can be seen between weak and strong electrolytes, as the latter are prac-

tically 100% dissociated in solution even at not very low concentrations, while weak electrolytes are only slightly dissociated into ions, and the less so the more concentrated the solution. Dilution of solutions causes an increase in the conductivity of solutions of strong electrolytes due to a decrease in the interaction between the ions, and an even greater increase for weak electrolytes, due to the shift in the equilibrium of dissociation towards ion formation. In all cases, therefore, $\Lambda_m$ tends to a limiting value, which is given the name of equivalent conductivity at infinite dilution, $\Lambda_o$. By examining the values of this parameter for various electrolytes, Kohlrausch formulated the law of independent ion migration, according to which the equivalent conductivity at infinite dilution of any one electrolyte is given by the sum of the limiting equivalent conductivities of the individual ions:

$$\Lambda_m^o = v_+\Lambda_+ + v_+\Lambda_+ \tag{3.3}$$

where $v_+$ and $v_-$ are the number of moles of cations and anions, respectively, which are created from the dissociation of 1 mole of the dissolved electrolyte; $\Lambda_+$ and $\Lambda_-$ are the limiting molar conductivities of the individual ions. Debye and Huckel developed a theory through which singe ion activity coefficients could be calculated, where the solute is completely dissociated as it is a strong electrolyte. The ions are considered not polarized spheres, each ion is surrounded more closely by ions of opposite charge than by ions of like charge. Using these assumptions they were able to calculate the average electric potential on each ion generated by the presence of other ions[20]. Onsarger later modified the theory by introducing the distortion of spherical symmetry caused by the electric field. Considering this effect and the effect of viscosity, Onsager formulated an expression for the calculation of molar conductance.

$$\Lambda_m = \Lambda_m^0 - (A + B\Lambda_m^0)c^{1/2} \tag{3.4}$$

where A and B are constants that depend only on known quantities, suchs as temperature, the charges of the ions, dieletric constat and viscosity of the solvent. Weak electrolytes are never fully dissociated. There is no limit of dilution below which the relationship between conductivity and concentration becomes linear.

## 3.2 Models of the electrode-solution interface

Once two phases come into contact takes place the interphase electrification. This phenomenon is of enormous importance in all electrochemical phenomena: from ATP production, to electrosynthesis, to the functioning of the membrane potential. The electrified interface has attracted great interest from the scientific community. Over the years, a number of increasingly complex models have been developed to enable the physical description of the electrochemical interface.

### Helmotz model

The first model to address the charge distribution on the electrode was theorised by Helmotz in 1853. This model involves two parallel charge planes of different polarity: one plane at the conductive interface of the electrode and the other located in the axis passing through the centre of the ionic conductors. The imaginary line through the ion centres defines the boundary known as the Outer Helmotz Plane (OHP). The region within this plane is called the Helmotz double layer, or, more simply, the double layer.

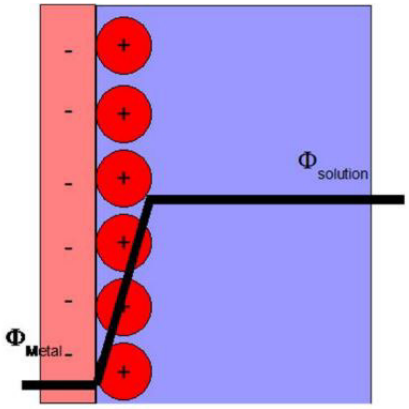


Figure 3.3: Helmotz model.

The model can be schematized as a parallel-faced capacitor with a capacitance depending only on the dielectric constant of the ionic conductor and the thickness of the double layer. However, this model is oversimplified, as it does not take into

account that the capacitance depends on several quantities such as the potential $V$, the temperature $T$ and the concentration of the ions in solution $c$.

## Gouy-Chapman model

In order to overcome the limitations of Helmotz's model, in particular the dependence of the capacitance on other parameters, Gouy-Chapman introduced a new description of the interface. In this model, a double layer is not considered, but a region of distributed charge (diffusive double layer) is theorised. It is therefore assumed that the electric potential in the double layer has an exponential trend. In this model the capacitance $C_d$ depends from V,T and c but some limits still remain, since the ions are considered points and the dissuse layer is considered to start form x=0, which make the model failing for highly charged double layers.

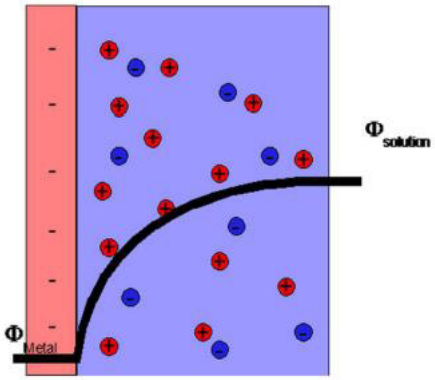


Figure 3.4: Gouy-Chapman model.

## Stern model

The Stern model, introduced in 1924, combines the two models described above. In fact, it assumes that some ions can be adsorbed on the electrode, as assumed by Helmotz, thus defining the so-called internal Stern Layer. Outside the Stern layer there is a diffusive layer, analogous to the Gouy-Chapman model. The electrical equivalent is represented by two capacitances in series.

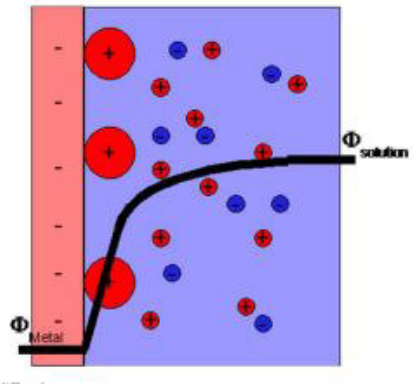


Figure 3.5: Stern model.

Stern model, however, does not take into account the presence of the ion hydration spheres, which are modelled as charged points. Also, the model assumes constant electrical permittivity and viscosity.

## Grahame model

In 1947, Grahame modified Stern's model by introducing a triple-layer model. The Stern layer is divided into two parts: Inner Helmotz Plane (IHP) and Outer Helmotz Plane (OHP). The first plane (IHP) contains the ions adsorbed on the electrode, while the OHP contains the solvated ions, surrounded by the hydration spheres, at the shortest distance from the electrode, but without touching it. Beyond the OHP plane we have the diffuse layer.

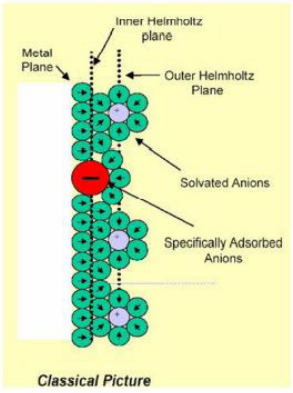


Figure 3.6: Grahame model.

## BDM model

Introduced in 1963 by Bockris, Devanthan and Muller, this model includes the action of the solvent at the electrode interface. They suggested that the attachment of solvent molecules may have a fixed alignment on the electrode surface. The layer of molecules has a great influence on the orientation of the electric field. This orientation has a great influence on the permittivity of the solvent, which varies with the strength of the field. Some of these molecules can be replaced by adsorbed ions. The IHP passes through the centers of these molecules. Specifically adsorbed, partially solvated ions appear in this layer. The solvated ions of the electrolyte are outside the IHP. The OHP pass through the centers of these ions. The diffuse layer is the region beyond the OHP. The BDM model actually more commonly used.

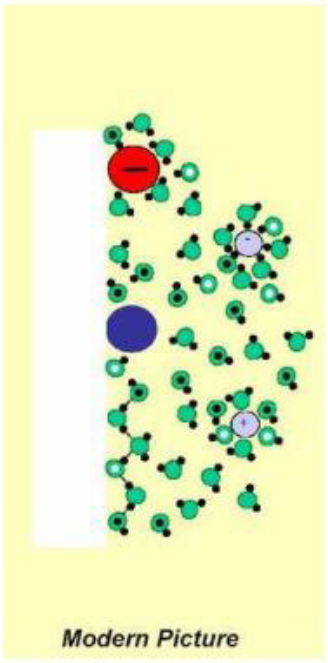


Figure 3.7: BDM model.

## 3.3 Electrodes and electrochemical cell

As already explained, when a piece of metal is placed in a solution containing ions, a charge separation takes place at the interface between the metal and the solution. This configuration is called an "electrode" and its fundamental characteristic, in addition to the aforementioned interphase electrification, is the transfer of charge by means of oxidoreductive processes. The potential of the electrode cannot be measured directly but requires connection to another electrode-electrolyte combination, thus forming the so-called electrochemical cell. The two half-cells must be connected by a conductive bridge or membrane. An electrical circuit is thus formed and the electromotive force of the cell can be measured as the difference between the electrode potentials in the two half-cells.

A typical example of an electrochemical cell is Daniel's cell. The two half-cells consist of copper and zinc electrodes placed in solutions containing respectively $CuSO_4$ and $ZnSO_4$. The two half-cells are joined by a salt bridge, i.e. a bridge containing an inert electrolyte like $NH_4NO_3$. The electrodes are joined by a wire, electrons flow from the zinc electrode to the copper electrode. At the same time, zinc is dissolved in the respective compartment, forming $Zn^{2+}$ ions, and $Cu^{2+}$ ions are transformed into metallic copper on the other electrode. The zinc electrode on which oxidation (loss of electrons) occurs is called the anode, while the copper electrode on which reduction (gain of electrons) occurs is called the cathode. This reaction can be expressed in terms of two half-cell reactions occurring at the electrodes:

$$\text{Anode: } Zn(s) \longrightarrow Zn^{2+}(aq) + 2e^-$$
$$\text{Cathode: } Cu^{2+}(aq) + 2e^- \longrightarrow Cu(s)$$

If we connect a voltmeter between the two cells, we measure an electromotive force between the two cells E=1.104 V (room temperature and equal ion concentrations). In generalized form, the equation of rection is:

$$Zn(s) + Cu^{2+}(aq) \longrightarrow Zn^{2+}(aq) + Cu(s) \tag{3.5}$$

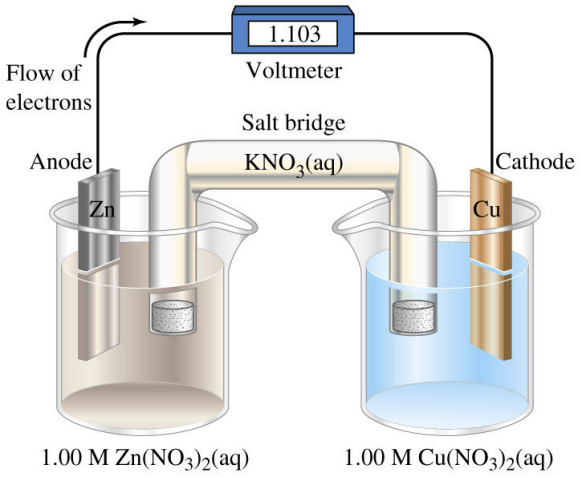


Figure 3.8: Illustration of Daniel's cell.

It is impossible to measure the potential of a single electrode, so a circuit composed by two electrodes is necessary to record an electromotive force. By convention, the potential of all electrodes is measured with respect to the standard hydrogen electrode or SHE. The potential of the SHE is conventionally set equal to zero, so the electromotive force measured will be the potential of the other electrode in the electrochemical cell. The Hydrogen electrode, however, is not very convenient for routine measurements as it involves hydrogen gas which is potentially explosive. Other electrodes, which are easy to set up, non-polarisable and have little variation in coefficients with temperature, are used as reference. Two examples are the silver-silver chloride electrode (Ag/AgCl) or the saturated calome electrode.

The considerations made up to now included a strong assumption, in fact as we assumed the same concentration of reduced and oxidised species. The Nerst equation is a logarithmic relationship that links the $fem$ of an electrochemical cell to variables such as temperature and the concentrations of the regent species. Considering a generic half-cell reduction reaction of an oxidised metal:

$$Me^{n+} + ne^{-} \longrightarrow Me$$

We can associate a variation of Gibbs free energy:

$$\Delta G = \Delta G^o + RT \ln \frac{a_{Me}}{a_{Me^{n+}}} \tag{3.6}$$

Since the variation of Gibbs free energy can be expressed as $\Delta G = -nFE$ we obtain:

$$-nFE = -nFE^0 + RT \ln \frac{a_{Me}}{a_{Me^{n+}}} \tag{3.7}$$

through simple algebraic calculations we obtain:

$$E = E^0 + \frac{RT}{nF} \ln \frac{a_{Me^{n+}}}{a_{Me}} \tag{3.8}$$

which in generalised form corresponds to:

$$E = E^0 + \frac{RT}{nF} \ln \frac{a_{Ox}}{a_{Red}} \tag{3.9}$$

The ratio between the oxidation and reduction activities can be replaced, in the case of very dilute concentrations, by the respective concentration, obtaining the following equation:

$$E = E^0 + \frac{RT}{nF} \ln \frac{[OX]}{[R]} \tag{3.10}$$

It is possible to carry out a base change from the natural logarithm to the logarithm in base 10 through the following relation $\ln x = 2.303 \log x$. Supporting the ratio $\frac{RT}{nF}$ with the respective numerical values and considering that often the reduced species is a metal, which possesses activity equal to 1, the equation is simplified to:

$$E = E^0 + \frac{RT}{nF} 0.0591 \log_{10}[R] \tag{3.11}$$

Througth this equation is possible calculate electrode potential in different work condition.

Two different configurations are used to carry out electrical measurements on electrochemical cells, depending on the current range to be measured or the potential applied between the electrodes:

- Two-electrodes cell: the potential is imposed between a working and a reference electrode. Current flows through the cell and is measured between the two electrodes. This configuration is not recommended for measurements requiring high current or large potential variations.
- Three-electrodes cell: the potential is imposed between working and reference, but the current is read between working and a third electrode called counter.

## 3.4 Voltammetric techniques

Voltammetric techniques make it possible to measure the presence or absence of an active species based on the change of current. Usually, the variation of current is measured as a function of a voltage, this pattern can be rappresented by a graph called voltammogram. Because they involve a wide potential range, voltammetry measurements are carried out in a three-electrode configuration. The voltammetric measurement techniques partially used in this thesis work are now presented: the linear sweep voltammetry (LSV) and the cyclic voltammetry (CV).

### Linear sweep voltametry (LSV)

In linear sweep voltammetry, after fixing a potential range, the current is measured from the lower limit of the range to the upper limit. The measurements are strongly influenced by the ramp rate $v$, calculated as the slope of the line of potential change.

In the LSV measurements the current is shown as a function of the change in potential over time. As we can see from the figure 3.9, at very low voltage the current is also very low; in fact, for these values there are no redox reactions, only breakdown currents are recorded. As the potential increases, the charges are attracted and redox reactions take place at the electrode interface, which causes an increase in the measured current. The current increases rapidly until the peak current is reached. When the peak is reached, the current begins to decrease due to diffusion limitations. In the case of a reversible reaction, the pico current can

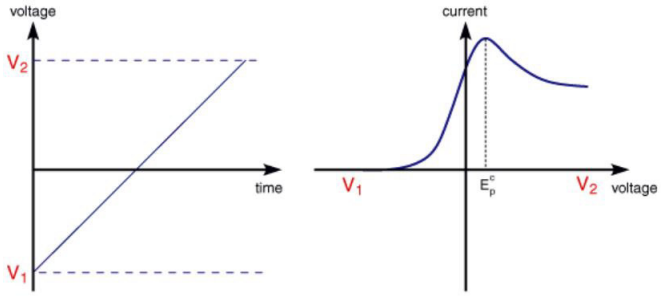


Figure 3.9: Example of LSV measurement: on the left, the potential ramp, on the right, the current as a function of voltage.

be calculated analytically using the Randles-Sevcik equation (in this case for the cathodic pico):

$$i_p = 2.686 * 10^5 n^{\frac{3}{2}} A D^{\frac{1}{2}} C_{Ox} v^{\frac{1}{2}} \tag{3.12}$$

Where n is the number of electrons transferred during the RedOx reaction, A is the electrode area, C the concentration (in this case of the oxidised species) and v the sweep rate. This last parameter, usually expressed in V/s, plays a fundamental role in determining the current. In fact, there is an increase in current as the sweep rate increases. However, the curves have a similar shape, the position of the pico does not change (figure 3.10).

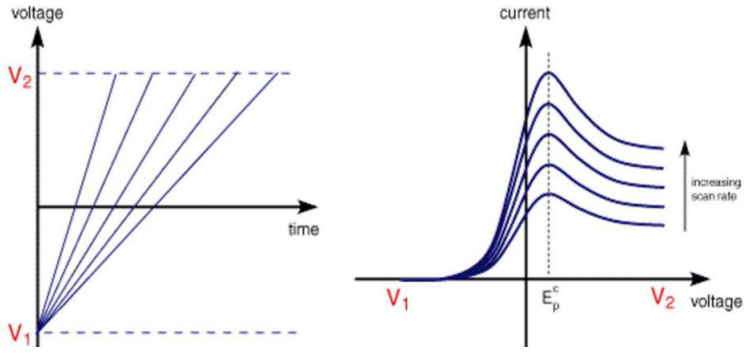


Figure 3.10: Effect of sweep rate variation on measurements.

## Cyclovoltammetry (CV)

Cyclovoltammetry is a potentiometric technique in which there is, as in LSV, a linear variation of voltage. In contrast to LSV, however, once the potential pico is reached, it is reversed back to its initial value. The anodic and cathodic peaks

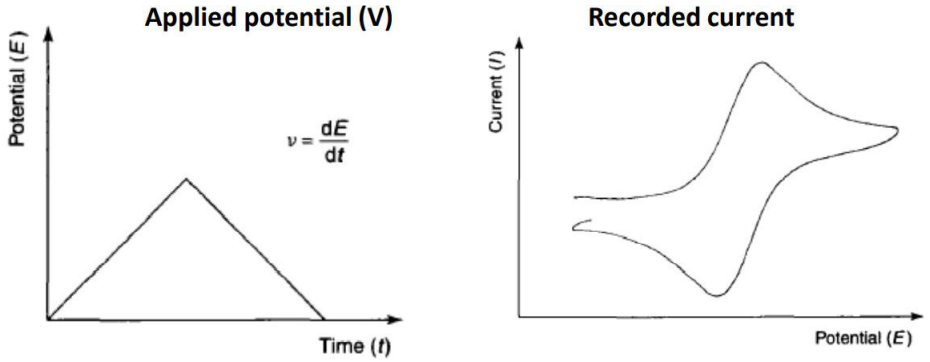


Figure 3.11: Example of CV measurement: on the left, the potential wave, on the right, the current as a function of voltage.

can be easily calculated through the Randles-Selvik equation:

$$i_p^{anode} = 2.686 * 10^5 n^{\frac{3}{2}} A D^{\frac{1}{2}} C_{Ox} v^{\frac{1}{2}} \tag{3.13}$$

$$i_p^{cathode} = 2.686 * 10^5 n^{\frac{3}{2}} A D^{\frac{1}{2}} C_{Ox} v^{\frac{1}{2}} \tag{3.14}$$

The significant parameters of a cyclovoltammetry experiment are the anodic peak currents $I_{pa}$ and cathodic peak currents $I_{ca}$ and their respective peak potentials $E_{pa}$ and $E_{pc}$. Through the CV is possible to calculate the standard redox potential, which is centred between the two peak potentials:

$$Eo = \frac{E_{pc} + E_{pa}}{2} \tag{3.15}$$

The shape of the CV curves, the current peaks and their respective potentials make it possible to state whether or not the process is reversible.

In fact, a process is reversible if the following conditions are verified:

1. The ratio of the modulus of the anodic peak to the cathodic peak is $\frac{|I_{pa}|}{I_{pc}} = 1$
2. The difference $\Delta E$, between the potentials of the two peaks, is: $\Delta E = \frac{0.056}{n}$ where n is the number of electrons transferred during the RedOx reaction.
3. The peak current is proportional to the square root of the scan rate: $i_p = cost(v)^{\frac{1}{2}}$

It must be remembered that the reversibility of the process depends not only on the RedOx reaction, but also on the experimental conditions and the type of electrode used.

## 3.5 Electrochemical Impedance Spectroscopy

Impedance techniques are used to monitor surface properties and changes by measuring the impedance between the electrode and solution. Ohm's law defines resistance in terms of the ratio between voltage and current: $R = \frac{E(t)}{I(t)}$.
Experimentally, circuit elements exhibit much more complex behaviour than simple ohmic behaviour. I have to introduce the concept of impedance $Z$ defined as the ability to resist the current flow after the application of an external bias.

The main impedance technique is called Electrochemical Impedance Spectrospy (EIS), it is a non-perturbative technique and allows time-dipendent information about the process in progress to be obtained. In recent years, EIS has found a lot of applications in the field of characterization of materials. It is routinely used in the characterization of coatings, batteries, fuel cells, and corrosion phenomena. It has also been used extensively as a tool for investigating mechanisms in electrodeposition, electrodissolution, passivity, and corrosion studies. In the biological field, EIS is widely used, some examples of applications include antibody-antigen association study, tuberculosis diagnosis or study of tissue structure for cancer detection [21]. In addition, EIS has been used to analyse and characterise different foods in the agri-food industry. In particular, there are several examples in the literature of how this technique has been used, for example, to assess the quality

of meat [22] or to characterise different types of milk [23].

The working principle of an EIS measurement is as follows: in order to measure $Z$ is externally imposed a small sinusoidal perturbation $V_0 \sin \omega t$ over a DC voltage, with $\omega$ the frequency [24]. The application of the potential, produces a sinusoidal current $I(t) = I_0 \sin(2\pi f t + \phi)$ superimposed on the DC current with $\omega$ the frequency and $\Phi$ the phase shift. We define the impedance as:

$$Z = \frac{V_0 \sin \omega t}{I_0 \sin(\omega t + \phi)} \tag{3.16}$$

As reported by Lisdat and Schafter in their article "The use of electrochemical impedance spectroscopy for biosensing" [25], the name impedance "spectroscopy" is derived from the fact that the impedance is generally determined at different frequencies rather than just one. Thus, an impedance spectrum is obtained that allows the characterisation of surfaces, layers or membranes as well as exchange and diffusion processes. For biosensing applications, frequency $\omega$ usually range from $1MHz$ up to about $1mHz/1Hz$. The voltage bias usually applied is in the order of $1mV$. Impedance is a complex number, it is useful to graph it through:

1. Nyquist diagram: projection of $Z$ in the plane $Imm(Z)$-$Re(Z)$.
2. Cole diagram: projection of $Z$ in the plane $Imm(Z) - \omega$.
3. Bode diagram: projection of the modulus $|Z| = [Re(Z)^2 + Im(Z)^2]^{\frac{1}{2}}$ and phase $Z = arctan[\frac{Im(Z)}{Re(Z)}]$ as a function of $\omega$ on a logarithmic scale.

Unlike amperometric and voltammetric techniques, usually EIS techniques involve the use of a two-electrode configuration. The current flowing between the working and reference electrodes must be small enough to avoid polarisation of the reference electrode. Depending on the type of electrochemical cell used, the spectrum obtained is analysed by using an equivalent circuit which may consist of various circuit elements describing the different physical and chemical properties of the system.

## Equivalent circuits for data fitting

### Without RedOx mediator

The characterisation of an electrochemical cell, with a supporting electrolyte, is modelled through a series of resistance and conductance. The impedance includes two components:

1. The resistance $R_s$ of the supporting electrolyte, which includes the characteristics of the solution, the working area and the inter-electrode distance.

2. The resistance $R_{el}$ related to the working electrode. This is usually smaller than $R_s$.

The Stern layers and the diffusive layer are modelled with a single equivalent capacitance, called the double layer capacitance $C_{dl}$. The calculated impedance is then:

$$Z = R - \frac{j}{\omega C}. \tag{3.17}$$

The Nyquist diagram consisting of a vertical line intercepting the real axis at $R = R_{el} + R_s$. The Bode diagram shows a decrease of the modulus once the frequency $\omega_0$ is reached, corresponding to an impedance $R_s + R_{el}$. The phase at low frequencies is equal to $-\frac{pi}{2}$, once the frequency is reached $\omega_0$ changes to 0.

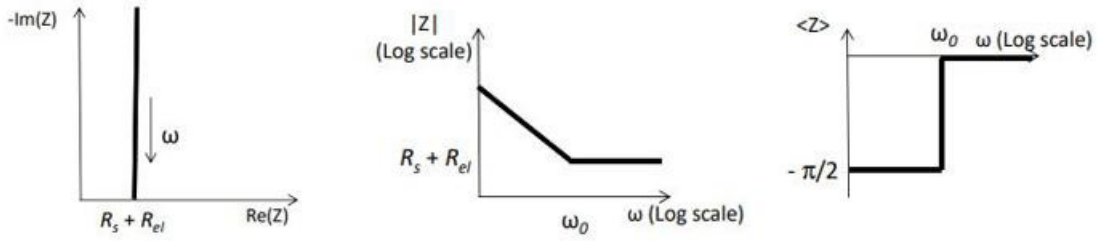


Figure 3.12: EIS measure without RedOx mediator: (a) Nyquist diagram; (b) Bode diagram: modulus; (c) Bode diagram: phase.

Experimentally, the capacitative behaviour is not observed, in order to achieve better maching of the data, the double layer capacitance is replaced by a constant

phase element $CPE$ with impedance:

$$Z_{CPE}(\omega) = \frac{1}{Y_0(j\omega)^n} \tag{3.18}$$

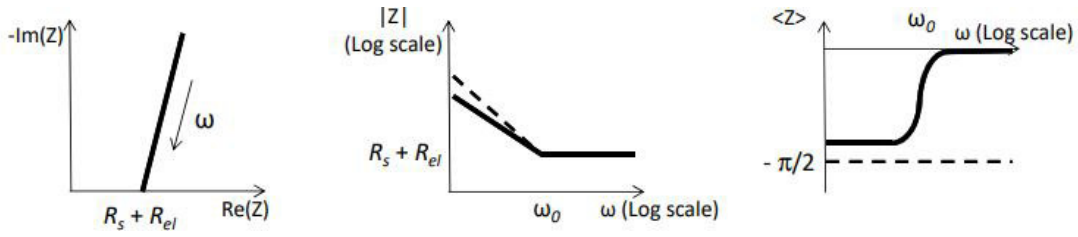


Figure 3.13: EIS measure without RedOx mediator, with CPE: (a) Nyquist diagram; (b) Bode diagram: modulus; (c) Bode diagram: phase.

This modelling involves a change in the expected graphs. In fact, as can be seen in the figure 3.13, the Nyquist presents a straight line inclined by $n\frac{\pi}{2}$, the phase does not present the step behaviour, it reaches 0 with a smooth trend. The modulus does not vary much, it only presents a lower slope at low frequencies.

### With RedOx medatior

The presence of a RedOx mediator, coupled to a supporting electrolyte, introduces the addition of a resistance in parallel to the double layer capacitance. This resistor, called charge transfer resistance $R_{ct}$, is used to model the current associated with the RedOx reaction occurring at the electrode interface. The branch containing the charge transfer resistor is called the faradic branch, the non-faradic branch the one containing the double layer capacitance.
The circuit impedence is:

$$Z = (R_s + R_{el}) + \frac{R_{ct}}{(1 + (\omega R_{ct} C_{dl})^2) - j\omega \frac{R_{ct}^2 C_{dl}}{1+(1+(\omega R_{ct} C_{dl})^2)}} \tag{3.19}$$

This equivalent circuit generates a semi-circular Nyquist diagram which intercepts the real axis at $R_s + R_{el}$ e $R_s + R_{el} + R_{ct}$. The diameter of the semicircle corresponds to $R_{ct}$. The Bode diagrams of this show the different frequency contributions of

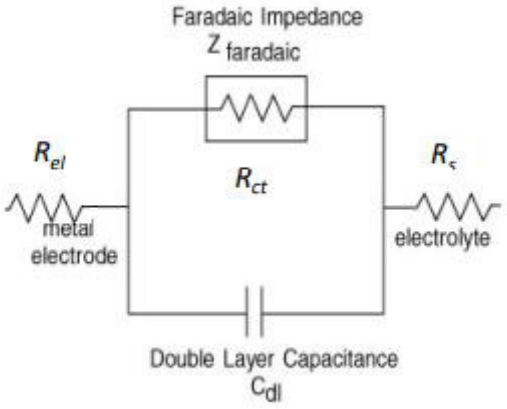


Figure 3.14: EIS measurements with RedOx mediator: equivalent circuit.

the electrical elements: at low frequencies we notice the influence of $R_s + R_{el} + R_{ct}$, as we continue to increase the frequency we see a decrease in the modulus due to $C_{dl}$ until it settles at $R_{el} + R_s$.

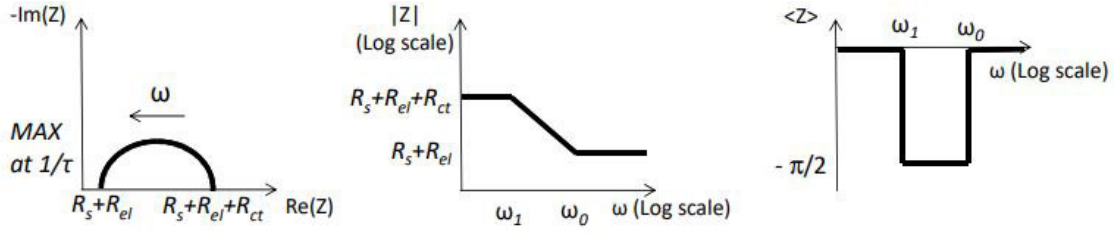


Figure 3.15: EIS measure with RedOx mediator, with CPE: (a) Nyquist diagram; (b) Bode diagram: modulus; (c) Bode diagram: phase.

### Low frequencies

A supplementary circuit element must be introduced to model the behaviour at low frequencies. In fact, experimentally, it is possible to observe a phase stabilisation at $-\frac{pi}{2}$ for low frequencies ($\omega < 100mHz$). This behaviour is caused by a diffusive process that takes place in the electrolyte: when the signal is very slow, the mediator molecules diffuse much further, contributing to the current measurement. In the modelling a new circuit element called Warburg element is added,

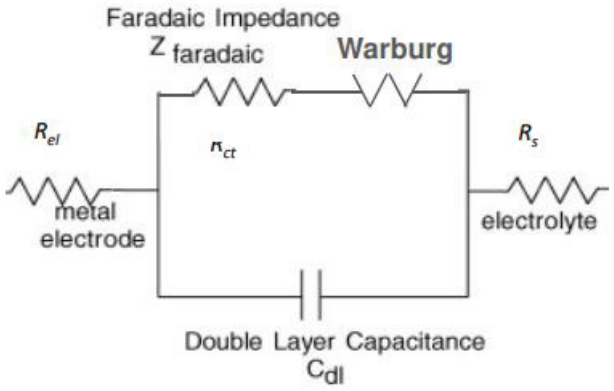


Figure 3.16: Randles cell.

which has impedance:

$$Z_{Ws} = \sigma\omega^{-\frac{1}{2}}(1-j) \tag{3.20}$$

$$\sigma = \frac{RT}{n^2F^2A\sqrt{2}}\left(\frac{1}{C^{*O}\sqrt{D_O}} + \frac{1}{C^{*R}\sqrt{D_R}}\right) \tag{3.21}$$

where $D_O$ and $D_R$ are the diffusion coefficients, $C^{*O}$ and $C^{*R}$ the concentrations, in the bulk, of the reduced and oxidised species, respectively. Usually, the diffusive layer is not infinite but is limited. In this case. the impedance of the Warburg element is modified to take this effect into account:

$$Z_{W_o} = \sigma\omega^{-\frac{1}{2}}(1-j)tanh[\delta(\frac{j\omega}{D})^{\frac{1}{2}}] \tag{3.22}$$

the diffusive layer and $D$ the average diffusive value of the two species. For high frequencies, i.e. $\omega \to \infty$, the hyperbolic tangent tends to 1, consequently the equation is simplified, returning equal to that with infinite diffusive layer $Z_{W_s}$. The equivalent circuit, including the Warburg element, is called a Randles cell.
In the Nyquist diagram, we have a line with slope $\pi/4$, ideally starting from point $R_s + R_{el} + R_{ct}$. When $\omega \longrightarrow 0$ the ions diffusion to the electrode becomes the dominating factor.

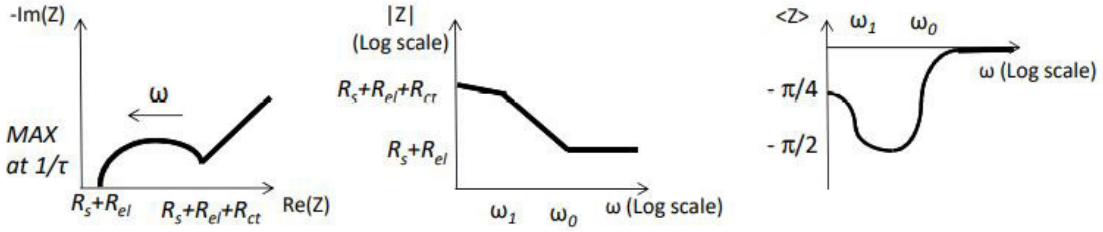


Figure 3.17: EIS measure with RedOx mediator, including Warburg element: (a) Nyquist diagram; (b) Bode diagram: modulus; (c) Bode diagram: phase.

For higher frequencies this issue is not relevent respect the interface charge transfer resistance and double layer formation. At very high frequencies the diffusion processes are excluded, only the resistance associated to the charge transport in solutions remains.

# Chapter 4

# Biosensor experimental characterization

## 4.1 Targets and methods

The goal of this thesis work is developing a sensor who can detect the presence of phages in milk sample with electrochemical measures. Based on the previously mentioned work by Rosati et.al [15], the sensor that I want to develop is conceptually very simple. In fact, the electrode surface does not need any treatment or funtionalization protocol. Moreover, I use solutions easily available on the market and I do not use high cost sensing technologies. The LAB (*L.Lactis*) present in the milk sample are deposited on the electrode. The electrical properties of the system change as a function of the number of bacteria deposited on the electrode. The presence of phages leads to the lysis of bacteria in the sample, as a result there is less bacteria deposited on the sensor, the electrical properties of the system vary differently to a sample without phages.

In the previous chapter, I introduced various measurement techniques for electrochemical characterisation. However, voltammetric techniques are not a valid alternative in this case of study, as they may involve too high currents would lead to electrical stress on the bacterial cells in solution and consequent lysis. I choose to characterise my device with electrochemical impedance spectroscopy (EIS), be-

cause this technique can monitor the superficial behaviour of electrochemical cell and model it with specific circuital models [26]. I opted to use the charge transfer resistance $R_{ct}$ of Randle's cell as sensing element. Theoretically, *L.Lactis* in solution settle on the sensing area of the sensor, obstruct the electron transfer and this behavior results in an increase of the transfer charge resistence $R_{ct}$. In a sample with phages, the virus lysis the bacteria, in consequence there are less bacteria deposited on the sensor and therefore a less $R_{ct}$ respect a sample without phage. Because the potential $V_{DC}$ of the EIS measurement is usually equal to the potential $E_0$, before performing the characterisation with the EIS measurements, I carried out cyclovoltammetry measurements with the aim of finding the potential $E_0$ of the test solutions, before adding the biological material.

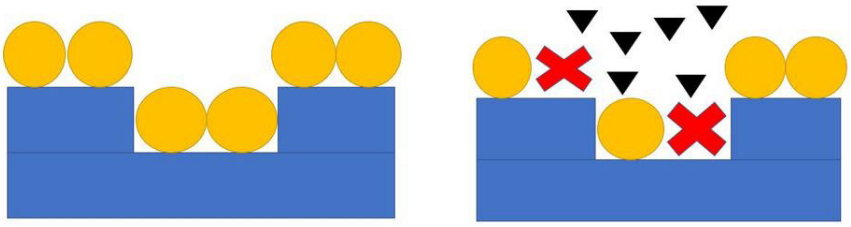

Figure 4.1: Illustration of sensors (in blue) and solution interface. *L.Lactis* deposition over the sensor (left). Phages lysis effect (rigth).

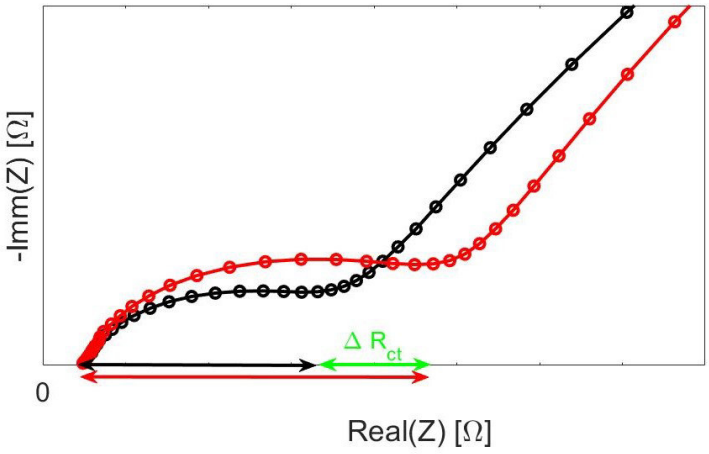


Figure 4.2: Nyquist diagram of two measure with a different bacteria density.

In order to charaterize the behaviur of the sensor with biogical material, I carried out EIS measures comparing the response of the sensor with the progressive increase of bacterial cells. The bacterial growth is monitored with optical absorbance measure at a wavelength of $600nm$. Theoretically, at the increase of absorbance, increases the number of bacterial deposited on sensing area and the $R_{ct}$ should increase. In each experimental test, I compared the trend of the measured optical absorbance with the $R_{ct}$ obtained during the course of the experiment, in order to verify the coherence between the absorbance measurements and the electrochemical measurements.

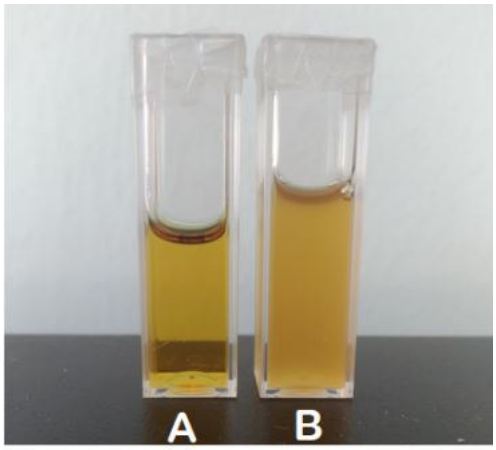


Figure 4.3: Cuvettes used in experimental test (a) without L.Lactis (b) solution with L.Lactis.

To give a qualitative view of the data, I have chosen to represent the impedance by Bode diagram and Nyquist diagram. In particular, through Nyquist diagram is possible to visually observe the course of the charge resistance by observing the amplitude of the semicircle, which become gradually greater as $R_{ct}$ increases.

## 4.2 Materials and Instrumentation

### Electrods DRP-C223AT

Screen-printed electrodes are devices used for electrochemical analyzes. These are formed by depositing inks of conductive, dielectric or resistive layers on top of an insulating layer (plastic or ceramic), through a screen printing process. Reliable devices are obtained, also resistant to temperature cycles and with good mechanical properties [13]. This process is stable and easily repeatable, allows to print different inks based on the type of application required. The devices used for electrochemical measurements are usually composed of three electrodes:

1. Working: electrode sensitive to the analyte of interest. Usually made in carbon, gold, platinum or silver.

2. Reference: approximation of the standard reference electrode. Its potential is constant and the working potential is measured in comparison with the latter.

3. Counter: electrode that completes the circuit allowing the passage of current. Usually made of the same material as the working.


Figure 4.4: Different type of electrodes developed by Metrohm DropSense.

In my thesis work I used DRP-C223AT electrodes manufactured by Metrohm DropSense. They have the following physical / geometric characteristics:

- Ceramic substrate: 33 x 10 x 0.5 mm (length, width, thickness).
- Electrical contacts in silver.

The electrochemical cell is composed of:

1. Working: Gold electrode, 1.6 mm diameter.
2. Counter: Gold electrode.
3. Reference: Silver electrode.

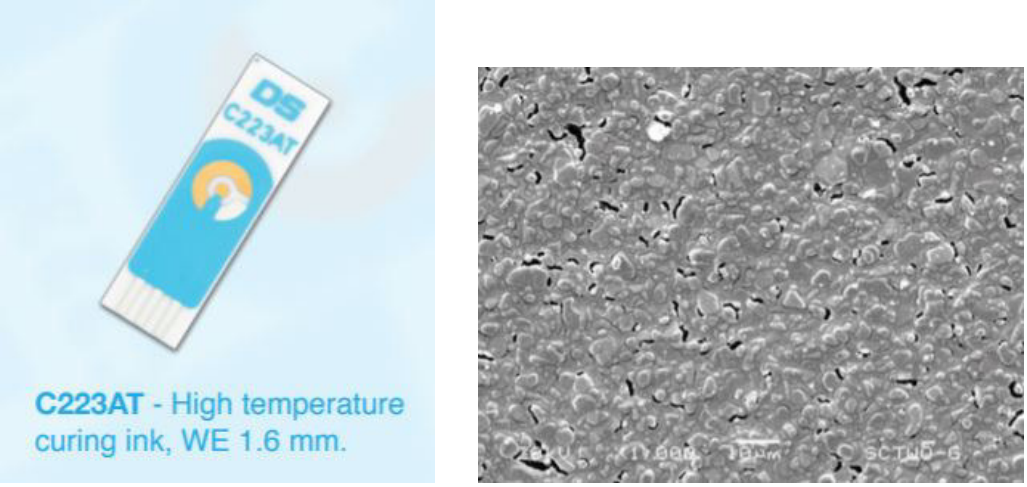


Figure 4.5: (a) DRP-C223AT sensor (b) DRP-C223AT surface.

They are marketed in packets of 75 units, which should remain at room temperature, protected from light and humidity, in order to not ruin their surface properties and consequently modify the response to the analyte of interest. All information and the photos, about these sensors, was taken from the official website of the manufacturing company *www.dropsens.com*.

The experimental set up involves the use of a PDMS (Polydimethylsiloxane, Sylgard 184) "electrochemical" unit with a hole in the sensing area. The unit is placed on the sensor and inserted into a PLA (Polylactic Acid) structure. To avoid the phenomenon of evaporation that could lead to measurement instability, the cell is always "coated" with a layer of laboratory Parafilm.

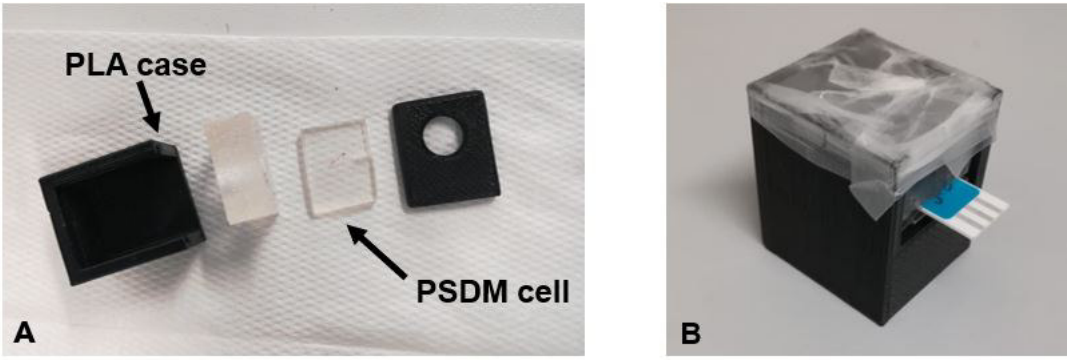


Figure 4.6: Experimental set-up: (a) "Electrochemical" unit assembled (b) Components of "Electrochemical" unit.

The electrical contacts are inserted into a DSC connector, also manufactured by Metrohm DropSense, which acts as an interface between the sensor and the potentiostat.

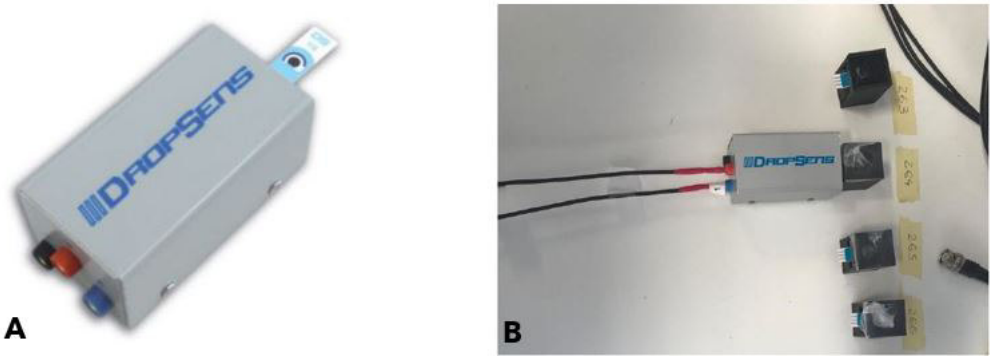


Figure 4.7: Experimental set-up: (a) Electrode placed into DCS connector, without "electrochemical" unit; (b) Experimental configuration, DCS connect with electrochemical cell.

## Instrumentation

To perform the EIS measurements, I used two different devices used as impedance analysers, which provide similar and comparable results, allowing me to use one or the other indiscriminately during the experimental tests. Whatever device is chosen, EIS measurements was carried out in a two-electrode configuration using the gold electrode as the working and the silver electrode as the reference.

Some measurements were carried out with the EmStat Pico potentiostat developed by PalmSens. As specified on the manufacturer's website (*www.palmsens.com*) this is a proven stand-alone potentiostat module that allows electrochemical measurements including EIS and CV. The device is connected to the sensor, located inside the DSC connector, via BNC cables.

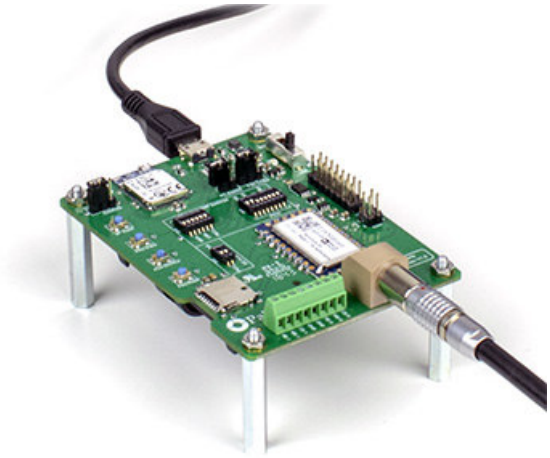

Figure 4.8: EmStat Pico.

The module features a USB output, making it integrable with a PC through a specific software called PSTrace. This software is required to set the measurement parameters and to view the graphs of the detected data in real time (Bode diagram and Nyquist diagram).

Other measure were carried out with 1260A Impedance Analyzer, one of the most widely used impedance analyzers in the world. This instrument is usually referred to as 'Solatron', and I will also be using this name during the discussion of the data obtained. One of the unique features of the Solatron is the wide frequency range it can inspect from $10\mu Hz$ to $32MHz$, provides excellent coverage for virtually all chemical and molecular mechanisms, all in one instrument. Solatron is connected to the PC with a USB cable and through specific software, called SMaRT, it is possible to set the experimental parameters of the EIS measurement, such as the input signal $V_{DC}$ and the sinusoidal perturbation $V_{ac}$. The software provides for the graphical display of the experimental phase through Nyquist and Bode diagrams, allowing to monitor the measurement in real time. The sensor, placed inside the DSC connector, is connected to the solatron via BNC cables.

Figure 4.9: 1260A Impedance Analyzer.

I used, for carried out CV measure, Model 404A fabricated by CH-Instrument. This is a potentiostat and also a galvanostat, it allowed to carry out cyclic voltammetries (CV). Apply a voltage drop between WE and RE and measures the current between WE and CE. The electrodes, located inside the DPS connector, are connected to the potentiostat via an adapter and BNC wires. As Solatron and Pico, I had to use specific software, for managing the experimental parameters.


Figure 4.10: Model 404A.

I needed a spectrophotometer to carry out optical absorbance measurements in parallel with electrochemical measurements. This was necessary to verify that the results obtained in electrochemistry were consistent with the data obtained in absorbance. The UV-30 SCAN is a high-performance scanning UV/Vis spectrophotometer for quality control applications. Allows automatic reference subtraction for the entire wavelength range. The application software, supplied with the instrument, enables PC control and includes all important quantitative and qualitative analysis methods. Optical ansorbnce was measured at $600nm$, a wavelength that is absorbed by the bacteria in solution, allowing me to monitor the *L.Lactis* growth.


Figure 4.11: Spectrophotometer ONDA UV-30 SCAN.

## Solutions

I used the RedOx test solution, which consists of the Ox/Red couple ferricyanide $[Fe(CN)_6]^{3-}$/ferrocyanide$[Fe(CN)_6]^{4-}$. The RedOX mediator was dissolved in

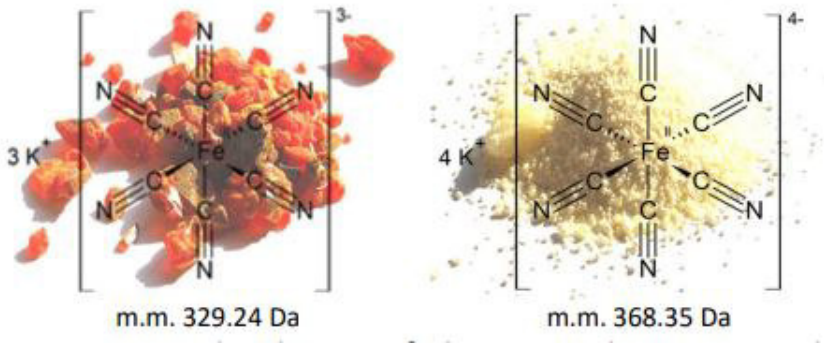


Figure 4.12: Molecules used for the preparation of ferricyanide/ferrocyanide solutions: (a) $[Fe(CN)_6]^{3-}$ (b) $[Fe(CN)_6]^{4-}$

M17 used as supporting electrolyte. Preparation procedure involves for first the preparation of two indipendent solutions at the same concentration, each containing one of two salts dissolved in M17. Knowing the concentration $c$ of mediator and the volume of solution $V$ to be obtained, the following relation is used to calculate the necessary moles $n$ of substance:

$$n = \frac{V}{c} \tag{4.1}$$

Once the moles have been calculated, calculate the required mass $M$:

$$M = nMM \tag{4.2}$$

where MM is the molecoular mass equal to 329.24 for ferricyanide $[Fe(CN)_6]^{3-}$ and 368.35 for ferrocyanide $[Fe(CN)_6]^{4-}$. Once the two solutions have been obtained, they are mixed to obtain ferri/ferrocyanide solution at the desired concentration. I opted to use a concentration of 10mm of $[Fe(CN)_6]^{3-/4-}$ dissolved in M17 as this is an ideal concentration for tests with bacteria cells.

To allow bacterial growth of *L.Lactis* I used M17 culture medium. It is specifically designe to improved growth of *Lactococcus* species and its bactereophages isolated from milk products. All information about this product has been taken from *www.himedialabs.com*.


Figure 4.13: Container of M17 broth powder before preparation.

| **Ingredients** | **Quantity [g/L]** |
|---|---|
| Peptic digest of animal tissue | 2.500 |
| Casein enzymic hydrolysate | 2.500 |
| Papaic digest of soyabean meal | 5.000 |
| Yeast extract | 2.500 |
| Beef extract | 5.000 |
| Lactose | 5.000 |
| Ascorbic acid | 0.500 |
| Disodium-$\beta$-glycerophosphate | 19.000 |
| Magnesium sulphate | 0.250 |

Table 4.1: Composition of M17 broth.

Lactic steptococci require a very complex medium for optimal growth. Glycerophosphate keeps the pH above 5.7, which is necessary because a lower pH could inhibit bacterial growth. Lactose is necessary for the metabolic activity of bacteria and ascorbic acid is stimulatory for the bacterial growth. Magnesium sulphate provides essential ions to the organisms. The preparation protocol consists of: suspend 42 g of powder in 1 litre of distilled water and let it soak; heat to boiling and dispense into suitable containers; sterilize by autoclaving at 121°C for 15 minutes.

## Software and Data Analysis

The analysis of the collected data was carried out through the MatLab R2021a software. MatLab is a numerical programming and computing platform used for data analysis, algorithm development and modeling (*www.matlab.com*). It combines a desktop environment optimized for iterative analysis and design processes with a programming language that expresses mathematical operations with matrices and arrays directly. Through this software the CV curves and the Bode and Nyquist diagrams for the EIS curves were obtained.

The software EISSA was used for the interpolation of the collected data and for the revalation of circuital parameters. This software allows to assemble suitable circuits for the interpolation of the experimental data. In addition to providing various elements for modeling such as resistors, capacitors, CPE or Warburg element, the software has functions of error estimation and coherence tests between data, thus allowing to obtain optimal values that represent our experimental process.

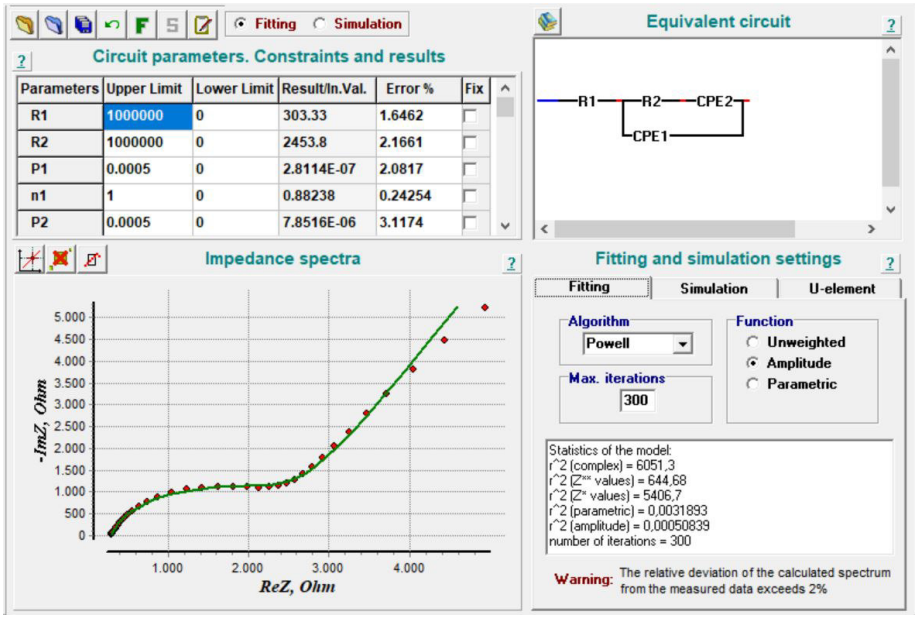


Figure 4.14: EISSA interface. Up-Left the estimated parameter with the respect error. Down-Left Nyquist diagram. Up-Right equivalent circuit. Down-Rigth simulation setting.

I used a circuit fitting slightly different from the Randle cell, in order to obtain a better estimate of the electrical circuit parameters. As can be seen in the figure 4.15, the Warburg element have been replaced with a CPE [15] called in my scheme CPE2. The circuit parameters calculated from the fitting of the data always showed an error of less than 5%.

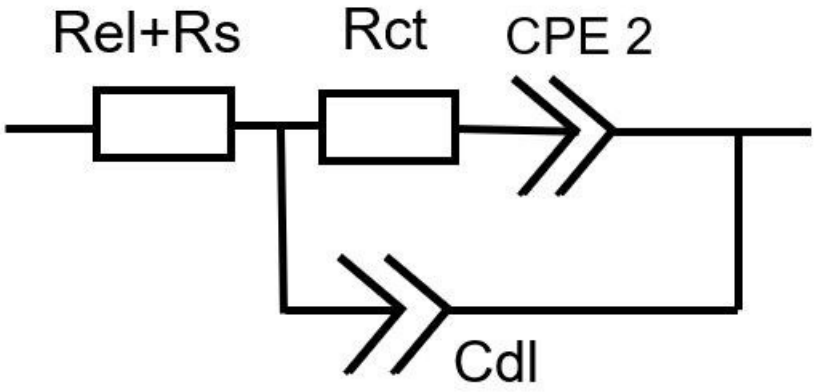


Figure 4.15: Schematization of the circuit used for data analysis.

## 4.3 Device stability

Firstly, I have carried out a series of tests to ensure that my device was able to give the most stable and repeatable response. Time stability is a fundamental requirement for the development of my device because during the experimental characterisation phase with biological material, I was interested in observing how the response of the device changes as a function of bacterial growth or phage activity. An excessively unstable response over time may not allow me to detect the biological activities I am interested in. Furthermore, another fundamental characteristic to be evaluated during the experimental characterisation of a biosensor is the stability of the measurements and the interchangeability between different devices. Even though this feature could seem obvious, it is actually not at all: sensors from the same batch may give completely different responses. In fact, there may be manufacturing errors, damage during packaging or during laboratory handling. I have carried out tests on several devices and assessed that the obtained error of the measurements , calculated through the standard deviation, was always less than or equal to 10%.

These stability tests were carried out with the 10mM $[Fe(CN)_6]^{3-/4-}$ and $M17$ solution. Before characterising the device through EIS measurements, I performed cyclic voltammetry (figure 4.16) measurements to calculate the $E_0$ potential. The cyclic voltammetry measurements were not carried out with biological material, as the high currents involved could lead to lysis of the bacteria. I found a potential $E_0$ equal to 0.091 mV.

In the first stability test I carried out EIS measurements at regular intervals over time. The measurement protocol was as follows:

1. Wash the sensor with milliQ.
2. Dry with compressed air.
3. Drop deposition.
4. EIS measurements every 30 min.

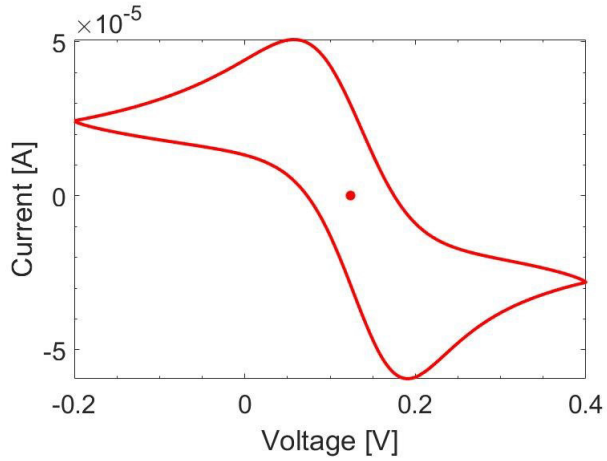


Figure 4.16: Ciclic voltammetry on DRP-C223AT with 10mM $[Fe(CN)_6]^{3-/4-}$ + M17.

I performed a total of 7 EIS measurements, for a total of 180 minutes of observation. I repeated the same tests following the same protocol, taking measurements every 30 minutes for a total of 180 minutes of observation.

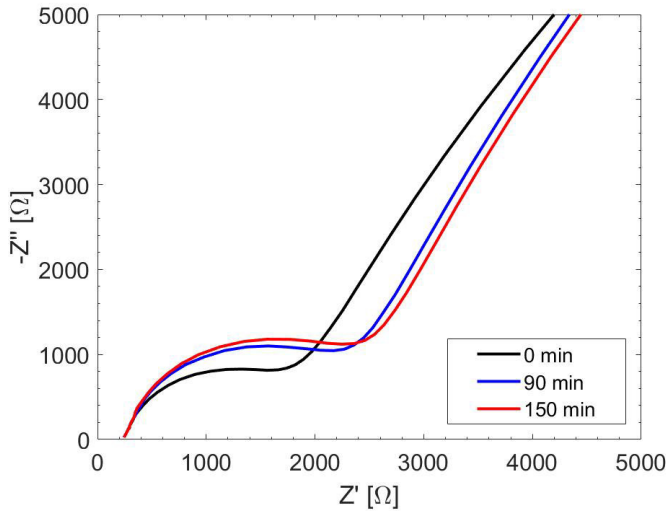


Figure 4.17: Stability test on DRP-C223AT with 10mM $[Fe(CN)_6]^{3-/4-}$ + M17:Nyquist diagram.

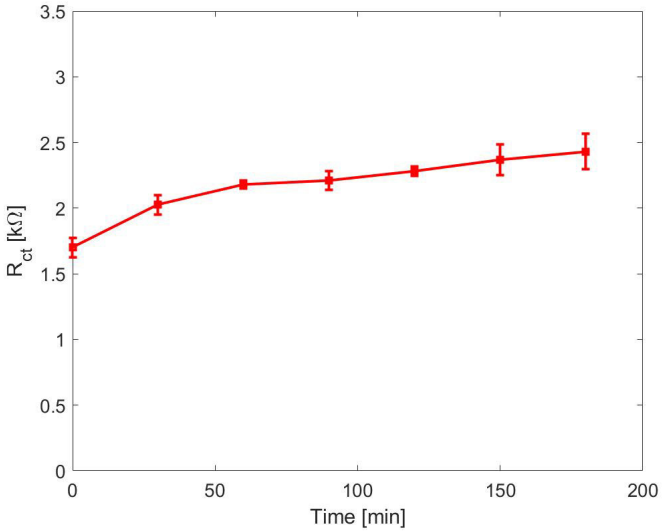


Figure 4.18: Stability test on DRP-C223AT with 10mM $[Fe(CN)_6]^{3-/4-}$ + M17: $R_{ct}$ in function of time.

The Nyquist diagrams of the measurements obtained at 0, 90 and 150 minutes from the start of the experiment are shown in figure 4.17. There is a slight increase in the semicircle of the Randle curve, indicating an increase in the resistance to charge transfer. From the trend of $R_{ct}$ over time (figure 4.18), I noted a growth trend as the experimental time increases. After 150 minutes of observation, the $R_{ct}$ is 1.49 times the initial value.

The measurement proved itself to be stable and the error on each measurement was less than 10%. It can clearly be seen that the charge transfer resistance increases in function of experimental time. Observing this experimental trend, I asked myself: is it possible that there is some kind of contamination following successive measurements with the same drop or is it just a typical behaviour of the device?

I therefore chose to test the device by changing the drop at each measurement. Between subsequent measurements, the device will be cleaned using a milliQ water and pressured air to eliminate any contamination. I followed a similar protocol to the previous one:

1. Wash the sensor with milliQ.
2. Dry with compressed air.
3. Drop deposition.
4. Wait 5 min.
5. EIS measurements
6. Drop removing.
7. Wash the sensor with milliQ.
8. Dry with compressed air.
9. Wait 30 min.
10. Repeate from 3 to 9.

I performed 10 EIS measurements, for a total of 270 minutes of the experiment. In order to simplify the graphical view, I will report in the Nyquist diagrams (figure 4.19) only the measurements at 0, 60 minutes, 120 minutes, 180 minutes and 270 minutes.

As we can see from the Nyquist diagram, the amplitude of the semicircle increases with time. From the trend of the $R_{ct}$ in time (figure 4.20) I see the same behaviour observed previously: as time increases, the $R_{ct}$ presents a linear increasing trend, arriving after 270 minutes at about 1.38 times the initial value. The error obtained in each measurement has always been less than 10%, allowing me to say that there is a good stability of the measurement and interchangeability between different devices. The increasing trend of $R_{ct}$ is confirmed, so I assume that this is a typical behaviour of the device. However, this behaviour should not affect the ability of

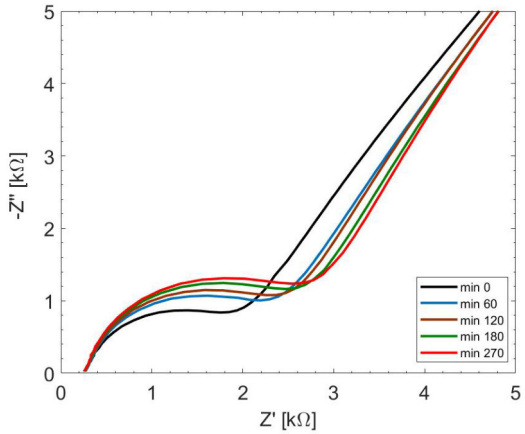


Figure 4.19: Stability test on DRP-C223AT with 10mM $[Fe(CN)_6]^{3-/4-}$ + M17 and drop change: Nyquist diagram.

the device to detect *L.Lactis* first. In fact, I expect that where bacteria will be present, the resistance to charge transfer will increase greatly in relation to the number of bacteria present in solution, compared to a sensor on which M17 + $10mM[Fe(CN)_6]^{3-/4-}$ solution has been deposited, which I will henceforth refer to as negative control.

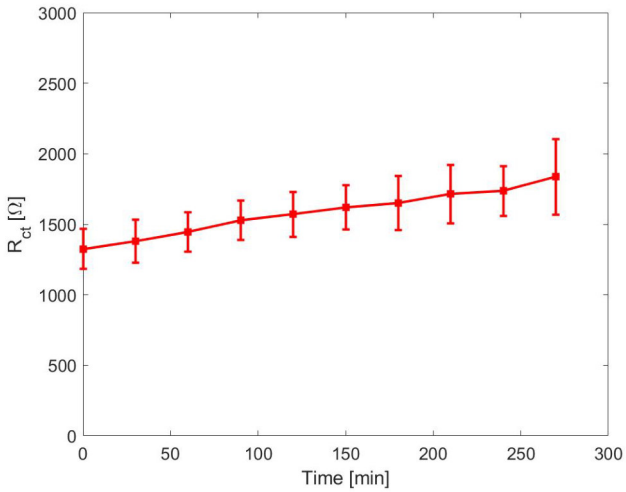


Figure 4.20: Stability test on DRP-C223AT with 10mM $[Fe(CN)_6]^{3-/4-}$ + M17 and drop change: $R_{ct}$ in function of time.

## 4.4 Experimental characterization with *L.Lactis*

Now that the response of our device has been evaluated and since this could be suitable for operating with biological material, I continued by adding *L.Lactis* in the solution containing 10 mM $[Fe(CN)_6]^{3-/4-}$ and $M17$. Analyses with biological material were carried out using EIS only, because other electrochemical measurement techniques involve potentials and currents that could lead to an inhibition of bacterial growth.

In parallel with the electrochemical measurements, I carried out absorbance measurements to check that there was consistency between the optical absorbance measurements and the electrical measurements. Throughout the treatment I will refer to optical absorbance as "OD". Ideally, as the OD increases, the bacterial concentration increases, resulting in an increase in the number of bacteria deposited on the working, which should lead to an increase in $R_{ct}$.

The solutions used were as follows:

| | **Negative Control** | **L.Lactis** |
|---|---|---|
| *L.Lactis* OD=0.5 | | $1200\mu L$ |
| 20mM FeCN in M17 | $3000\mu L$ | $3000\mu L$ |
| M17 | $2520\mu L$ | $1320\mu L$ |
| **Total Volume** | $6000\mu L$ | $6000\mu L$ |

Table 4.2: Solution composition, characterisation of DRP-C223AT with *L.Lactis* in solution.

As can be seen from the table **??** in the composition of the solutions I used 20mM $[Fe(CN)_6]^{3-/4-}$ in M17. In order to obtain the desired concentration of 10mM $[Fe(CN)_6]^{3-/4-}$, I inserted a quantity of 20mM equal to half of the desired total volume, which will then be diluted by adding the other components of the solution. Bacteria are added to the solution from an initial OD of 0.5. In all my tests, *L.Lactis* are always added 1/5 of the total volume of solution desired, so as to start from a very low OD around 0.1 in the solution, allowing us to monitor growth over long periods. The solutions were completed by adding M17 to obtain the desired final volume.

For these tests I used the "Solatron" impedance analyser using the following parameters: frequency range [100kHz-1Hz]; numbers of points per decade 10; $V_{DC}$ corresponding to the potential previoulsy found from CV measures $E_0 = 0.091V$; potential $V_{AC}$ fixed at $10mV$. During all experimental tests before carrying out the actual test, I carried out pretest measurements with solutions free of biological material, to make sure that the sensors all behaved in the same way or were not accidentally damaged inside the container. In order to simplify the graphical view, I decided to show the Bode and Nyquist diagram of only three measurements taken at the starting minute, an intermediate time and the final time.

### 4.4.1 Drop-In

The first experimental approach used for detecting bacteria in solutions has been renamed Drop-In, as the drop once deposited on the sensor is never removed. The protocol consists of:

1. Wash with milliQ water.
2. Dry with jet air.
3. Deposition of $90\mu L$ of solution.
4. Wait 15 min.
5. EIS measurements.
6. OD meausure.
7. Wait 30 min.
8. Repeat from 4 to 7.

The Drop-In protocol is experimentally simple to perform, as it only requires subsequent measurements to be made without touching the experimental set-up in any way. An advantage of this protocol is that it limits any interactions due to electrochemical unit movement. Indeed, bacterial growth could be affected by

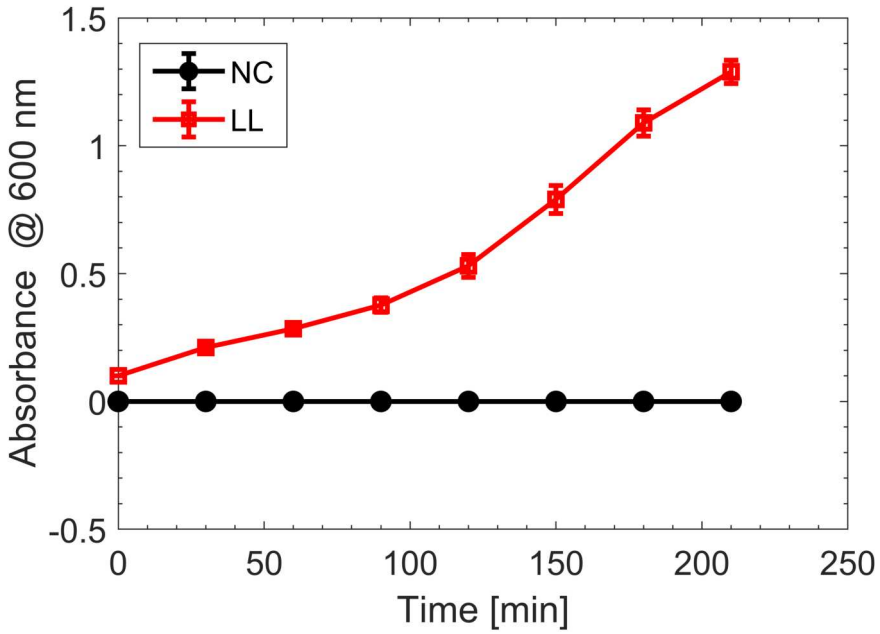


Figure 4.21: Drop-In method: OD (600 nm) in function of time, characterisation of DRP-C223AT with *L.Lactis* in solution.

electrochemical unit movement. By minimising movement I am sure to have a bacterial growth which is consistent with what I can have in vivo samples. From the figure 4.21, in the solution containing the negative control the absorbance remains the same, indicating the absence of any contamination. In the solution containing *L.Lactis*, an increase in OD over time can be seen, indicating the advent of bacterial growth. The development of the curve reflects what is expected from the theoretical growth curve. Up to 90 minutes there is a latency phase in which growth is very slow. In this phase the bacteria are gradually reproducing. As time goes on, there is an exponential growth phase where the bacteria make the most of the environmental resources and reproduce very quickly.

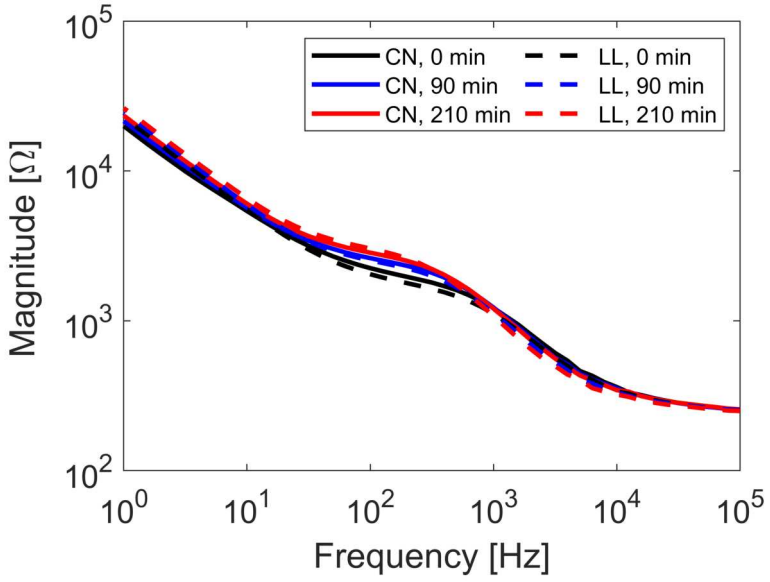


Figure 4.22: Drop-In method: Modulus of Bode diagram, characterisation of DRP-C223AT with *L.Lactis* in solution.

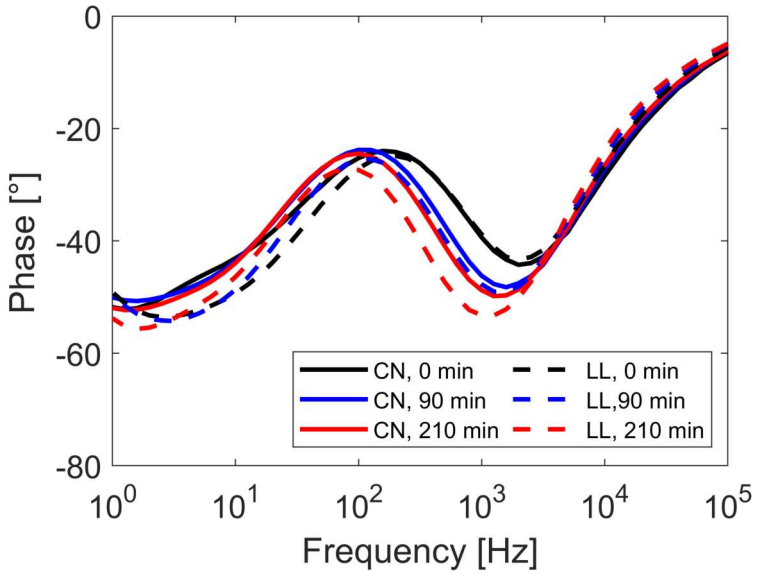


Figure 4.23: Drop-In method: phase of Bode diagram, characterisation of DRP-C223AT with *L.Lactis* in solution.

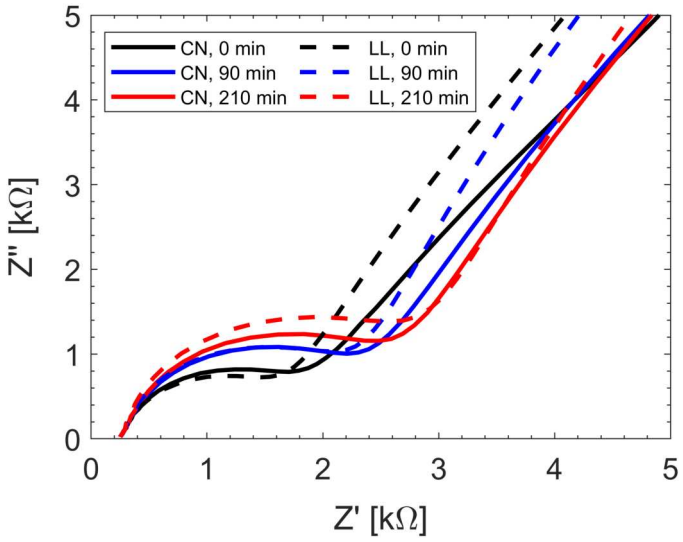


Figure 4.24: Drop-In method: Nyquist diagram, characterisation of DRP-C223AT with *L.Lactis* in solution.

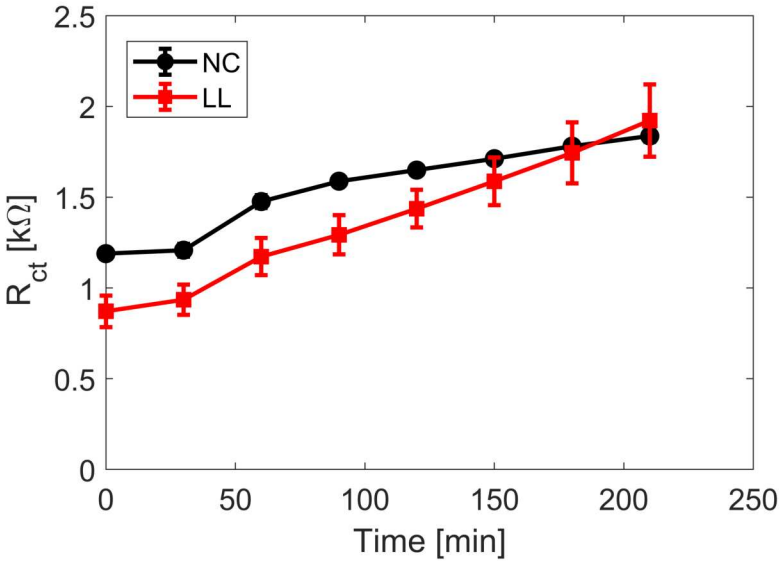


Figure 4.25: Drop-In method: $R_{ct}$ in function of time, characterisation of DRP-C223AT with *L.Lactis* in solution.

The figure 4.22 shows the modulus of the impedance as the frequency varies. As time increases, there is not a substantial difference between sensors where bacteria are present or not, the curves are almost overlapping. The phase of the impedance as a function of frequency (figure 4.23) shows the same trend as the modulus, the measurements over time are very similar. Between $10^2$ Hz and $10^3$ Hz there is a shift in phase as time increases, this behaviour appears to be similar in both negative control and in the sensor with bacteria. From the Nyquist diagram (figure 4.24) an increase in the amplitude of the semicircle can be seen, indicating a possible increase in $R_{ct}$, both in the negative control sensor and in the sensor with bacteria.

Theoretically, once a large amount of bacteria in solution has been reached, many of them should settle on the surface of the electrode, blocking the passage of electrons and consequently there is a much greater charge transfer resistance than the negative control. As can be seen from the figure, the trend of $R_{ct}$ over time is almost completely similar between the sensor with the bacteria and the negative control sensor. It is not possible to correlate the electrochemical measurements with the absorbance measurements. The curves are almost similar, so I wondered whether bacterial growth actually took place in the electrochemical unit. The reference electrode is made of silver, which is a powerful inhibitor of bacterial growth. Is it possible that the reference electrode inhibited bacterial growth in the cell?

### 4.4.2 Spill-Out

In order to test whether or not the reference electrode affects bacterial growth, I have developed a specific protocol that involves replacing the drop at each measurement, allowing me to continuously monitor what is happening in the electrochemical unit in relation to the bacterial growth observed in absorbance. The protocol is called "Spill-Out" and involves the following steps:

1. Wash with milliQ water.
2. Dry with jet air.
3. Deposition of $90\mu L$ of solution.
4. OD measure.
5. Wait 15 minutes.
6. EIS measurements.
7. Remove the drop.
8. Wash with milliQ water.
9. Dry with jet air.
10. Wait 30 minute.
11. Repeat from 3 to 10.

This protocol is appropriate for monitoring sensor in parallel, but it needs a specificity timetable. The Spill-Out protocol is experimentally more complicated to set up than Drop-In, the cuvettes are moved continuously and this could greatly influence bacterial growth. Furthermore, it is fundamental don't move the sensor during the measure, because the bacterial could disperse in the solution and consequently give me a wrong revelation of $R_{ct}$.

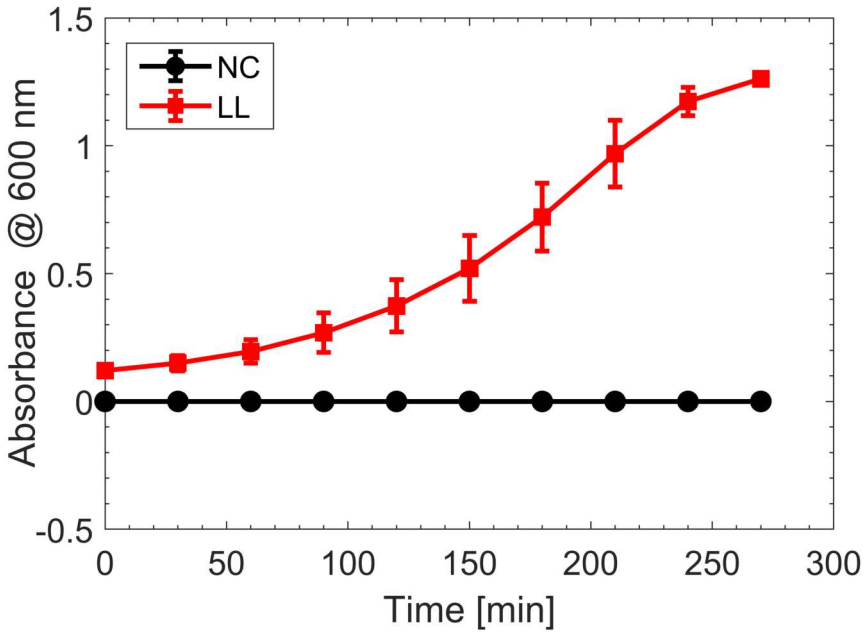


Figure 4.26: Spill-Out method: OD (600 nm) in function of time, characterisation of DRP-C223AT with *L.Lactis* in solution. Spill-Out.

From the figure 4.26, the trend in absorbance over time is reported. As in the case of the Drop-In protocol, the trend is consistent with what was expected in theory. After an initial adaptation phase where growth is slower, from minute 120 the bacteria begin to grow exponentially to an optical absorbance of over 1.200. At 240 minutes a stationary phase is reached, the nutrients of the culture have been consumed, the bacteria proliferation and the bacteria which are dying, are in equilibrium. In fact, if I had gone ahead and had measured OD after 300 minutes, I would probably have detected a decrease in OD, as the nutrients were no longer present and the bacteria would no longer be able to replicate themselves and would die.

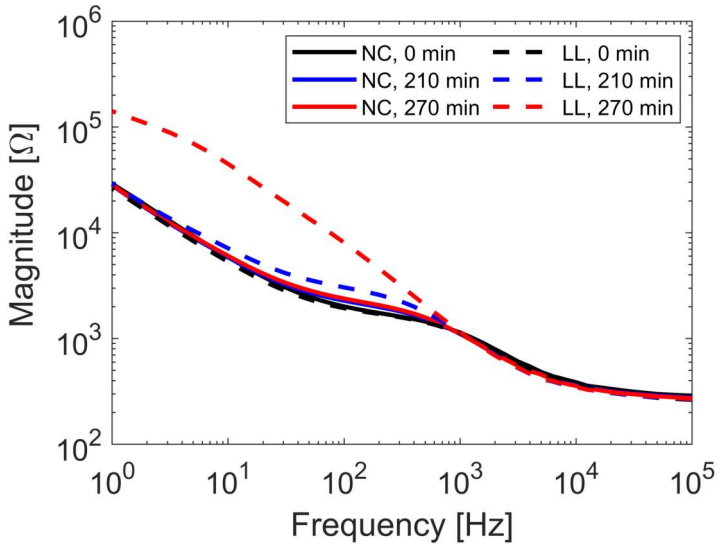


Figure 4.27: Spill-Out method: modulus of Bode diagram, characterisation of DRP-C223AT with *L.Lactis* in solution. Spill-Out.

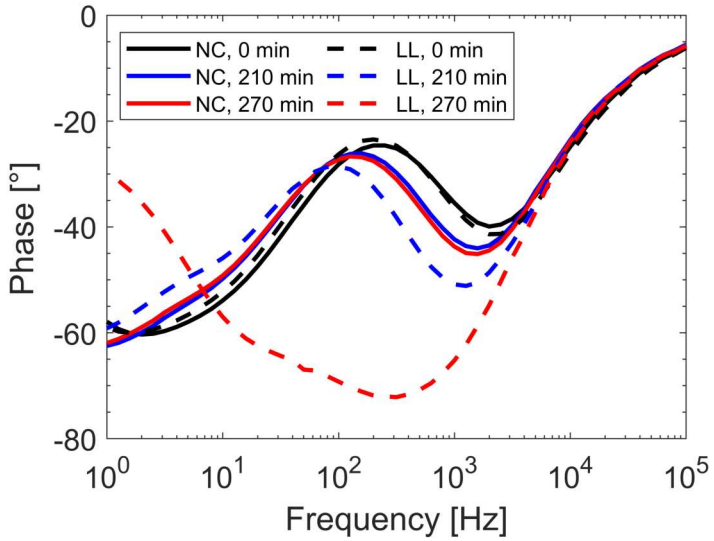


Figure 4.28: Spill-Out method: phase of Bode diagram, characterisation of DRP-C223AT with *L.Lactis* in solution. Spill-Out.

The figure 4.27 shows the modulus of the Bode diagram. For the negative control curves, at different times, are superimposable for all frequencies. In the sensor on which the bacteria are deposited, the curve at 270 minutes is not superimposed on the curve at 0 minutes. The curves are superimposable for high frequencies, but around $10^3$ down to lower and lower frequencies, the curve on which bacteria depositated starts to increase more and more. At $\omega = 1$ Hz, the curve at 270 minutes is one order of magnitude larger than that at time 0. From the phase of the impedance as a function of frequency (figure 4.28),there is a phase shift between $\omega = 10^2$ and $\omega = 10^3$ for both sensors. Observing the trend of the curve with the bacteria at 270 minutes, I asked myself: can I use the phase shift at a specific frequency to detect bacteria in solution?

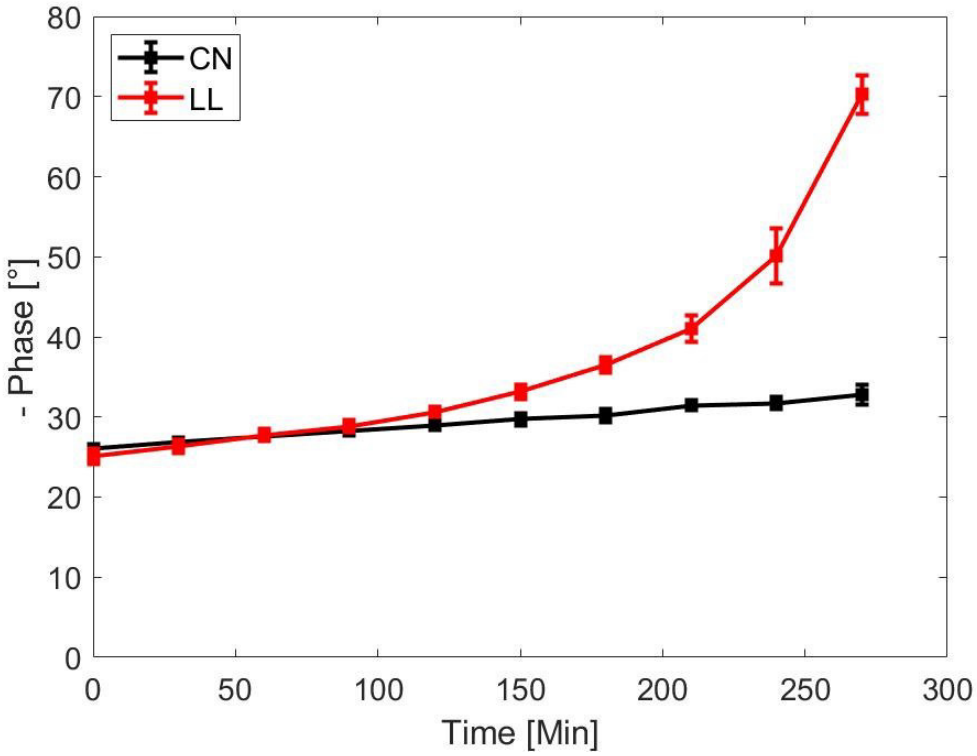


Figure 4.29: Spill-Out method: phase variation at 400 Hz, characterisation of DRP-C223AT with *L.Lactis* in solution. Spill Out.

In the figure 4.29 the phase at 400Hz is shown in function of time. The value of 400 Hz is chosen because at that specific frequency I observe the maximum shift between the curves. In the sensor on which the negative control solution has been deposited, the phase increases slightly as the time of the experiment increases, having a variation of the final phase with respect to the initial one equal to $\Delta\phi = 6.32°$. A growth trend is also observed on the sensors on which the bacteria have been deposited, however, the phase change is $\Delta\phi = 45.16°$, over 7 times that of the negative control. The phase change at 400 Hz is consistent with the results obtained in absorbance: as the number of bacteria in solution increases over time, the phase at 400 Hz increases too. I can use this phase variation to detect bacteria in solution.

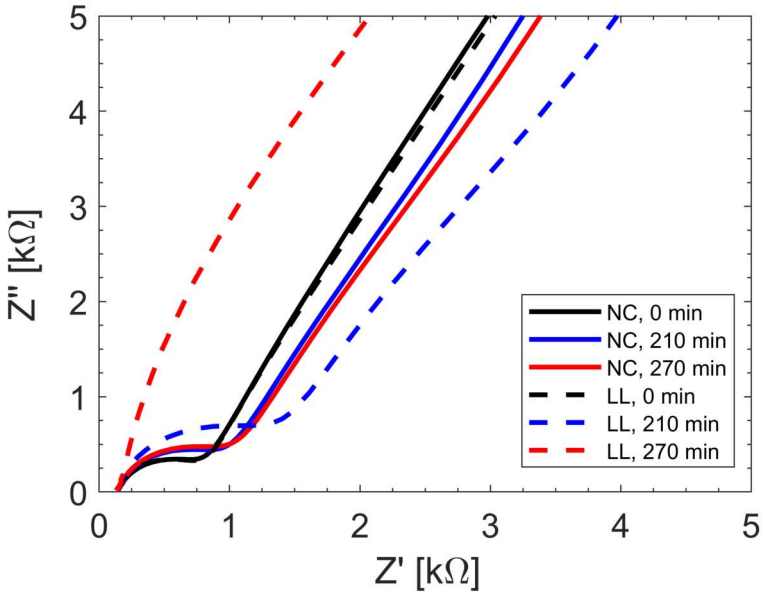


Figure 4.30: Spill-Out method: Nyquist diagram, characterisation of DRP-C223AT with *L.Lactis* in solution.

From the Nyquist diagram (figure 4.30), the negative control sensor shows the same behaviour for more or less the entire duration of the experiment. In the sensors on which the bacteria were deposited, up to 210 minutes, a clear increase in the amplitude of the Randle cell semicircle can be seen, which indicates an increase in

the charge transfer resistance $R_{ct}$. At 270 minutes there is a change of the curve, the typical semi-circle of the Randle cell is no longer visible. This happens because there is a lot of bacteria deposited on top of the working electrode which prevents the passage of current. At this point, the system can no longer be described by Randle's model, and it is not possible to calculate the charge transfer resistance.

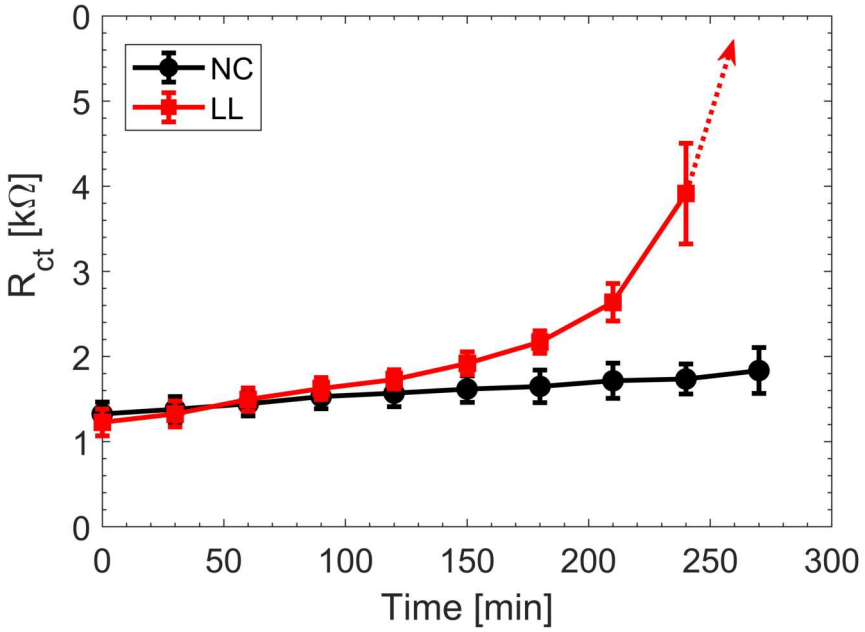


Figure 4.31: Spill-Out method: $R_{ct}$ normalized respect its initial value in function of time, characterisation of DRP-C223AT with *L.Lactis* in solution.

In the figure 4.31 the trend of $R_{ct}$ normalized with respect to the initial value is shown, which I will call $R^n_{ct}$, as the time of the experiment increases. These values (at the i-th time $t_i$) were obtained by using the following formula:

$$R^n_{ct}(t_i) = \frac{R_{ct}(t_i)}{R_{ct}(t_0)} \tag{4.3}$$

From the figure 4.31, the $R_{ct}$, in the sensor on which the solution without bacteria was deposited, shows a growth trend, but still much less than in the sensor on which the solution containing the bacteria was deposited. In fact, at 270 minutes, the negative control is 1.2 times the intial value of $R_{ct}$, while in the sensor with

bacteria is 2 times higher. The readings of the electrochemical system are consistent with the absorbance readings.

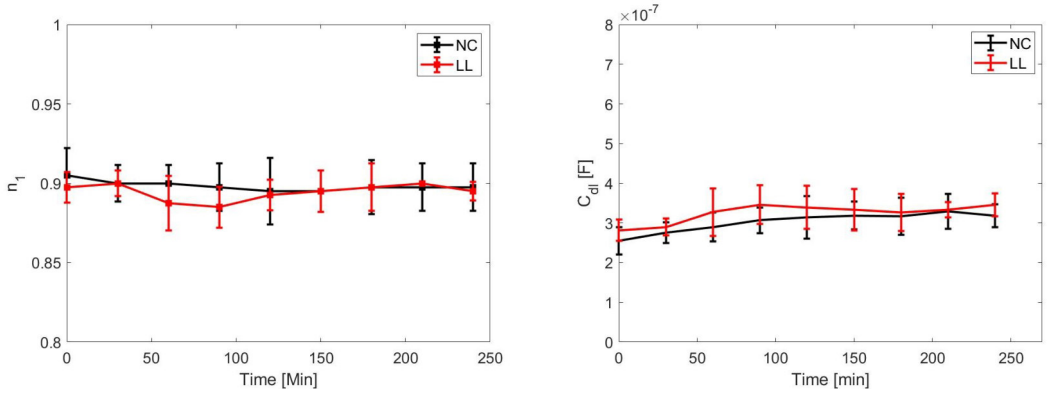


Figure 4.32: Spill-Out method:$C_{dl}$ and $n_1$ in function of time, characterisation of DRP-C223AT with *L.Lactis* in solution.

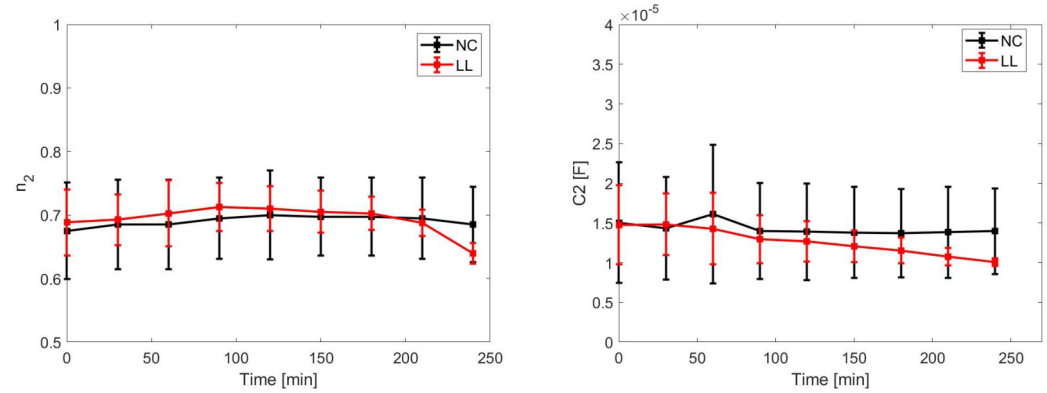


Figure 4.33: Spill-Out method: $CPE2$ and $n_2$ in function of time, characterisation of DRP-C223AT with *L.Lactis* in solution.

In the figures 4.34, 4.32 and 4.33, the resistance $R_s$, the $C_{dl}$ (base $C_{dl}$ and exponent $n_1$) and the $CPE$ (base $CPE$ and exponent $n_2$) are represented as a function of the time of the experiment. From the overall trend of the graphs, it can be seen that the electrical parameters remain stable, whether or not *L.Lactis* is present in the solution. As it can be seen above, the only parameter that varies substantially in relation to bacterial growth is the charge transfer resistance $R_{ct}$, therefore I

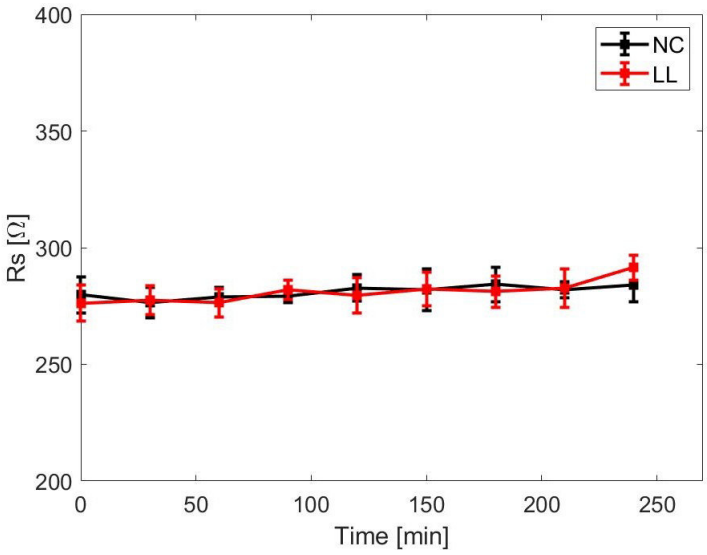


Figure 4.34: Spill-Out method: $R_s$ in function of time, characterisation of DRP-C223AT with *L.Lactis* in solution.

can use this parameter for the detection of bacteria in solution. In addition, the phase difference $\phi$ at 400 Hz has also shown to be a good parameter, as it also decreases as the number of *L.Lactis* increases. In the light of the obtained results, I demostrate that the DRP-C223AT are able to identify the presence of *L.Lactis* in solution, with Spill-Out protocol.

## 4.5 Stability with phage buffer

The phages are stored in a refrigerator in a saline solution called phages buffer. Before adding the phages to the solution, it is necessary to characterise the behaviour of the sensor in the presence of the phages buffer, because this presence in solution could change the performance of the device or even affect bacterial growth. The following solutions were used:

| | **Negative Control** | **L.Lactis** | **Phage Buffer** |
|---|---|---|---|
| Buffer | $480\mu L$ | | $480\mu L$ |
| *L.Lactis* OD=0.5 | | $1200\mu L$ | $1200\mu L$ |
| 20mM FeCN in M17 | $3000\mu L$ | $3000\mu L$ | $3000\mu L$ |
| M17 | $2520\mu L$ | $1800\mu L$ | $1320\mu L$ |
| **Total Volume** | $6000\mu L$ | $6000\mu L$ | $6000\mu L$ |

Table 4.3: Solution composition, characterisation of DRP-C223AT with Phage Buffer in solution.

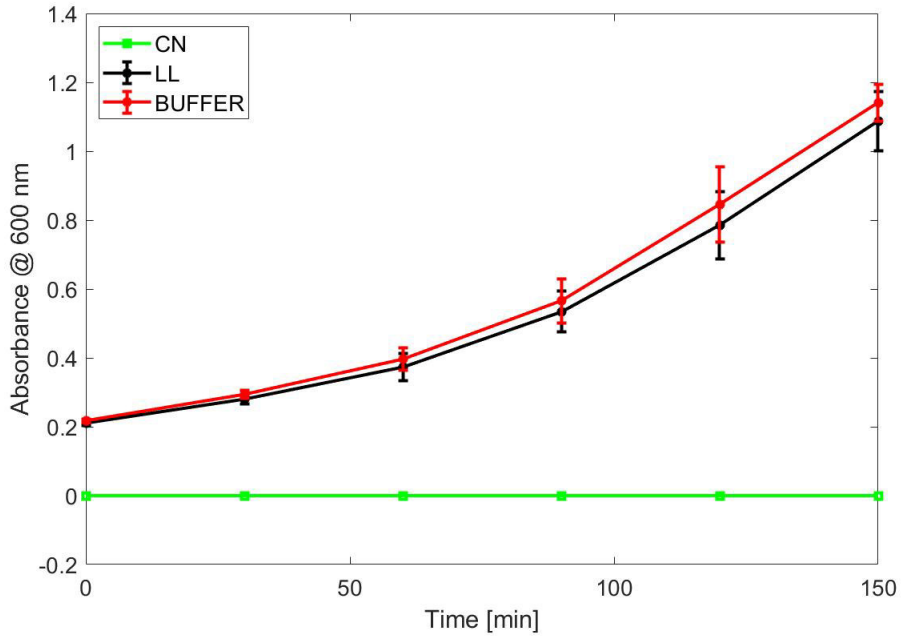


Figure 4.35: OD (600 nm) in function of time, characterisation of DRP-C223AT with phage buffer in solution.

The solutions were made up using the same methodology as in the previous experiment. Measurements were collected every thirty minutes throughout the duration of the experiment. The absorbance was calculated using the absorbance of the M17+FeCN+Phage Buffer solution as the zero value. The figure 4.35 shows the varation of absorbance over time. All the curves in which bacteria are present, show a similar growth trend, the bacterial growth is not inhibited by the presence of phage buffer in solution.

For a better visualisation, I show in the Bode diagrams (figures 4.36 and 4.37) and in the Nyquist diagram (figure 4.38) only the measurements at time 0, at 90 minutes and 150 minutes.

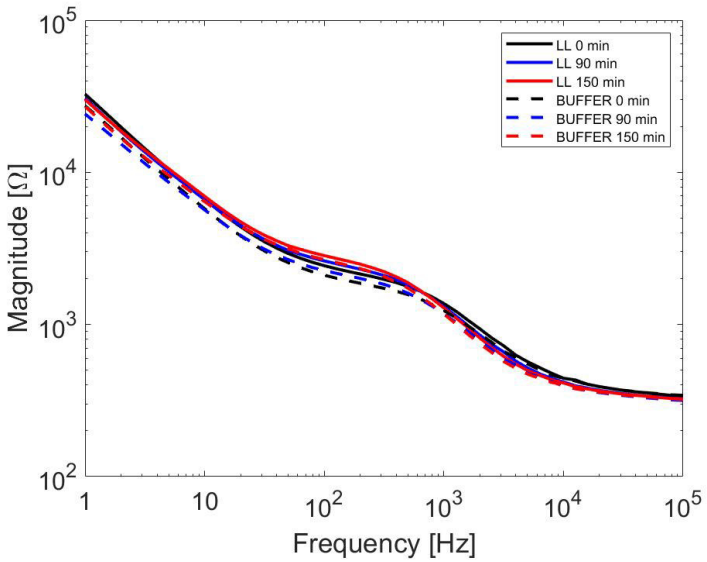


Figure 4.36: Nyquist Diagram, characterisation of DRP-C223AT with Phage Buffer in solution.

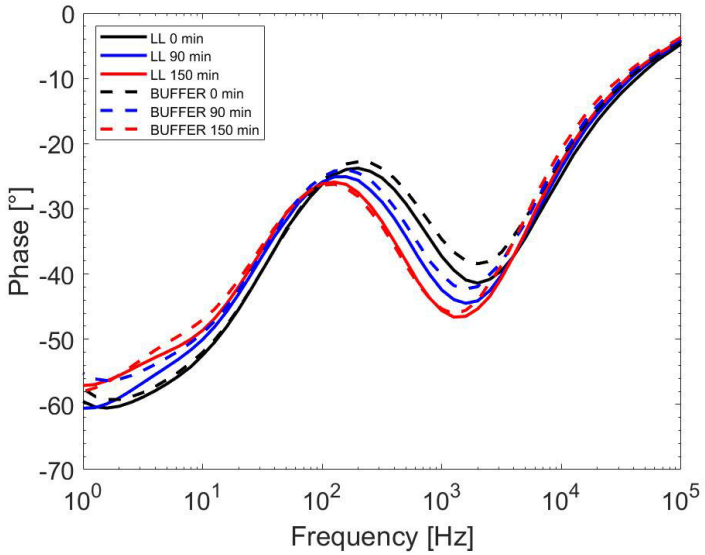


Figure 4.37: Nyquist Diagram, characterisation of DRP-C223AT with Phage Buffer in solution.

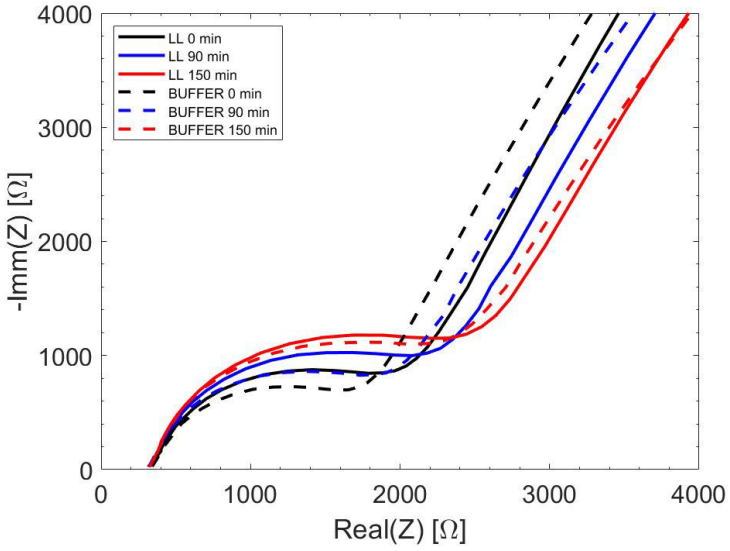


Figure 4.38: Nyquist Diagram, characterisation of DRP-C223AT with Phage Buffer in solution.

In the Bode diagrams there are similar trends in both sensors: the magnitude remains unchanged, the impedance tends to increase over time at low frequencies; the phase presents the already noted shift with the passage of time between $\omega = 10^3$ and $\omega = 10^4$. In the Nyquist diagram the behaviour of the two sensors is also similar; as the time of the experiment passes, and therefore as the number of bacteria in solution increases, there is an increase in the semicircle, indicating an increase of the charge transfer resistance.

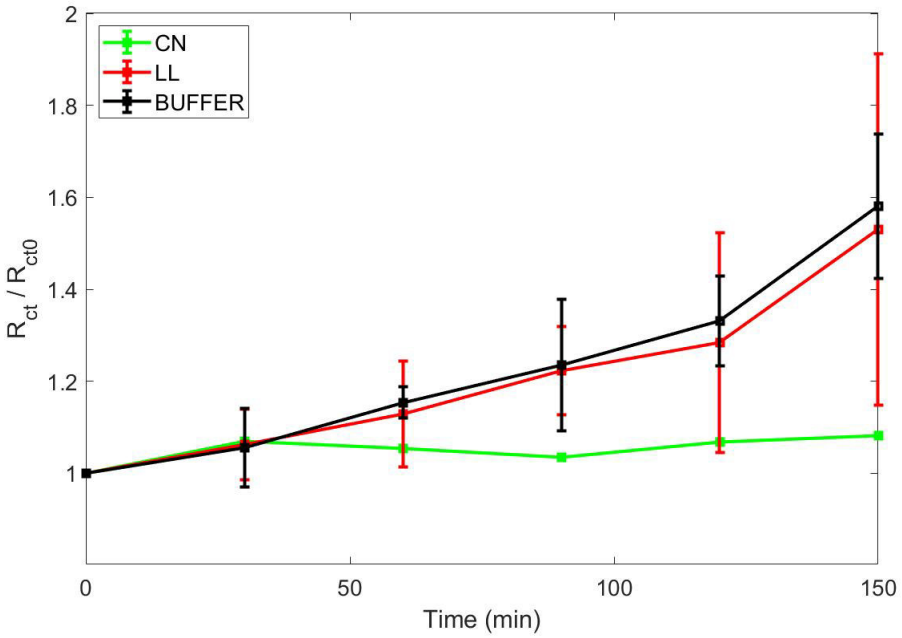


Figure 4.39: $R_{ct}$ in function of time, characterisation of DRP-C223AT with Phage Buffer in solution.

The figure 4.39 illustrates the evolution in time of normalized charge transfer resistance with respect to the initial value $R^n_{ct}$, calculates using the formula 4.3. The $R_{ct}$ of the negative control sensor remains roughly stable throughout the experiment, confirming the slightly increasing trend noted in previous tests, $R_{ct}$ becomes approximately 1.08 times respect to the initial value. In the other sensors, whether buffer is present or not, there is a substantial increase in the resistance to charge transfer. The trend of the curves is consistent with the OD obtained values.

As in the unbuffered characterisation, I focus on the phase at 400 Hz. Figure 4.40 shows the variation of phase $\Delta\phi$ at 400 Hz in function of time. These values at time i is obtained by the difference between the phase at time i $\phi_i$ and the phase at time zero $\phi_0$. Where the bacteria are not present the phase changes from the initial value by about three degrees. The presence of buffer does not affect the phase variation. The phase variation at 400 Hz is also shown in the presence of buffer to be a sensitive parameter for the growth of *L.Lactis* in solution.

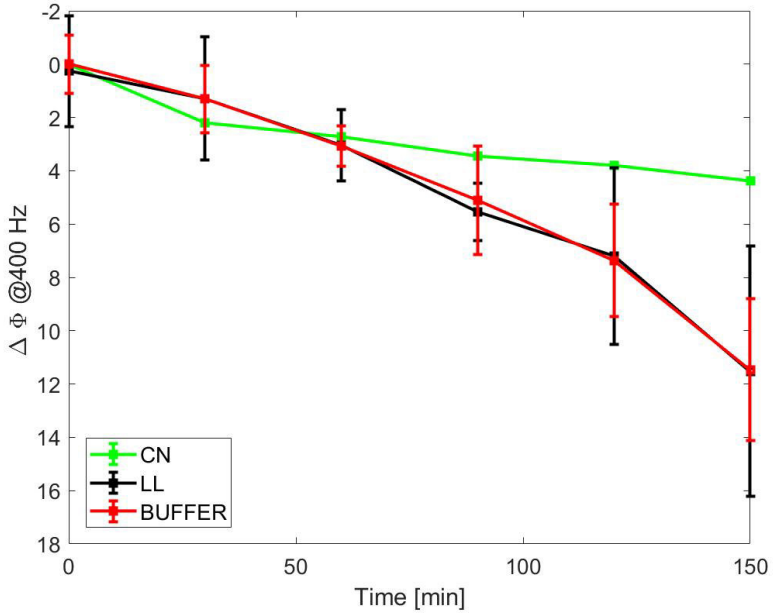


Figure 4.40: Variation of phase at 400 Hz $\Delta\phi$ in function of time, characterisation of DRP-C223AT with Phage Buffer in solution.

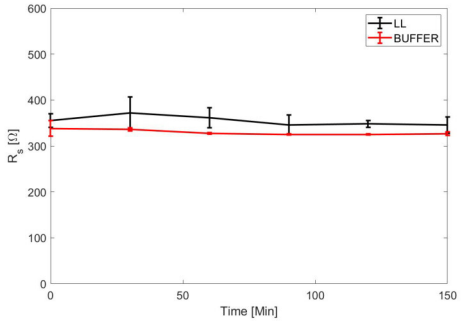


Figure 4.41: $R_s$ in function of time, characterisation of DRP-C223AT with Phage Buffer in solution.

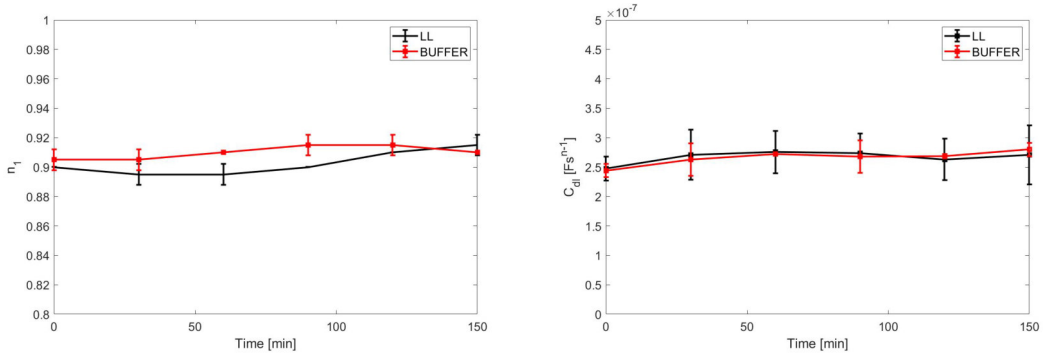


Figure 4.42: $Y_{C_{dl}}$ and $n_1$ in function of time, characterisation of DRP-C223AT with *L.Lactis* in solution. Spill-Out method.

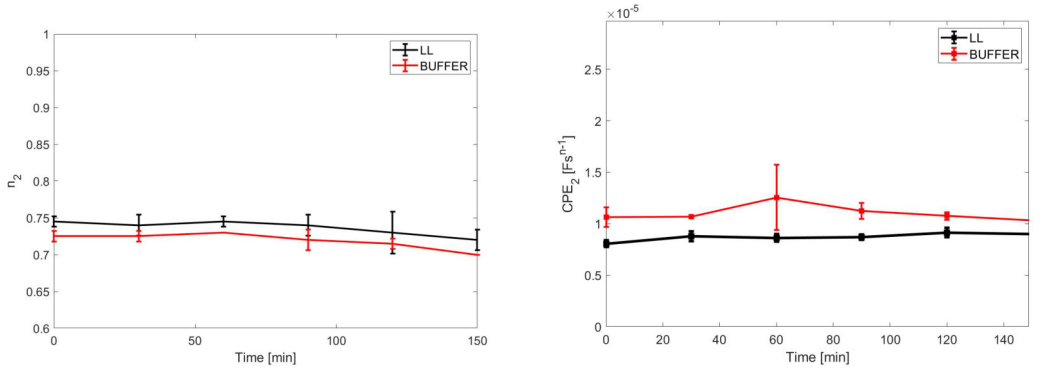


Figure 4.43: $Y_{CPE2}$ and $n_2$ in function of time, characterisation of DRP-C223AT with *L.Lactis* in solution. Spill-Out method.

In the figures 4.41, 4.42 and 4.43, the resistance $R_s$, the $C_{dl}$ and the $CPE2$ are represented as a function of the time of the experiment. All circuit parameters except for $R_{ct}$, as seen above, remain constant over time in both the unbuffered and buffered sensor cases. For all electrical parameters there is no obvious difference between sensors with and without buffer. I can say that the presence of the phage buffer does not affect our electrochemical system and does not change the ability of our sensor to detect *L.Lactis*. I am ready to verify whether or not my device are able to discirminate the presence of phage in my test solution.

## 4.6 Biosensing of *L.Lactis* Phages

I proceeded to characterise the device in the presence of bacteriophages in solution. The addition of phages in solution should lead theoretically to bacterial lysis and consequently $R_{ct}$ should be lower respect to a sample without phages, where bacteria are free to proliferate. The solutions used were as follows:

| | **Negative Control** | ***L.Lactis*** | **Phages** |
|---|---|---|---|
| Phages | | | $240\mu L$ |
| Buffer | $480\mu L$ | $480\mu L$ | $240\mu L$ |
| *L.Lactis* | | $1200\mu L$ | $1200\mu L$ |
| 20mM FeCN in M17 | $3000\mu L$ | $3000\mu L$ | $3000\mu L$ |
| M17 | $2520\mu L$ | $1800\mu L$ | $1320\mu L$ |
| **Total Volume** | $6000\mu L$ | $6000\mu L$ | $6000\mu L$ |

Table 4.4: Solution composition, characterisation of DRP-C223AT with M17, $[Fe(CN)_6]^{3-/4-}$, *L.Lactis* and phages.

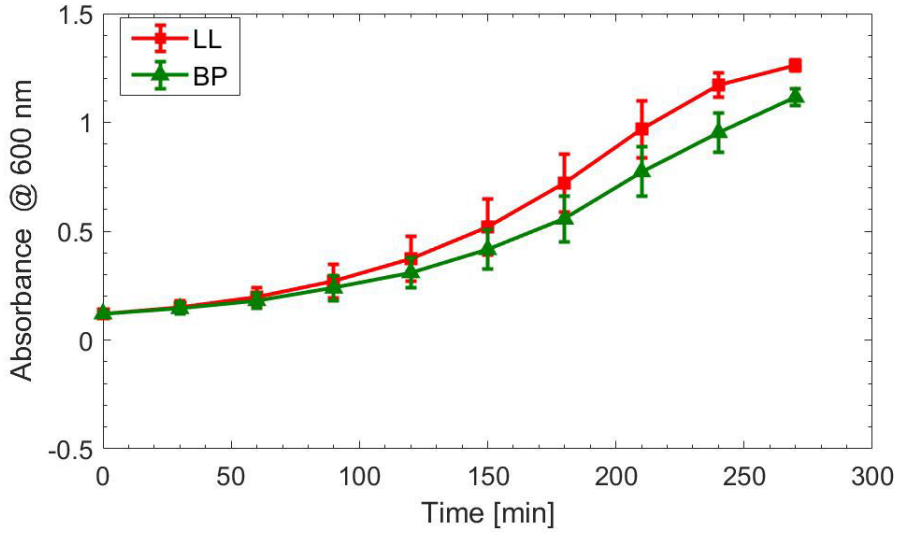


Figure 4.44: OD (600nm) in function of time, characterisation of DRP-C223AT with M17, $[Fe(CN)_6]^{3-/4-}$, *L.Lactis* and phages.

In the figure 4.44 is reported the evolution of the bacterial growth in absorbance. Absorbance measurements were carried out using the negative control solution as zero-base. Absorbance measurements of the negative control are not shown in the figure because it is always stable equal to 0. For the first minutes of the experiment there is not much difference between the curve with only *L.Lactis* and the curve containing *L.Lactis* and phage. Up to 150 minutes, the growth rate of the bacteria is much higher than the phage activity, so the curves grow in a similar way. About 100 minutes into the experiment, the curve begins to increase in slope, changing from a straight line to an exponential trend. This behaviour is consistent with what was expected in theory. At minute 150, the curves begin to distance themselves. This indicates that phage activity has begun and is visibly slowing down bacterial growth, but not inhibiting it completely. After 240 minutes, the curves decrease in slope, reaching a sort of platou, the numbers of bacteria are stationary. However, there is a clear difference between the OD of solutions containing bacteria and solutions containing only phages.

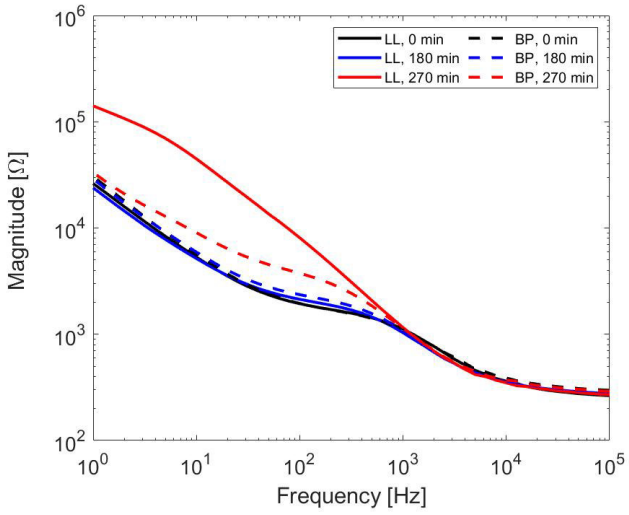


Figure 4.45: Modulus of Bode diagram, characterisation of DRP-C223AT with M17, $[Fe(CN)_6]^{3-/4-}$, *L.Lactis* and phages.

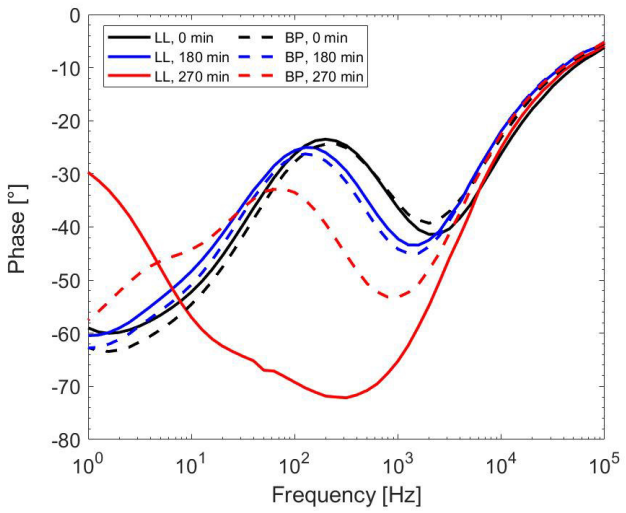


Figure 4.46: Phase of Bode diagram, characterisation of DRP-C223AT with M17, $[Fe(CN)_6]^{3-/4-}$, *L.Lactis* and phages.

From the modulus of impedance as a function of acquisition frequency (figure 4.45), at minute 270 there is an increase of one order of magnitude in the impedance at low frequencies in the sensor which contains only bacteria (red continuos curve), compared to the detection at time zero (black continuos curve). The increase is also noticeable where phages are present, however it is much smaller (dashed red curve) than the increase with only bacteria. At high frequencies the curves are all overlapping, either at different times, with only bacteria or bacteria and phages. As I already noted during the bacterial-only characterisation, the phase (figure 4.46) shows a shift, as time varies, between $10^2$ and $10^3$, for both sensors. But if there is a kind of explosion of the curve where only bacteria are present (continuous red curve) this effect is not observed where phages are present (dashed red curve).

In the figure 4.47 I represent the Nyquist diagram. At minute 270 the semicircle has completely disappeared in the sensors on which the bacteria-only solutions were deposited: the bacteria deposited on the impedance are so many that they block the electron transfer, the curve follows the pattern described above without the RedOx mediator. At the same time, in sensors where phages are present, the

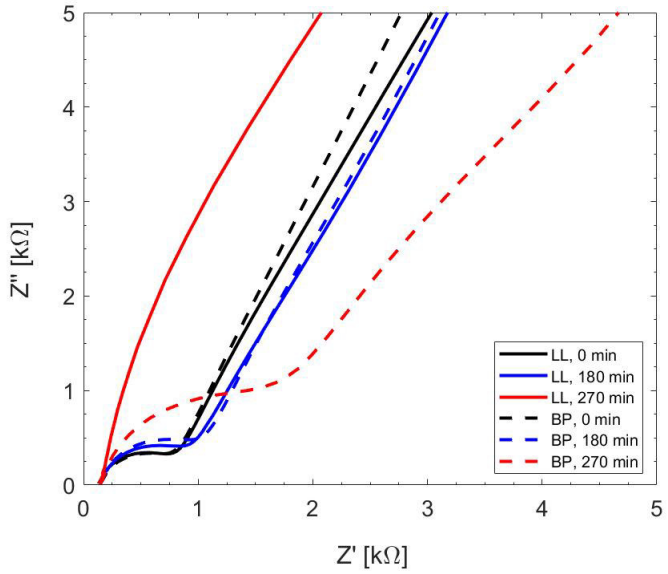


Figure 4.47: Nyquist Diagram, characterisation of DRP-C223AT with M17, $[Fe(CN)_6]^{3-/4-}$, *L.Lactis* and phages.

curves show a larger semicircle as time increases, but there is no real explosion of the curve as in the previous case, it is still possible to calculate the charge transfer resistance.

In the figure 4.48 is shown the trend of $R_{ct}$ normalized with respect to the initial value $R^n_{ct}$ calculated with 4.3. From the figure 4.48 the curve, on which the negative control has been deposited, remain more or less constant with the passage of time, there is no noticeable increase in $R_{ct}$, in according to what I found in my stability test. In the other curves, in which the bacteria are present, there is a substantial increase in the ratio with the passage of time. The bacterial growth observed by the absorbance measurements is therefore confirmed also in electrochemistry. From minute 180 there is a clear division between the curves containing only bacteria and the curves containing phages, a sign that phage lysis activity is taking place, a fact also confirmed by the values obtained in absorbance. At 240 minutes the $R^n_{ct}(t_i)$ in the sensors on which the bacteria have been deposited

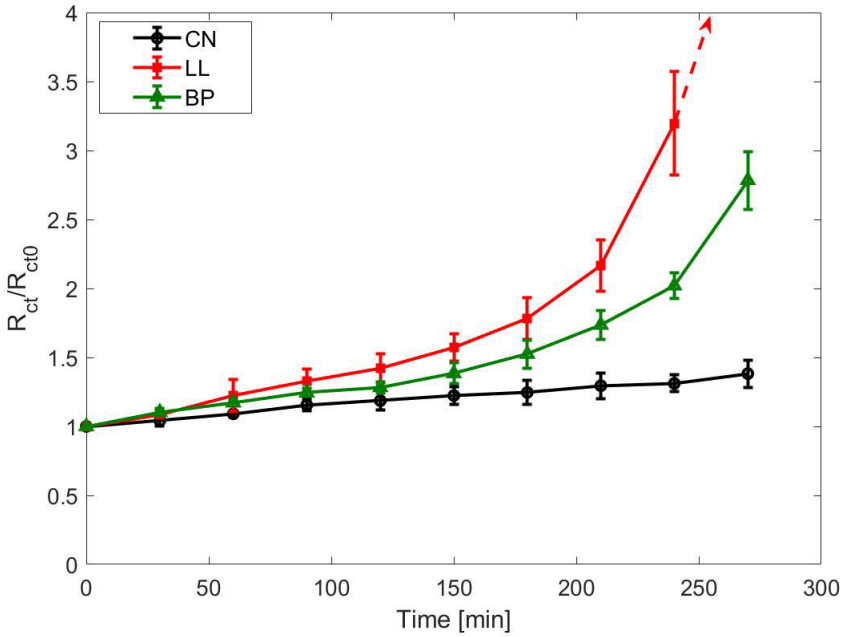


Figure 4.48: $R_{ct}^{n}$ in function of time, characterisation of DRP-C223AT with M17, $[Fe(CN)_6]^{3-/4-}$, *L.Lactis* and phages.

is almost 3, indicating that the $R_{ct}$ has increased almost three times compared to its initial value, while in the sensors with the phages the ratio is about 2. I can therefore say that the $R_{ct}$ is a good sensing parameter, as it is sensitive to bacterial growth and phage lysis.

As done previously, I evaluate the phase variation at $\omega = 400$ Hz, and as can be seen from the figure 4.49, I obtaine consistent results with both optical density and charge transfer resistance readings. The phase shows small variation in the negative control sensor, exhibiting a slight tendency to decrease with time. Similar to $R_{ct}$, in sensors with bacteria, there is a similar trend in phase for the first few minutes of the experiment, the phase gradually decreasing as the bacteria grow. As time progresses, and thus as the bacteria grow in solution, the phase decreases, but the presence of the phages in solution slows this effect. At both 240 minutes and 270 minutes there is a clear division of the curves. Phase has also been shown to be a good parameter for detecting both bacterial growth and the presence of

phages in solution.

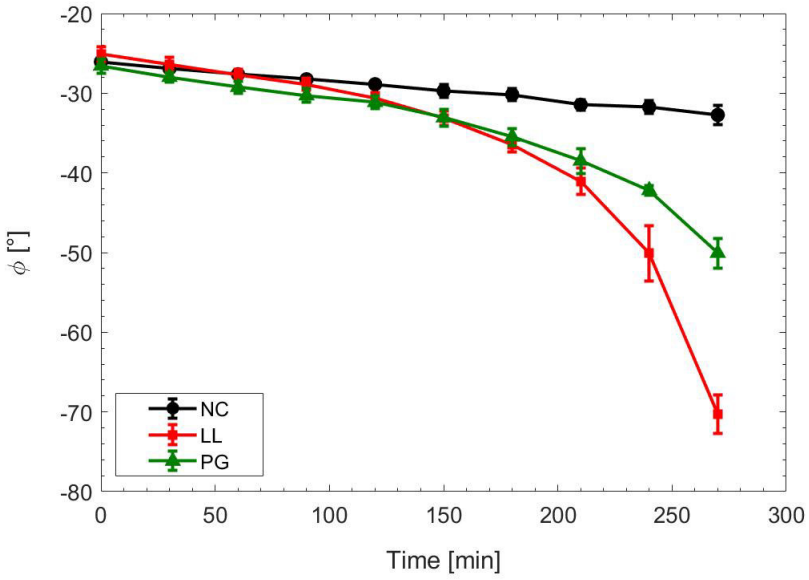


Figure 4.49: Phase at 400 Hz in function of time, characterisation of DRP-C223AT with M17, $[Fe(CN)_6]^{3-/4-}$, *L.Lactis* and phages.

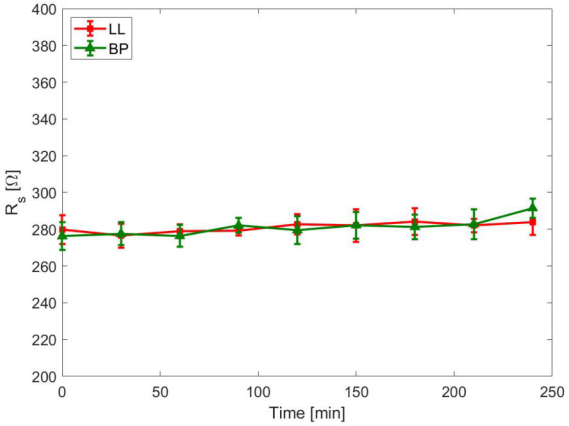


Figure 4.50: $R_s$ in function of time, characterisation of DRP-C223AT with M17, $[Fe(CN)_6]^{3-/4-}$, *L.Lactis* .

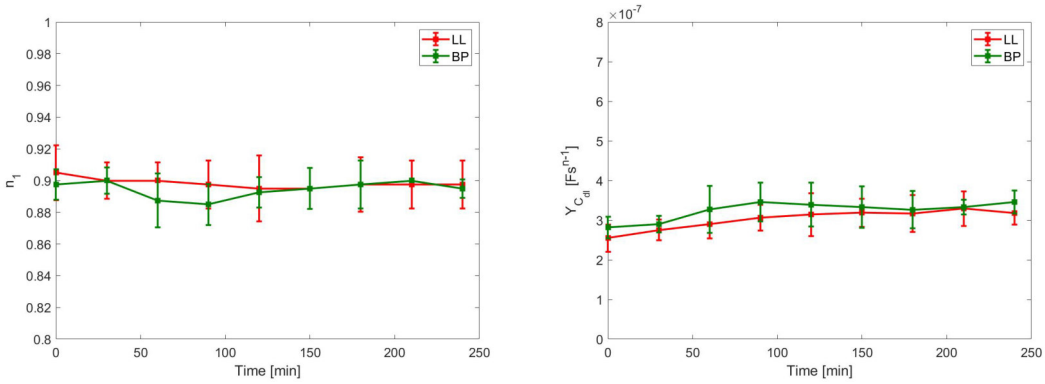


Figure 4.51: $Y_{C_{dl}}$ and $n_1$ in function of time, characterisation of DRP-C223AT with M17, $[Fe(CN)_6]^{3-/4-}$, *L.Lactis* and phages.

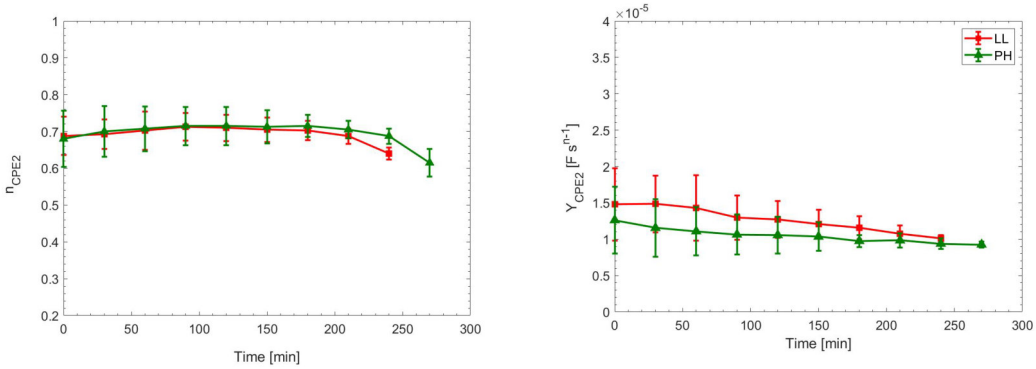


Figure 4.52: $Y_{CPE2}$ and $n_2$ in function of time, characterisation of DRP-C223AT with M17, $[Fe(CN)_6]^{3-/4-}$, *L.Lactis* and phages.

In the figures 4.50, 4.51 and 4.52, the resistance $R_s$, the $C_{dl}$ (base $Y_{dl}$ and exponent $n_1$) and the $CPE2$ (base $Y_{CPE}$ and exponent $n_2$) are represented as a function of the time of the experiment. All circuit parameters, except for the charge transfer resistance, show the same trend over the time despite the presence or not of phages in solution. I am able to detect successfully the presence of *L.Lactis* phages in solution through two parameters:

- The variation of charge transfer resistance in function of time.
- The phase variation at 400 Hz in function of time.

## 4.7 Response with different phages concentration

I continued by testing the performance of the device with different phage concentrations. I used three different phage concentrations: $10^9$ UFP, $10^8$ UFP and $10^7$ UFP. The solutions used were as follows:

| | **LL** | **9 UFP** | **8 UFP** | **7 UFP** |
|---|---|---|---|---|
| Phages $10^9$ UFP | | 240 $\mu L$ | | |
| Phages $10^8$ UFP | | | 240 $\mu L$ | |
| Phages $10^7$ UFP | | | | 240 $\mu L$ |
| Buffer | 480 $\mu L$ | 240 $\mu L$ | 240 $\mu L$ | 240 $\mu L$ |
| *L.Lactis* OD=0.5 | 1200 | 1200 $\mu L$ | 1200 $\mu L$ | 1200 $\mu L$ $\mu L$ |
| 20 mM FeCN in M17 | 3000 $\mu L$ | 3000 $\mu L$ | 3000 $\mu L$ | 3000 $\mu L$ |
| M17 | 1320 $\mu L$ | 1320 $\mu L$ | 1320 $\mu L$ | 1320 $\mu L$ |
| **Total Volume** | 6000 $\mu L$ | 6000 $\mu L$ | 6000 $\mu L$ | 6000 $\mu L$ |

Table 4.5: Solution composition, characterisation of DRP-C223AT with M17, $[Fe(CN)_6]^{3-/4-}$, *L.Lactis* and phages at different concentration.

The solutions were composed following the same methodology used in previous experiments. These tests were carried out using the potentiostat "EmStat Pico". The parameters of the EIS measure were as follows: frequency range [100kHz-1Hz]; number of points per decade 10; $V_{DC}$ corresponding to the potential $E_0 = 0.091V$; potential $V_{AC}$ fixed at $10mV$. I carried out a pretest to check that the sensors all had the same behaviour. For the pretest I used a solution composed as follows:

| **20 mM FeCN in M17** | **Phage Buffer** | **M17** | **Total Volume** |
|---|---|---|---|
| 500 $\mu L$ | 40 $\mu L$ | 460 $\mu L$ | 1000 $\mu L$ |

Table 4.6: Pretest solution composition, characterisation of DRP-C223AT with M17, $[Fe(CN)_6]^{3-/4-}$, *L.Lactis* and phages at different concentration.

I had to partially modify the spill-out protocol:

1. Wash with milliQ water;
2. Dry with jet air;
3. Deposition of $90\mu L$ of solution;
4. Carry out OD measurement;
5. Wait 15 minute;
6. EIS measurements;
7. Remove the drop;
8. Wash with milliQ water and dry with jet air;
9. Wait 60 minute;
10. Repeat from 3 to 9.

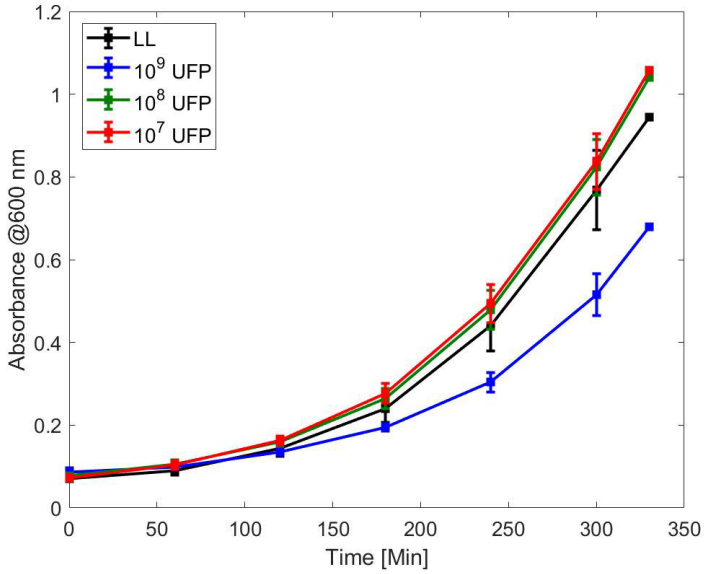


Figure 4.53: OD (600nm) in function of time, characterisation of DRP-C223AT with M17, $[Fe(CN)_6]^{3-/4-}$, *L.Lactis* and phages at different concentration.

I made an additional measurement at 330 minutes after the start of the experiment. The absorbance value of the pre-test solution was used as the zero value. In this experiment, I started with a slightly lower concentration of bacteria at time 0 respect the previous experiment. In the first 120 minutes the bacteria grow very slowly compared to previous experiments, as can be seen from the OD values reached in all the sensors, which never exceed 0.2, while in the last experiment at 120 minutes I had already reached an OD of 0.3 or even higher. From the figure 4.53, where no phages are present (black curve) the bacterial growth follows the theoretical curve, presenting a linear growth phase up to 120 minutes and then entering an exponential growth phase. In this experiment, the plateau of the curve is not reached despite 330 minutes of the experiment. This effect is linked to the low initial bacterial concentration. The bacteria started with a lower concentration than in previous experiments and consequently their growth was delayed. The trend of the curves is similar until the 180th minute, from there is a marked slowdown in growth in the blue curve, representing the sensor on which the solution containing the highly concentrated phages has been deposited. The same phenomenon does not occur for lower phage concentrations. In fact, the green and the red curves behave similarly to the black curves, where no phage is present. This phenomenon may be closely linked to the fact that bacterial growth is too slow. In fact, the bacteria have grown too little to prevent viral replication in the early stages of the experiment. Slow growth may be due to the initial concentration of bacteria or other environmental factors such as the temperature of the environment.

From the modulus of impedance as a function of frequency (figure 4.54), at 330 minutes there is a slight increase in impedance at 0 Hz, for all sensors regardless of whether phages are present or not. The phase (figure 4.55) show the usual shift between $10^2$ and $10^3$ between the measurement at time zero (solid lines) and at the 330th minute (dashed lines). The curves at the same time, irrespective of whether or not phages are present in solution, show a similar trend and are almost completely superimposable. In the figure 4.56 I report the Nyquist diagrams of the measurements at time 0 and time 330 for each sensor. As expected, there is an increase of the semicircle in all curves, indicating an increase of $R_{ct}$. In contrast to

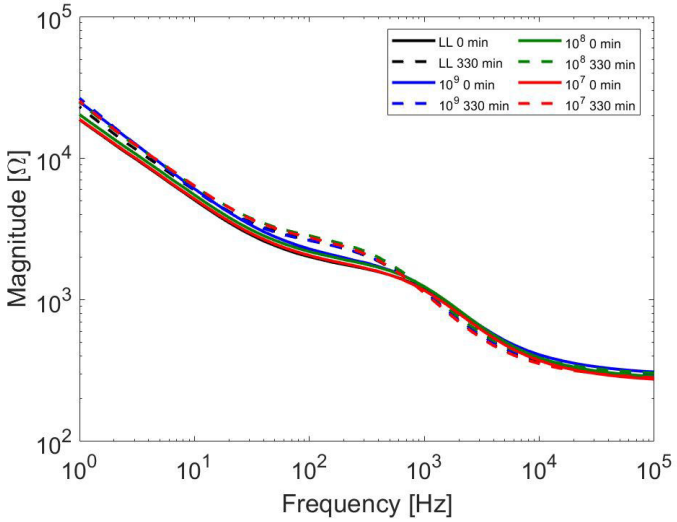


Figure 4.54: Modulus of Bode Diagram, characterisation of DRP-C223AT with M17, $[Fe(CN)_6]^{3-/4-}$, *L.Lactis* and phages at different concentration.

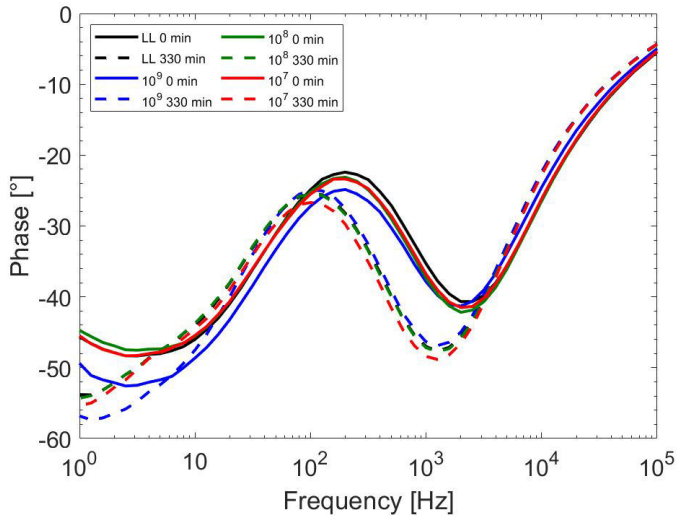


Figure 4.55: Phase of Bode Diagram, characterisation of DRP-C223AT with M17, $[Fe(CN)_6]^{3-/4-}$, *L.Lactis* and phages at different concentration.

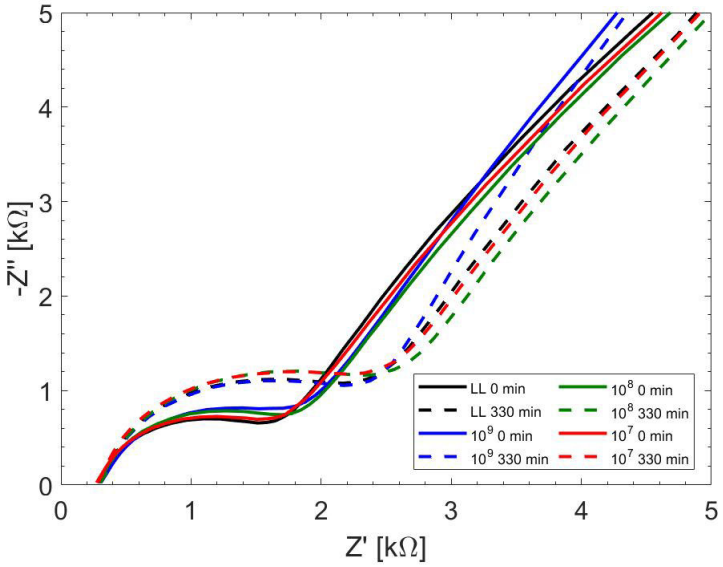


Figure 4.56: Nyquist diagram, characterisation of DRP-C223AT with M17, $[Fe(CN)_6]^{3-/4-}$, *L.Lactis* and phages at different concentration.

the previous experiment, I am not able to visually distinguish the phage activity, since the low bacterial growth did not lead to an explosion of the curve, despite the long running time of the experiment.

The figure 4.57 shows the normalized charge transfer resistance $R_{ct}^n$ obtained through the formula 4.3. The trend is similar in all sensors for almost the entire duration of the experiment. This fact confirms what I saw in the absorbance, the bacterial growth is very slow in time and even after 300 minutes of experiment there is not a high concentration of bacteria, consequently I do not have the explosion of $R_{ct}$. At 300 minutes the phage activity seems not to occur for the lower phage concentrations, as seen in absorbance, the curves all grow in a similar way. While in absorbance there is for the solutions containing the highest concentration phages a slowdown in OD, between 180 and 240 minutes from the start of the experiment. There is a slowdown in the growth of $R_{ct}$ but not as noticeable as that seen in the previous experiment. At minute 300, for the sensors without phage I

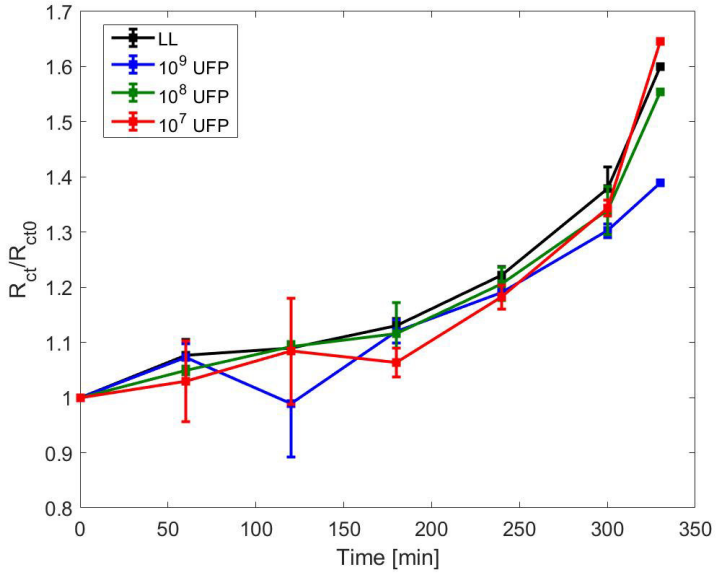


Figure 4.57: $R_{ct}^{n}$ in function of time, characterisation of DRP-C223AT with M17, $[Fe(CN)_6]^{3-/4-}$, *L.Lactis* and phages at different concentration.

obtain an average increase of 1.38 times from the initial value, while I obtain an average increase of 1.30 from the initial value for the sensors on which the highest concentration of phage was deposited. Observing the behaviour at 330 minutes there is a clear difference between the curves, in fact the blue curve appears much lower than the others.

The phase at 400 Hz also behaves similarly to the charge transfer resistance in this case. The figure (4.58) show the phase variation $\Delta\phi$ in function of time. All sensors show a decreasing phase trend as the experimental time increases. If this trend is entirely similar between the sensor with the bacteria and the sensors with the phages at the lowest concentrations, there is less phase variation in the sensor on which the solution with the highest concentration of bacteria has been deposited.
This experiment do not leave me entirely satisfied. I expect that as the number of phages in solution increases, I would first get a lower absorbance and consequently a lower increase in $R_{ct}$. In absorbance it is clearly seen that no inhibition of bacterial growth occurs. I exclude that this behaviour is due to the type of solutions

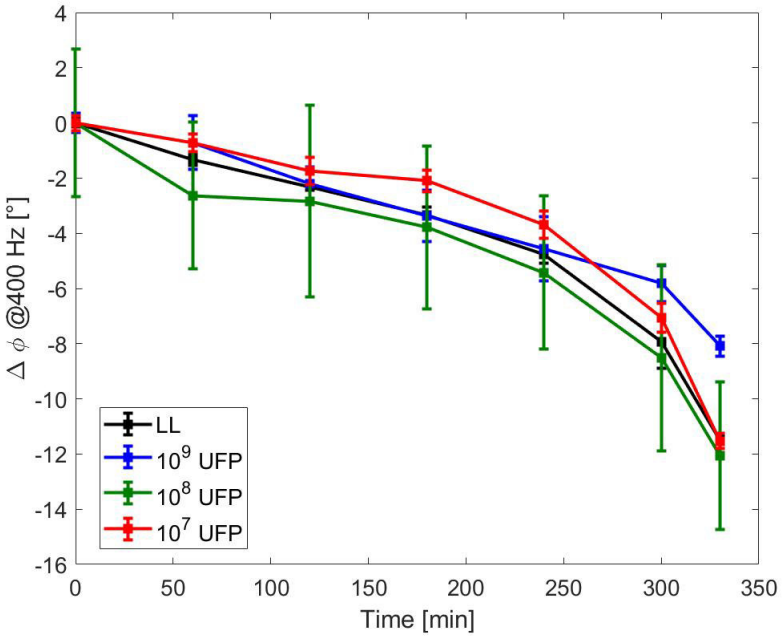


Figure 4.58: Variation of phase at 400 Hz $\Delta\phi$ in function of time, characterisation of DRP-C223AT with M17, $[Fe(CN)_6]^{3-/4-}$, *L.Lactis* and phages at different concentration.

used, since in previous experiments, with a concentration of between $10^7 UFP$ and $10^8 UFP$, I was able to observe both in absorbance and in electrochemistry bacterial lysis. Could this behaviour be due to the experimental conditions?

In fact, both bacterial growth and phagic activity are affected by a number of environmental factors, such as light radiation, temperature, humidity and osmotic pressure. In addition, bacterial growth can be promoted by shaking the cuvette. In order to control all these environmental factors, especially the operating temperature, future tests will be carried out by placing the cuvettes in a static incubator at 25°C. The cuvette containing the solution to be deposited is removed from the incubator just in time to take the solution and measure its absorbance, trying to shake it as little as possible. Inside the incubator, the cuvettes are covered with parafilm in order to prevent any kind of evaporation phenomenon, which would lead to an increase in $[Fe(CN)_6]^{3-/4-}$ concentration and consequently to an in-

correct measurement.

However, even though this experiment does not go as hoped, I am still able to demonstrate that my device can detect the presence of phage in an ideal solution. I was able to detect this with two parameters: the $R_{ct}$ and the phase change at 400 Hz. I can move on to testing the device by adding milk samples to the solution, checking the behaviour of my device under working conditions close to a real sample.

# Chapter 5

# Experimental tests with milk samples

## 5.1 First characterisation with milk in solution

I proceeded to characterise the device in the presence of milk in solution. The composition of the solution used was as follows:

| **Milk** | **20 mM FeCN in M17** | **M17** | **Total Volume** |
|---|---|---|---|
| 80 $\mu L$ | 500 $\mu L$ | 420 $\mu L$ | 1000 $\mu L$ |

Table 5.1: Solution composition, characterisation of DRP-C223AT with M17, $[Fe(CN)_6]^{3-/4-}$ and milk.

Before characterisation through EIS measurements, I carried out a cyclic voltammetry measurement to find the $E_0$ potential of the new solution. The potential $E_0$ was calculated by averaging the voltage of the two peaks of the measurement, the cathodic and the anodic, according to the formula 3.15. A potential $E_0 = 0.071V$ was obtained.

EIS measurements were carried out with the 'Solatron', monitoring two sensors in parallel, using the following parameters: frequency range [100kHz-1Hz]; number of points per decade 10; $V_{DC}$ corresponding to the potential $E_0 = 0.071V$; potential $V_{AC}$ fixed at $10mV$.

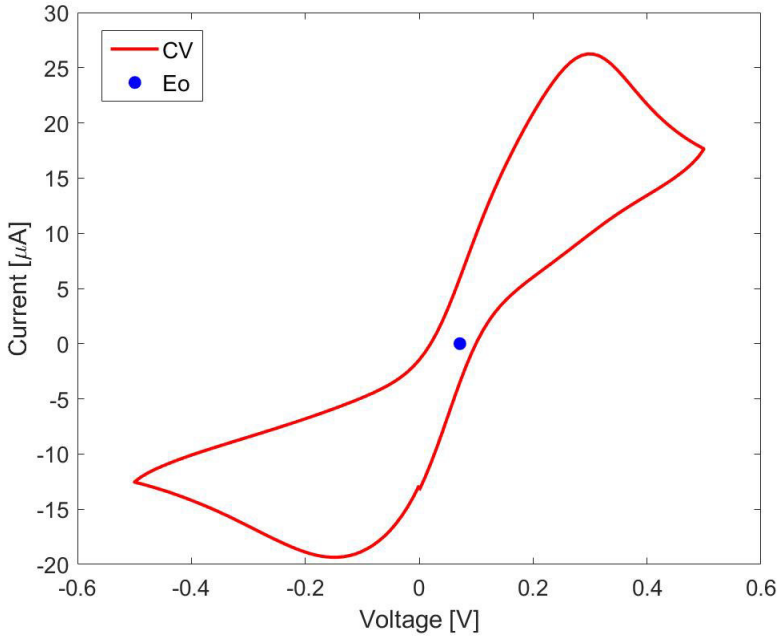


Figure 5.1: Cyclic voltammetry, characterisation of DRP-C223AT with M17, $[Fe(CN)_6]^{3-/4-}$ and milk.

I followed the Spill-out protocol but in this test measurements were taken at 0 minutes, 60 minutes, 140 minutes and 200 minutes after the start of the experiment.

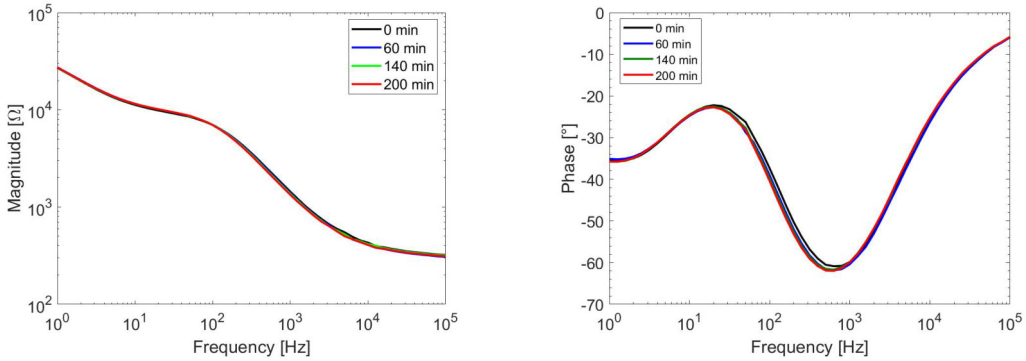


Figure 5.2: Bode diagram, characterisation of DRP-C223AT with milk in solution.

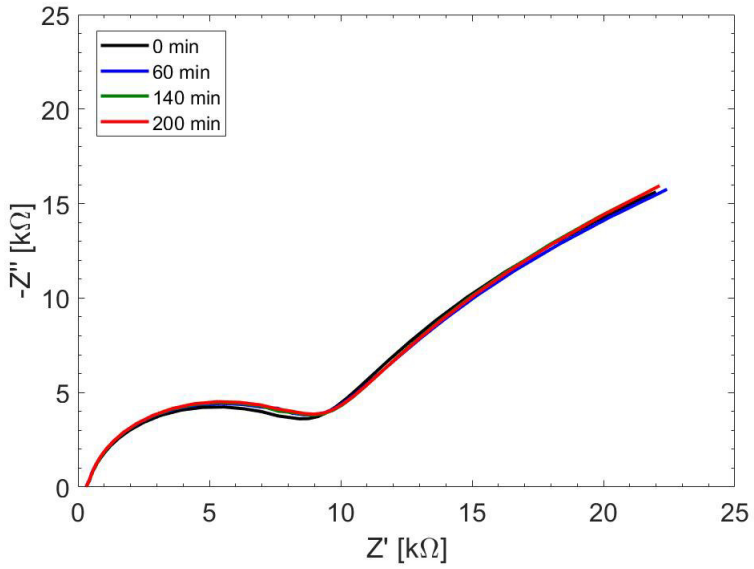


Figure 5.3: Nyquist diagram, characterisation of DRP-C223AT with milk in solution.

As can be seen from the Nyquist diagram 5.3 and Bode diagrams, the response of the sensor is stable at the drop change and in time, in fact the curves are almost superimposable. The table 5.2 shows the values of $R_{ct}$ and phase variation at 400 Hz, with the corresponding percentage errors. The $R_{ct}$ values are much larger than in previous experiments where milk was not present in solution. I am not particularly surprised by this value, in fact it is exactly what I expected. In fact, there are many different types of molecules in milk, such as proteins or fats, which

| **Time** | $R_{ct}$ [Ω] | **Err.** | $\phi$ **@400 Hz** [°] | **Err.** |
|---|---|---|---|---|
| **Min 0** | 8821,5 | 4,03 % | -58,1 | 1,72 % |
| **Min 60** | 9278,5 | 2,20 % | -59,6 | 1,51% |
| **Min 140** | 9482 | 1,40 % | -60,1 | 0,83% |
| **Min 200** | 9660,5 | 0,22 % | -60,6 | 0,49 % |

Table 5.2: Characterisation of DRP-C223AT with milk in solution: rilevazioni a 0, 60, 120 e 240 minuti di OD, $R_{ct}$ e $\phi(\omega = 400Hz)$

could have settled on the sensor and obstructed the passage of the current. The obtained $R_{ct}$ shows the increasing trend which I had also observed in the solutions without milk. There is minimal phase variation at 400 Hz, which is in agreement with what was observed in ideal solution without milk sample. The other circuit

| Time | $Y_{C_{dl}}$ $[Fs^{n-1}]$ | Err % | n1 | $Y_{CPE}$ $[Fs^{n-1}]$ | Err | n2 |
|---|---|---|---|---|---|---|
| 0 min | 2,72E-07 | 2,97E-08 | 0,89 | 1,64E-05 | 7E-08 | 0,6 |
| 60 min | 2,82E-07 | 2,12E-08 | 0,89 | 1,64E-05 | 0 | 0,6 |
| 140 min | 2,94E-07 | 2,12E-08 | 0,89 | 1,61E-05 | 7E-08 | 0,6 |
| 200 min | 2,97E-07 | 1,98E-08 | 0,89 | 1,59E-05 | 4E-07 | 0,6 |

Table 5.3: Characterisation of DRP-C223AT with milk in solution: values of $C_{dl}$ (base $Y_{C_{dl}}$ and exponent $n_1$) and $CPE2$ (base $Y_{CPE}$ and exponent $n_2$)

| Time | $R_s$ [Ω] | Err. % |
|---|---|---|
| Min 0 | 329 | 1,27 % |
| Min 60 | 319,5 | 1,09% |
| Min 140 | 329 | 0,42 % |
| Min 200 | 320 | 1,31 % |

Table 5.4: Characterisation of DRP-C223AT with milk in solution: values of $R_s$.

parameters, i.e. $R_s$ $C_{dl}$ and $CPE2$, also show stable behaviour as the time of the experiment passes. The errors associated with each measurement are very low, confirming the interchangeability between devices and the reproducibility of the measurement.

I proceeded to evaluate the response of the sensor by adding the *L.Lactis* to the solution with milk. I also decided to characterise the behaviour in the presence of phage buffer in solution. I used the four different solutions and monitored the behaviour of four sensors in parallel, following the well-known spill-out protocol. OD and EIS measurements were carried out at time 0, 60 minutes, 140 minutes and 200 minutes after the start of the experiment. Absorbance, at 600 nm, was measured using the solution containing milk and buffer (M+BF in the table **??**) as "zero".

| | **M** | **M+LL** | **M+BF** | **M+LL+BF** |
|---|---|---|---|---|
| **Milk** | 480 $\mu L$ | 480 $\mu L$ | 240 $\mu L$ | 240 $\mu L$ |
| **L.Lactis OD=05** | | 1200 $\mu L$ | | 1200 $\mu L$ |
| **Phage Buffer** | | | 240 $\mu L$ | 240 $\mu L$ |
| **20 mM FeCN in M17** | 3000 $\mu L$ | 3000 $\mu L$ | 3000 $\mu L$ | 3000 $\mu L$ |
| **M17** | 2520 $\mu L$ | 1320 $\mu L$ | 2520 $\mu L$ | 1320 $\mu L$ |
| **Total Volume** | 6000 $\mu L$ | 6000 $\mu L$ | 6000 $\mu L$ | 6000 $\mu L$ |

Table 5.5: Solution composition, characterisation of DRP-C223AT with M17, $[Fe(CN)_6]^{3-/4-}$, *L.Lactis* and milk.

| | **M** | **M+BF** | **M+LL** | **M+LL+BF** |
|---|---|---|---|---|
| **Min 0** | 0.320 | 0 | 0.353 | 0.014 |
| **Min 60** | 0.328 | -0.005 | 0.370 | 0.016 |
| **Min 140** | 0.345 | -0.001 | 0.360 | 0.034 |
| **Min 200** | 0.339 | 0.006 | 0.365 | 0.039 |

Table 5.6: OD values (600 nm), characterisation of DRP-C223AT with M17, $[Fe(CN)_6]^{3-/4-}$, *L.Lactis* and milk.

From table 5.6, OD values remain constant over time in all the solutions, indicating the lack of bacterial growth in the solutions in which the *L.Lactis* was placed. Therefore, it is not possible to relate the measurements obtained in electrochemistry to the absorbance measurements.

I ask myself what could have influenced the lack of bacterial growth. Could it be due to possible contamination? This possibility is improbable because OD measurements remain constant over time, if there had been any contamination from an external biological agent I would observe a change in absorbance at 600nm. The second option that came to my mind is: is it possible that there are some molecules in milk that inhibit the growth of *L.Lactis* in solution?

## 5.2 Characterisation with processed milk

In order to stimulate bacterial proliferation, the milk was treated firstly to remove the fat content and secondly to precipitate the casein. The used protocol was as follows:

1. Centrifuge the cold milk at 10000 RPM for 5 minutes;
2. Extract and centrifuge the supernatant;
3. Lower the pH of the supernatant to precipitate the casein. Add 70 $\mu L$ of HCl 37% to 9 mL of supernatant. The pH of the supernatant is 6.5, the desired pH is 4.6. You will notice casein clusters when you are at approximately the desired pH;
4. Centrifuge at 10000 RPM for 5 minutes;
5. Remove the supernatant and store it in the fridge. The treated milk will not have the classic milky white colour, but will be practically transparent (filtered milk).

The characterisation was carried out by comparing the response of the device to four different solutions:

| | **M** | **M+LL** | **M+BF** | **M+LL+BF** |
|---|---|---|---|---|
| **Treated milk** | 480 $\mu L$ | 480 $\mu L$ | 240 $\mu L$ | 240 $\mu L$ |
| **L.Lactis** | | 1200 $\mu L$ | | 1200 $\mu L$ |
| **Phage Buffer** | | | 240 | 240 $\mu L$ |
| **20 mM FeCN in M17** | 3000 $\mu L$ | 3000 $\mu L$ | 3000 $\mu L$ | 3000 $\mu L$ |
| **M17** | 2520 $\mu L$ | 1320 $\mu L$ | 2520 $\mu L$ | 1320 $\mu L$ |
| **Total Volume** | 6000 $\mu L$ | 6000 $\mu L$ | 6000 $\mu L$ | 6000 $\mu L$ |

Table 5.7: Solution composition, characterisation of DRP-C223AT with M17, $[Fe(CN)_6]^{3-/4-}$, *L.Lactis* and processed milk.

The test was conducted with the Spill-Out protocol. EIS measurements on a single sensor were taken every 60 minutes, for a total of 240 minutes of the experiment. These measurements were made with the impedance analyser "EmStat Pico" using the following parameters: frequency range [100kHz-1Hz]; number of points per

decade 10; $V_{DC}$ corresponding to the potential $E_0 = 0.071V$; potential $V_{AC}$ fixed at $10mV$. The OD was measured against a "zero" value corresponding to the OD value of solution "M". In order to limit environmental interference and promote bacterial growth, the solutions were placed in a static incubator at 25°C.

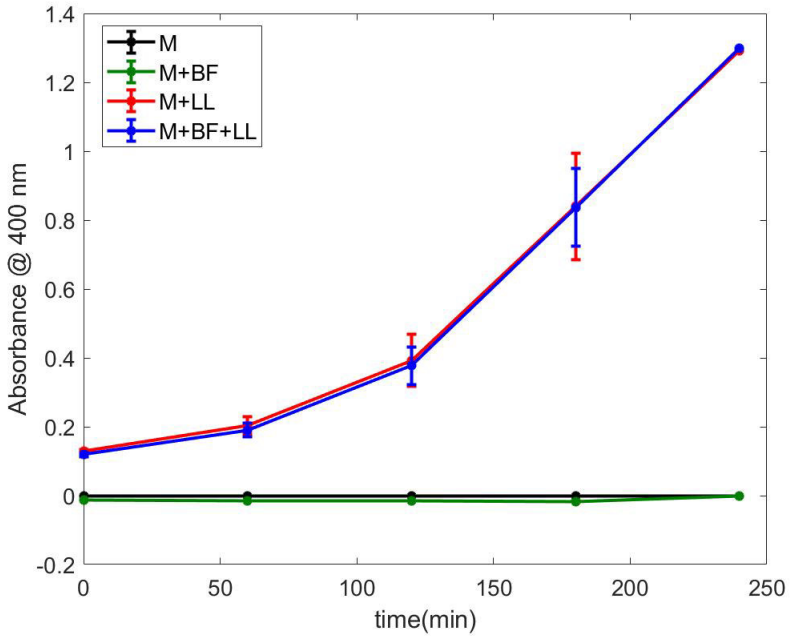


Figure 5.4: OD values (600 nm) as a function of time, characterisation of DRP-C223AT with M17, $[Fe(CN)_6]^{3-/4-}$, *L.Lactis* and processed milk.

From the figure 5.4, there is an increase in OD over time in solutions containing bacteria, indicating that bacterial growth has taken place. The two curves follow the same trend, despite the presence of the buffer, confirming in absorbance what was seen previously without the milk: the presence of the buffer does not affect bacterial growth, even in this type of solution.

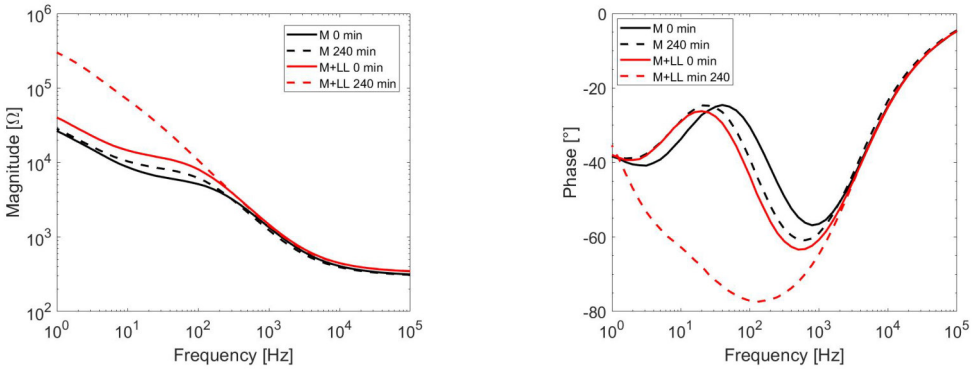


Figure 5.5: Bode diagrams, characterisation of DRP-C223AT with M17, $[Fe(CN)_6]^{3-/4-}$, *L.Lactis* and processed milk.

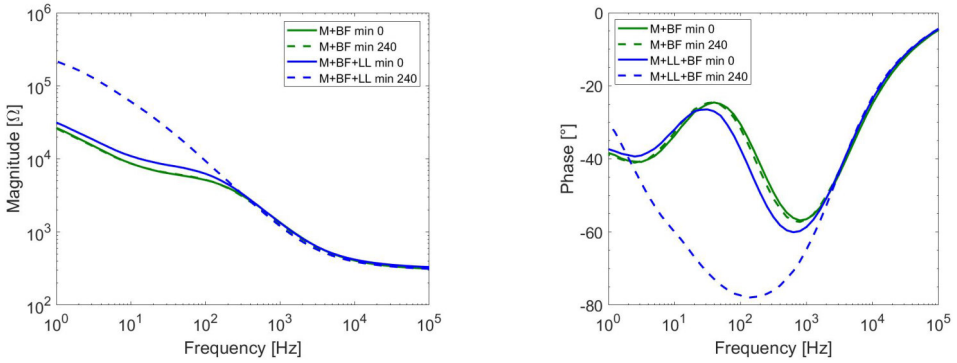


Figure 5.6: Bode diagrams, characterisation of DRP-C223AT with M17, $[Fe(CN)_6]^{3-/4-}$, *L.Lactis*, phage buffer and processed milk.

In the figure 5.5 I represent the Bode diagrams of the sensors characterised with milk and *L.Lactis*. The trend observed in the characterisation with the ideal sample is confirmed: in time the modulus increases for the low frequencies where the *L.Lacts* while it remaines substantially unchanged for the negative control sensor; the phase presentes the usual shift with both solutions, but at 240 minutes there is a change of the curve in sensor with bacteria. As can be seen from the Bode diagrams (figure 5.6), the presence of phage buffer in solution does not change the behaviour of the measurement, in fact the curves are almost completely analogous to those without buffer. In figure (5.7), the Nyquist diagrams also show the same

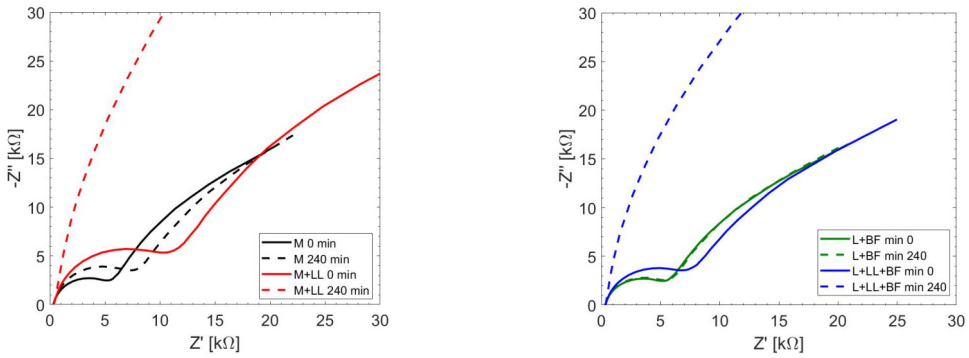


Figure 5.7: Characterisation of DRP-C223AT with M17, $[Fe(CN)_6]^{3-/4-}$, *L.Lactis* and processed milk: Nyquist diagram (a) without phage buffer; (b) with phage buffer.

trend regardless of the presence of phage buffer. Where bacteria are present at 240 minutes there is the usual explosion of the curve due to the deposition of bacteria on the electrode which block the passage of electrons.

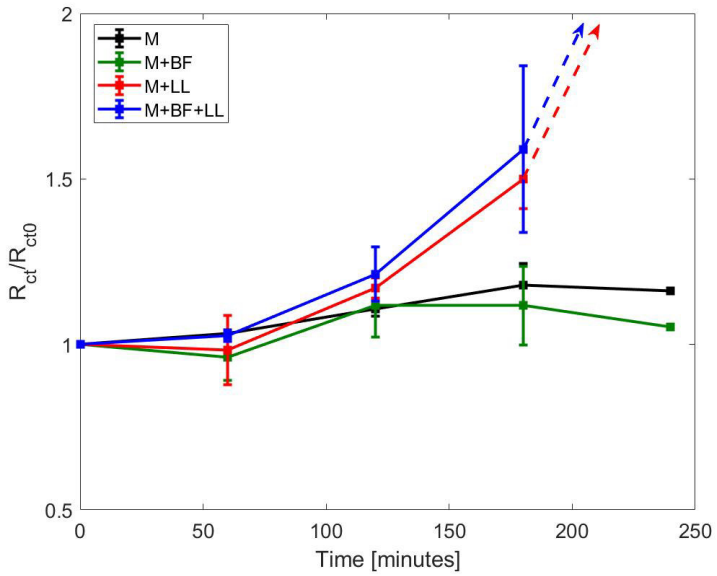


Figure 5.8: $R_{ct}^n$ as a function of time, characterisation of DRP-C223AT with M17, $[Fe(CN)_6]^{3-/4-}$, *L.Lactis* and processed milk.

Figure 4.57 shows the normalized charge transfer resistance $R_{ct}^{n}$ obtained through the formula 4.3. The $R_{ct}$ increases very little in the sensors on which the solutions without bacteria become 1.2 times the initial value. The growth trend of the M and M + BF curves is very similar, the buffer has no effect on the measurement. In sensors on which solutions with bacteria have been deposited the increase of $R_{ct}$ is greater reaching 1.5 (solution without buffer) and 1.6 times (solution with buffer) compared to the initial value.

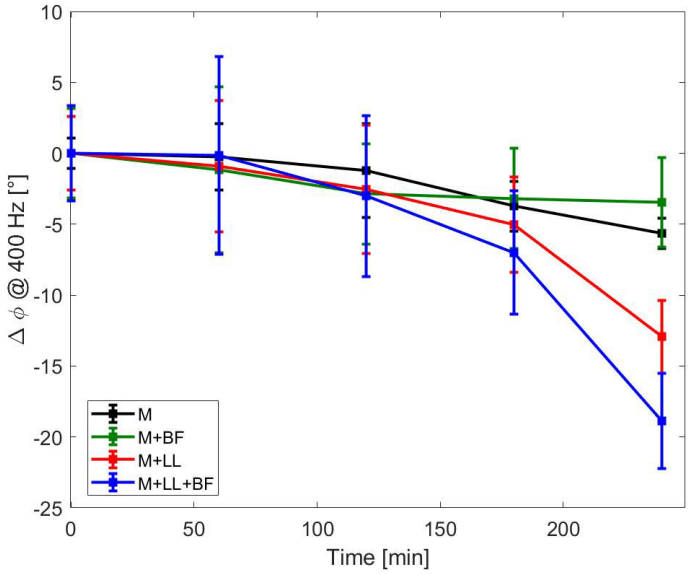


Figure 5.9: Phase variation at 400 Hz $\Delta\phi$, characterisation of DRP-C223AT with M17, $[Fe(CN)_6]^{3-/4-}$, *L.Lactis* and processed milk.

Analysis of the phase change at 400 Hz (figure 5.9) confirme what I have already seen in the ideal solution: the negative control, regardless of whether or not there is buffer, shows a slight decrease in phase with the passage of time; the sensors with the bacteria show a clear decrease in phase with a change of almost 20°. I have verified that, as the OD increases, there is an increase in the charge transfer resistance and a decrease of phase at 400 Hz in function of time. I can therefore state that device is able to monitor the growth of *L.Lactis* even when the milk is put into solution, getting closer and closer to an ideal working condition.

## 5.3 Response with phages and milk

Having reached this point, I proceeded to add the phages to the solution with treated milk, thus testing the performance of the device in a condition very similar to that of an on field application. I used the following solutions:

| | **C.Negative** | **L.Lactis** | **Phages** |
|---|---|---|---|
| **L.Lactis OD=0.5** | | 1200 $\mu L$ | 1200 $\mu L$ |
| **Milk** | 240 $\mu L$ | 240 $\mu L$ | 240 $\mu L$ |
| **Phages** | | | 240 $\mu L$ |
| **Phage Buffer** | 240 $\mu L$ | 240 $\mu L$ | |
| **20 mM FeCn in M17** | 3000 $\mu L$ | 3000 $\mu L$ | 3000 $\mu L$ |
| **M17** | 2520 $\mu L$ | 1320 $\mu L$ | 1320 $\mu L$ |
| **Total Volume** | 6000 $\mu L$ | 6000 $\mu L$ | 6000 $\mu L$ |

Table 5.8: Solution composition, characterisation of DRP-C223AT with M17, $[Fe(CN)_6]^{3-/4-}$, *L.Lactis*, processed milk and phages.

The "Spill-out" protocol was applied, taking measurements every 30 minutes on the same sensor, for a total of 300 minutes of observation (11 EIS measurements on the same sensor). The experiment was carried out using the potentiostat "EmStat Pico" with the following experimental parameters: frequency range [100kHz-1Hz]; number of points per decade 10; $V_{DC}$ corresponding to the potential $E_0 = 0.071V$; potential $V_{AC}$ fixed at $10mV$.

In line with the previous experiments, a pretest was carried out in order to verify that all sensors behaved in the same way. To promote bacterial growth, the cuvette was placed in a static incubator at 25°C. The ODs were measured against a zero, corresponding to the OD of the cuvette containing the negative control solution at the time the solutions were created. OD values are graphed as a function of time in the figure 5.10. The trend of the curve shows an expected trend for the negative control curve, which in fact always remains equal to zero. Where only bacteria are present, the curve corresponds to the theoretical one, the bacteria grow following the typical exponential trend, reaching a plateau between 270 and 300 minutes from the start of the experiment. Where phages are present for the first 90 minutes of the experiment following the theoretical trend assumed, the

bacterial growth is similar to that which occurs in the cuvettes where phages are not present. At 120 minutes, the OD begins to slow down its growth, a sign of the beginning of phage activity. At 180 minutes, there is a decrease in OD, in both cuvettes, which reaches a platou around 0.030, even lower than the starting OD which was 0.120.

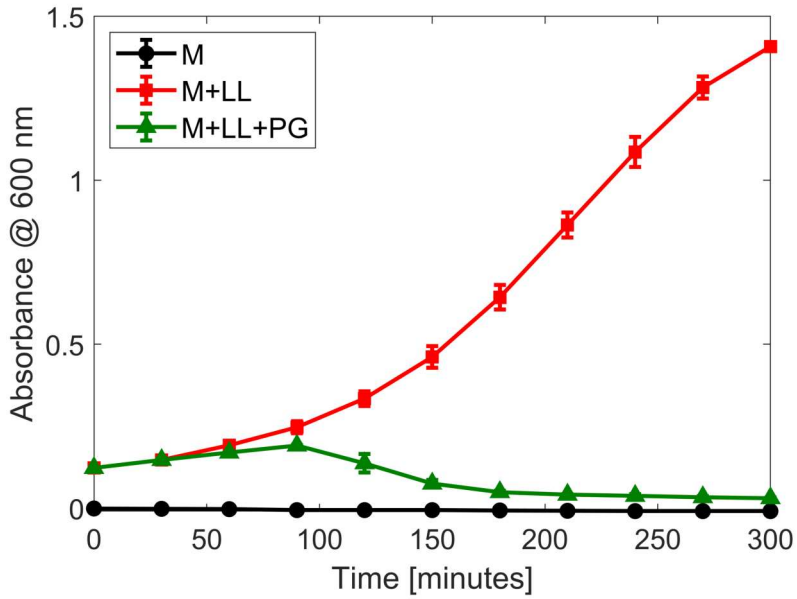


Figure 5.10: OD(600nm) in function of time, characterisation of DRP-C223AT with M17, $[Fe(CN)_6]^{3-/4-}$, *L.Lactis*, processed milk and phages.

In the figures 5.11, 5.12 and 5.13 the modolus of the Bode diagram, the phase of the Bode diagram and the Nyquist diagram are shown respectively. I decide to report only the first and last measurements (minute 300), in order to simplify the graphic visualisation. The modulus as a function of frequency shows the already verified increase at low frequencies (red dashed curve) for the solution with L.Lactis, while for both the negative control and where phages are present we do not notice any particular changes between the curve at time 0 and time 300, the curves are superimposable.Tthere is a change in the shape of the curve of the phase where bacteria are present. The phase shows a similar pattern between the negative control and the sensor with phages in solution, with the just observed frequency shift between $10^2$ and $10^3$. From the Nyquist diagram (figure 5.13), as

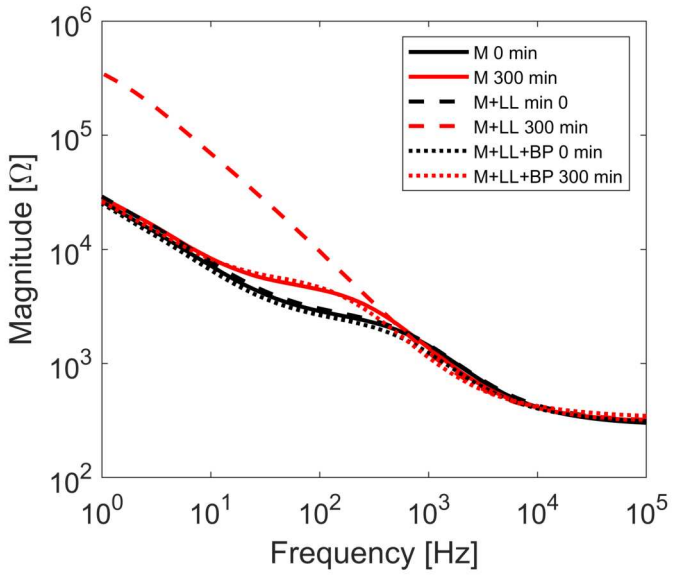


Figure 5.11: Modulus of Bode diagram, characterisation of DRP-C223AT with M17, $[Fe(CN)_6]^{3-/4-}$, *L.Lactis*, processed milk and phages.

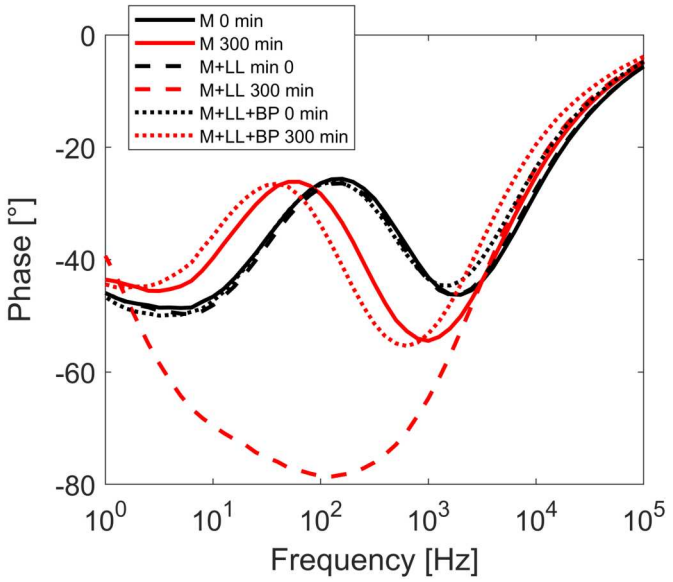


Figure 5.12: Phase of Bode diagram, characterisation of DRP-C223AT with M17, $[Fe(CN)_6]^{3-/4-}$, *L.Lactis*, processed milk and phages.

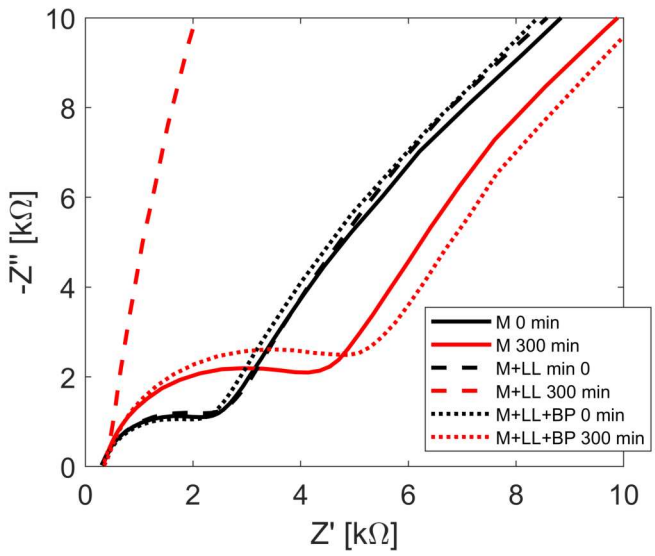


Figure 5.13: Nyquist diagram, characterisation of DRP-C223AT with M17, $[Fe(CN)_6]^{3-/4-}$, *L.Lactis*, processed milk and phages.

could be expected from the OD values, there is an explosion of the curve for the sensors on which the solution containing only the bacteria has been deposited. At minute 300, the shape of the curve changes, the semicircle disappears, the charge transfer resistance cannot be calculated.

The figure 5.14 shows the variation of $R_{ct}^n$ over time, calculated using the formula 4.3. The curves show that the resistance to charge transfer increases markedly where bacteria are present, reaching up to 10 times the initial value. The other curves show a very similar growth trend. The phase variation at 400 Hz confirms what I have seen from the trend in $R_ct$ and what I have seen in optical density. The phase change is much greater where only bacteria are present, whereas at the inhibition of bacterial growth due to the action of phages, there is clear decrease in phage change, comparable with the negative control (without bacteria and without phages).

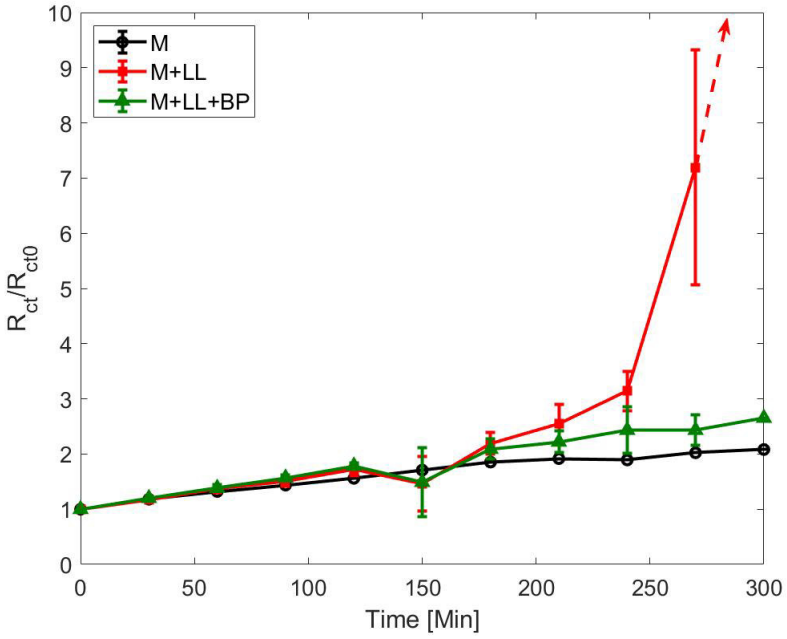


Figure 5.14: $R^n_{ct}$ in function of time, characterisation of DRP-C223AT with M17, $[Fe(CN)_6]^{3-/4-}$, *L.Lactis*, processed milk and phages.

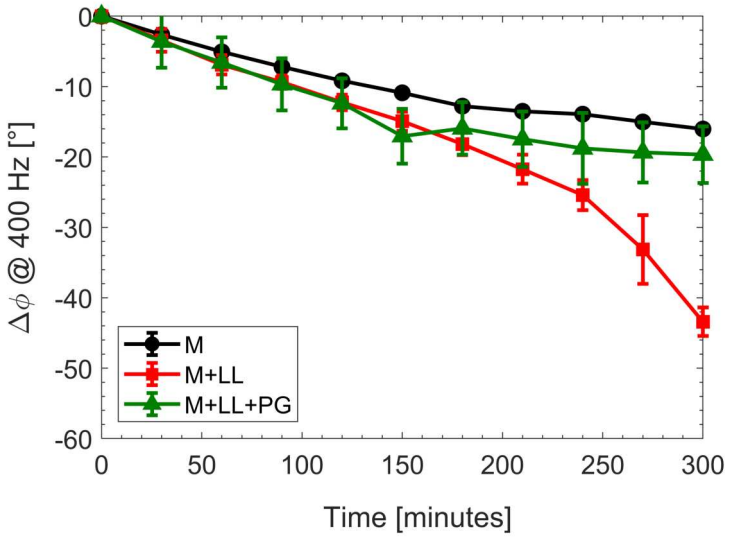


Figure 5.15: Phase variation at 400 Hz $\Delta\phi$, characterisation of DRP-C223AT with M17, $[Fe(CN)_6]^{3-/4-}$, *L.Lactis*, processed milk and phages.

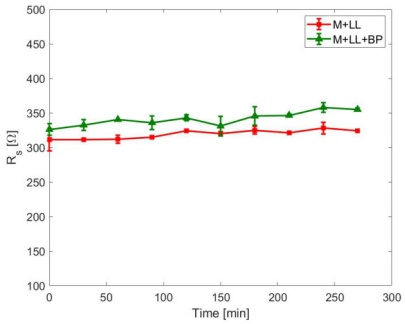


Figure 5.16: $R_s$ in function of time, characterisation of DRP-C223AT with M17, $[Fe(CN)_6]^{3-/4-}$, *L.Lactis*, processed milk and phages.

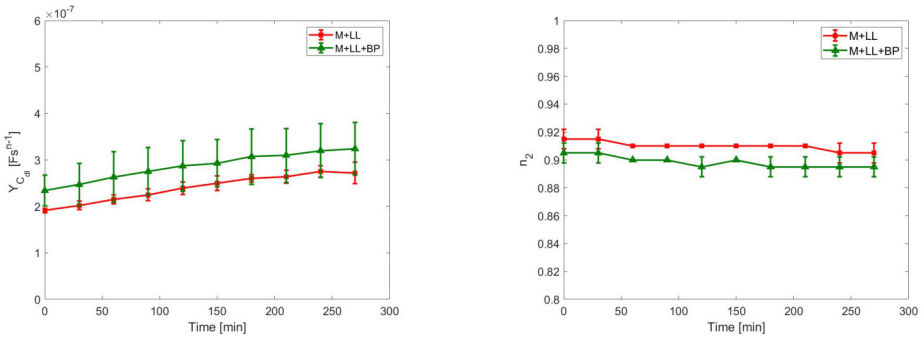


Figure 5.17: $Y_{C_{dl}}$ and $n_1$ in function of time, characterisation of DRP-C223AT with M17, $[Fe(CN)_6]^{3-/4-}$, *L.Lactis*, processed milk and phages.

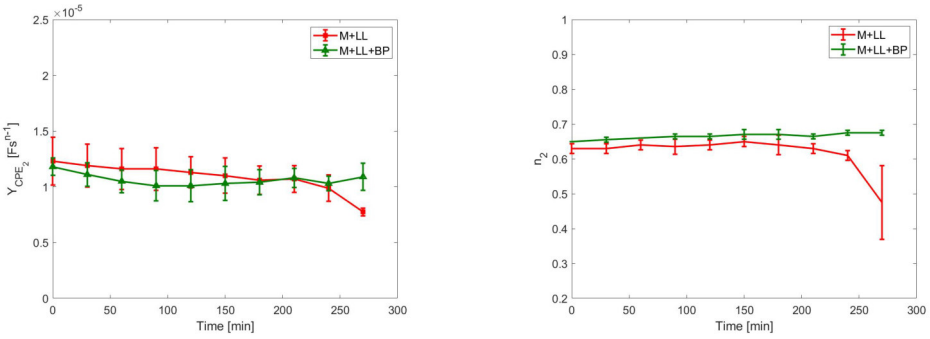


Figure 5.18: $Y_{CPE2}$ and $n_2$ in function of time, characterisation of DRP-C223AT with M17, $[Fe(CN)_6]^{3-/4-}$, *L.Lactis*, processed milk and phages.

The other circuit parameters $R_s$, $C_{dl}$ and $CPE2$, represents respectively in the figures, remain all constant in time, consistently with what was observed in the tests with solutions without milk samples. With this experiment I detect the presence of L.Lactis phages in a solution that is close to what might be an ideal sample. The trend in optical densities showed a behaviour that I had not noticed before: the phages overcame completely the bacterial growth, probably in the presence of milk the phages have a higher lytic capacity which exceeded the bacterial growth rate.

# Chapter 6

# Conclusions

The presence of phages in milk leads to several serious repercussions for the dairy industry such as: product waste with consequent environmental repercussions, production delays and economic damage. At the state of art, there are several techniques currently used for phage detection in the dairy environment, but they have common drawbacks: long observation time; high cost; need of trained personnel; specific instrumentation required. The development of an electrochemical biosensor could be an optimal solution for fast, efficient, economical, portable and user-friendly detection. However, developing a sensor with this goal is complicated, requires time and a huge number of experimental tests.

Screen printed sensor DRP-C223AT, manufactured by Metrohm DropSense, was selected for this purpose. I performed a preliminary characterisation using 10 mM $[Fe(CN)_6]^{3-/4-}$ as the RedOx mediator and M17 as the supporting electrolyte. The device proved to be stable over time, stable to solution drop change and capable of giving a repeatable response. The sensor proved to be capable of detecting the presence of *L.Lactis* in the test solution, but I had to develop a specific protocol called Spill-Out, which involves changing the drop at each measurement. The bacteria in solution settle on the electrode and they obstruct the transport of electrons at the electrode-solution interface.

As the number of bacteria in solution increase, I noted:

- An increase of charge transfer resistance $R_{ct}$ in function of time.
- A decrease of phase at 400 Hz in function of time.

Phages in solution cause bacterial lysis, consequently, compared to a control in which the phages are not present, there are less bacteria in the sample. I was able to detect this phenomenon by looking at:

- Lower increase of charge transfer resistance compared to sample without phages.
- Lower decrease of phase at 400 Hz compared to sample without phages.

In the second phase of my work, I wanted to get closer to a real sample, so I added treated milk in solution. I was again able to detect the presence of bacteriophages in solution with the variation of $R_{ct}$ and the variation of phase at 400 Hz. However, the use of $R_{ct}$ has a limitation: for a high density of bacteria in solution, the charge transfer resistance can not be calculated. The phase variation at 400 Hz has proven to be an optimal parameter for detecting bacteriophages in solution. Furthermore, compared to $R_{ct}$, the phase variation can be calculated by focusing on a single frequency, unlike $R_{ct}$ for which detection requires the inspection of a large frequency range.

In this thesis work, I have proposed a new biosensing technique capable of detecting the inhibition of bacterial growth caused by *L.Lactis* bacteriophages in both ideal solutions and solutions containing treated milk samples. Future work must be carried out with the aim of introducing the device into the market. The first step will be the study and the optimisation of the detection methods under different experimental conditions. Indeed, there are many factors that could influence the performance of the device, such as the ambient temperature or the composition of the test solutions. Then, the device should be tested with different amounts of phages in order to understand its sensitivity. Finally, the device should be characterised with untreated milk and shown to be able to detect effectively phages in the real sample.

# List of Figures

# List of Tables

# Bibliography


[1] F.P.Douillard and W.M.deVos, "Functional genomics of lactic acid bacteria: from food to health," *Microbial Cell Factories*, 2014.

[2] J.Blaya, Z. Barzoedeh, and G.LaPointe, "Symposium review: Interaction of starter cultures and nonstarter lactic acid bacteria in the cheese environment," *American Diary Science Association*, 2018.

[3] J.W.Sanders, G.Venema, and J.Kok, "Environmental stress responses in lactococcus lactis," *FEMS Microbiology Reviews*, 1999.

[4] M.Wels *et al.*, "Comparative genome analysis of lactococcus lactis indicates niche adaptation and resolves genotype/phenotype disparity," *Frontiers in Microbiology*, 2019.

[5] E.Lavezzo, "Course of medical biotechnologies," 2020/2021.

[6] G.Giraffa *et al.*, *Microbgy in Dairy Processing: Challanges and Opportunities*, ch. 13, pp. 233–246. 2018.

[7] J.Garneau and S.Moineau, "Bacteriophages of lactic acid bacteria and their impact on milk fermentations," *Microbiological Cell Factory*, 2011.

[8] A.Magadan *et al.*, *Handbook of Diary Foods Analysis*, ch. 22, pp. 473–486. 2009.

[9] A.Paccagnella, "Corso di biosensori," 2019/2020.

[10] M. H. Ly-Chatain *et al.*, "Direct quantitative detection and identification of lactococcal bacteriophages from milk and whey by real-time pcr: Application

for the detection of lactococcal bacteriophages in goat's raw milk whey in france," *International Journal of Microbiology*, 2011.

[11] O.Michelsen *et al.*, "Detection of bacteriophage-infected cells of lactococcus lactisby using flow cytometry," *Applied and Enviromental Microbiology*, 2007.

[12] S. Favero, "Corso di tecnologia e strumentazione biomedica 2018/2019," 2019.

[13] S.Cinti, "Elettrodi stampati e sostenibilita;" *Chimica Analitica*, 2018.

[14] K.Rathee *et al.*, "Biosensors based on electrochemical lactate detection: Acomprehensive review," *Elsevier-Biochemistry and Biophysics Reports*, 2015.

[15] G.Rosati *et al.*, "Silver nanoparticles inkjet-printed flexible biosensor for rapid label-freeantibiotic detection in milk," *Elsevier, Sensors and Actuators B: Chemical*, 2018.

[16] D.L.Alecandre *et al.*, "A rapid and specific biosensor for salmonella typhimurium detection in milk," *Food and Bioprocess Technology*, 2018.

[17] Z.A.Ahovan *et al.*, "Bacteriophage based biosensors: Trends, outcomes and challenges," *Nanomaterials*, 2020.

[18] C.Garcìa-Aljaro *et al.*, "On-chip impedimetric detection of bacteriophages in dairy samples," *Elsevier: Biosensors and Bioelectronics*, 2008.

[19] G.Palleschi, "Biosensori in medicina," *Caleidoscopio*.

[20] R. Chang, *Chimica Fisica 1.* Zanichelli, 2006.

[21] P.Aberg *et al.*, "Electrical impedance spectroscopy and the diagnostic accuracy for malignant melanoma," *Experimental Dermatology*, 2011.

[22] M. Oliver *et al.*, "Evaluation of the electrical impedance spectroscopy (eis) equipment for ham meat quality selection," *Meat Science*, 2001.

[23] A.M.Lopes *et al.*, "Milk characterization using electrical impedance spectroscopy and fractional models," *Food Analytical Methods*, 2018.

[24] M. Grossi and B. Riccò, "Electrical impedance spectroscopy (eis) for biological analysis and food characterization: a review," *Journal of Sensors and Sensors Systems*, 2017.

[25] F.Lisdat and D.Schafer, "The use of electrochemical impedance spectroscopy for biosensing," *Bioanalytical Chemestry*, 2008.

[26] E. B. Bahadir and K. Sezgintürk, "A review on impedimetric biosensor," *Artificial Cells, Nanomedicine, and Biotechnology*, 2014.

[27] R. Chang, *Chimica Fisica 2.* Zanichelli, 2006.

[28] O. Abollino *et al.*, "Principi ed applicazioni di sensori elettrochimici," *La Chimica e l'industria*, 2014.

[29] S. M. Mariángeles Briggiler Marcó and A. Quiberoni, "Bacteriophages and dairy fermentations," *Landes Bioscience*, 2012.

[30] M. Amiri *et al.*, "Electrochemical methodologies for the detection of pathogens," *Sensors Acs*, 2018.

[31] B. Meshram *et al.*, "Biosensor and its application in food and dairy industry," *International Journal of Current Microbiology and Applied Sciences*, 2018.

[32] Y. Sui and C. A.Zorman, "Inkjet printing of metal structures for electrochemical sensor applications," *Journal of The Electrochemical Society*, 2020.

# Acknowledgements

I would like to express my profound gratitude to my co-supervisor, Dr. Stefano Bonaldo, for his advice, support and encouragement during the course of this study.

I wish to express my gratitude to my supervisor, Prof. Alessandro Paccagnella, who assisted and guided me throughout this project.

Special thanks to all ARC staff, in particular to Dr. Elisabetta Pasqualotto, Dr. Erica Cretaio and Arianna Zanini.